Missouri S&T Library and Learning Resources

Scholars' Mine

Doctoral Dissertations | Student Theses and Dissertations

Spring 2015

Active - passive spent fuel interrogation using neutrons and photons

Tayfun Akyurek

Follow this and additional works at: https://scholarsmine.mst.edu/doctoral_dissertations

 Part of the Nuclear Engineering Commons

Department: Nuclear Engineering and Radiation Science

Recommended Citation

Akyurek, Tayfun, "Active - passive spent fuel interrogation using neutrons and photons" (2015). *Doctoral Dissertations*. 3084.
https://scholarsmine.mst.edu/doctoral_dissertations/3084

This thesis is brought to you by Scholars' Mine, a service of the Missouri S&T Library and Learning Resources. This work is protected by U. S. Copyright Law. Unauthorized use including reproduction for redistribution requires the permission of the copyright holder. For more information, please contact scholarsmine@mst.edu.

ACTIVE - PASSIVE SPENT FUEL INTERROGATION USING NEUTRONS AND PHOTONS

by

TAYFUN AKYUREK

A DISSERTATION

Presented to the Faculty of the Graduate School of the

MISSOURI UNIVERSITY OF SCIENCE AND TECHNOLOGY

In Partial Fulfillment of the Requirements for the Degree

DOCTOR OF PHILOSOPHY

in

NUCLEAR ENGINEERING

2015

Approved by

Shoaib Usman, Advisor

Xin Liu, Co-Advisor

Hyoung K. Lee

Ayodeji B. Alajo

Joseph Smith

© 2015
TAYFUN AKYUREK
All Rights Reserved

PUBLICATION DISSERTATION OPTION

This dissertation consists of the following five articles that have been published, submitted for publication or will be submitted for publication:

Paper I entitled "GM Counter Dead-time Dependence on Applied Voltage, Operating Temperature and Fatigue", presented from page 9 to 36 in this dissertation, has been published in Radiation Measurement, 2015, Volume 73, Pages 26-35.

Paper II entitled "A Comparison of Traditional and Hybrid Radiation Detector Dead-time Models and Detector Behavior", presented from page 37 to 64 in this dissertation, has been accepted in Progress in Nuclear Energy, March 21th, 2015,

Paper III entitled "Portable Spectroscopic Fast Neutron Probe and ^{3}He Detector Dead-time Measurements", presented from page 65 to 86 in this dissertation, will be submitted to Progress in Nuclear Energy.

Paper IV entitled "Characterization of Best Candidate Isotopes for Burnup Analysis and Monitoring of Irradiated Fuel", presented from page 87 to 124 in this dissertation, has been published in Annals of Nuclear Energy, 2014, Volume 69, Pages 278-291.

Paper V entitled "Spent Fuel Interrogation Using Delayed Fast Neutron Counting at Missouri University of Science and Technology Reactor", presented from page 125 to 163 in this dissertation, have been submitted to Progress in Nuclear Energy (Under Review).

ABSTRACT

This dissertation consists of three main parts. The first part is devoted to the comprehensive dead-time calculations with different detectors and conditions using different dead-time models as well as computer simulations. The minimum time that must separate two detectable events is called the counting system's dead-time. If events take place during the system's dead-time, they will not be recorded and will be lost. Such lost information is very important in many applications including high-intensity spectroscopy and nuclear spent fuel interrogations. The second part, a multitude of fission products identified as candidates have been scrutinized for their suitability of burnup analysis and spent fuel analysis for irradiated Mixed Oxide (MOX) fuels. Best isotopes obtained for analysis by investigating half-life, photon energy, fission yield, branching ratios, production modes, thermal neutron absorption cross section and fuel matrix diffusivity. ^{132}I and ^{97}Nb are identified as good isotope candidates for MOX fuel on-line burnup analysis. The third and most important part, in terms of time spent and effort, deals with spent fuel analysis using non-destructive (NDA) delayed fast neutron measurement technique for safeguard purposes. The spent fuel investigation experiment was held in Missouri University of Science and Technology Research Reactor (MSTR) which is a swimming pool type reactor and licensed to operate at 200 kilowatts power. The core of the reactor consists of 15 fuel elements with low-enriched Uranium-235. Using the NDA technique, the reactor fuel burnup and ^{235}U - ^{239}Pu conversion values calculated. The fast neutron measurements were taken with a liquid scintillator detector which its dead-time value calculated to be 101.2 μs for paralyzing dead-time model and 254.8 μs for non-paralyzing model.

ACKNOWLEDGMENTS

I would like to thank my advisor, Dr. Shoaib Usman for training, teaching, guiding me during the Ph.D. program. I could not complete this project without his help and encouragement. I also need to thank my dissertation committee members, Dr. Xin Liu for his support as my co-advisor, Dr. Ayodeji Alajo for his advice and the useful interactions we had throughout the PhD program, Dr. Hyoung Lee and Dr. Joseph Smith for all their ideas and discussions.

I also received tremendous amount of help from the Missouri University of Science and Technology Reactor staff. Bill Bonzer and Craig Reisner helped me to complete my spent fuel analysis experiments. My friends in Nuclear Engineering department contributed to my dissertation. I appreciate their ideas, discussions, assistance and work. I also would like to thank to Turkish Ministry of National Education for their support to receive my Master's and Ph.D. degree in United States.

I remember the day of enrolling my primary school in 1988, I was so excited and cheerful. I never lost my passion to learn something new during 26 years. Today is the last day of my school time and I will never forget those years and still continue learn something new. I thank my family who have been a source of encouragement and emotional support which was needed for all those years. I would have accomplished nothing without them throughout my life. Last, but far from least, I thank my wife, Zeynep Akyurek, who never stop supporting me at all times. I would never complete my graduate school without your patience, encouragement, and love. Beside all of those thanks to everybody, I need to apologize to my daughter, Zehra, for not being able to spend more time during my Ph.D. program.

TABLE OF CONTENTS

LIST OF ILLUSTRATIONS

Paper III

Paper V

LIST OF TABLES

NOMENCLATURE

Symbol	Description
n	True count rate
m	Observed count rate
τ	Dead-time
τ_p	Paralayzable dead-time
τ_{np}	Non-Paralayzable dead-time
f	Paralyzing factor
P+U	Patil and Usman
L+G	Lee and Gardner
GM	Geiger-Muller
NP	Non-paralyzing
P	Paralyzing

1. INTRODUCTION

1.1. DEAD-TIME OF RADIATION DETECTION SYSTEMS

High intensity radiation measurements such as spent fuel monitoring with spectroscopy are affected by detection system's dead-time and pulse pile-up problems [1]. In detector systems, a minimum time interval required between two events so that they can be recorded as an independent event. This minimum time interval is called the counting system's dead-time [2, 3]. All events occurring during this dead-time are lost in a detection system. Researchers have been developing counting system's dead-time model that would describe the behavior of the detection system. The two idealized models (paralyzing and non-paralyzing) have been introduced that help researchers to correct their counting loss [4]. Recently, new dead-time models developed that estimate the count loss, however, no detector exactly follows any of these models [5, 6]. In reality, counting loss estimation lies between paralyzing and non-paralyzing extreme models.

The two-source method is commonly used to measure a detecting system's total dead-time. The method is based on measuring the counting rate from two sources, both individually and in combination. The measured counting rate of combined sources will be less than the sum of individual sources counting rates because the observed counting losses are non-linear. The dead-time can be calculated from the difference between the two sources [7, 8]. However, several assumptions must be made regarding the system's intrinsic characteristics after the data is collected, before the dead-time can be calculated. Detailed dead-time calculation of two source method can be found further in paper I section. Another method commonly used to measure a system's total dead-time is the decaying source method [9]. This technique, essentially, requires a short-lived isotope; it is based on

that isotope's decaying behavior. This method has several advantages for measuring the dead-time and ability to validate assumption of system being paralyzable or non-paralyzable. Unfortunately, for this method a large amount of time is needed to determine the dead-time.

1.2. SPENT FUEL INTERROGATION USING PHOTONS AND NEUTRONS

Spent fuel investigations have been continuing using neutron and gamma detection for safeguard purposes and reprocessing control. There are two groups of techniques available; "passive" measurement of delayed neutrons and gamma and "active" interrogation by either a pulsed neutron source or a weak steady state source and subsequently monitoring the gamma and/or neutron emissions [10]. The lost counts because of the dead-time during data collection should be added to the collected data for spent fuel analysis.

Commercial nuclear fuel reprocessing was banned by the United States government, interrupting the U.S. reprocessing industry between 1977 and 1981. European countries such as France developed the reprocessing technology and incorporated Mixed OXide (MOX) fuel into their nuclear fuel cycle. France have showed that MOX fuel can be integrated into a Uranium fueled core without risking the safety of the plant and proliferation. Recently, the U.S. nuclear power industry have been interrogating the MOX fuel. The megatons to megawatts program is an encouragement for investigating the MOX fuel [11]. Therefore, better tools and techniques are necessary for measuring burnup and spent fuel monitoring for MOX fuel.

Gamma (photon) measurement is a non-destructive technique (NDA) for spent fuel analysis. Using NDA gamma measurement method, emitted photons by irradiated fuel

assemblies can be analyzed to determine parameters such as burnup, cooling time, and qualitative verification of the irradiation history [12]. Willman and et. al., have discriminated MOX fuel from LEU fuel using ^{134}Cs ^{137}Cs and ^{154}Eu isotopes as cooling time and irradiation history indicators [13]. Dennis and Usman reported that ^{106}Ru is another isotope which can be used potential burnup indicator [14]. Another NDA technique for spent fuel interrogation is neutron measurement. When ^{238}U is exposed to neutron radiation, it leads to the production of ^{244}Cm. Spontaneous fission of ^{244}Cm provides a source of "delayed neutron". Since the half-life of ^{244}Cm is 18.1 years, neutron intensity from ^{244}Cm is a measure of burnup [15]. This technique is highly sensitive to cooling time, and initial enrichment for the spent fuel.

Additionally, chemical assay with mass spectroscopic techniques have historically been applied to determine isotopic composition of spent nuclear fuel but these techniques requires fuel sample destruction and can take a long time for sample analysis and results [16].

Missouri University of Science and Technology research reactor (MSTR) is a "swimming pool" reactor licensed to operate at 200 kW power. The research reactor is first nuclear reactor in Missouri and its core contains low enriched Uranium (LEU). Detailed core and fuel information of MSTR will be discussed in paper V section. The reactor can be used for burnup analysis and discrimination of Pu and U content using nondestructive gamma and delayed neutron measurements. All radiation measurements need to be corrected using either non-paralyzing dead-time or paralyzing dead-time model depend on detector behavior.

1.3. RESEARCH OBJECTIVES

The main objective of this study is to determine best isotopes for MOX fuel for online burnup analysis and spent fuel monitoring as well as developing a technique which can discriminate Pu content from U using NDA method. The secondary objective of this study is to determine the dead-time of different radiation detectors under different conditions. MS&T research reactor was used to determine burnup value of a particular spent fuels using NDA method. The reactor has been burning 15 nuclear fuel elements in the core since 1992 and producing Pu. Therefore, Pu conversion of the fuel elements was determined. To achieve all the objective of this study, the following specific works accomplished:

1. Obtain the dead-time measurement of different detectors under different conditions and understand the behavior of detectors to correct the lost counts for high intensity radiation measurements. Compare the different dead-time models using computational simulations under different conditions.
2. Determining best isotopes for online burnup analysis, spent fuel monitoring, and historical fuel monitoring for MOX fuel. Best isotopes obtained by investigating half-life, photon energy, fission yield, branching ratios, production modes, thermal neutron absorption cross section and fuel matrix diffusivity.
3. Interrogate the MSTR nuclear spent fuel elements and calculate the U fuel burnup values using NDA method. Fast delayed neutron energy spectra were taken for each spent and fresh fuels. Observing delayed neutron

emission rates of the spent and fresh fuel elements Pu conversion was calculated.

1.4. DISSERTATION ORGANIZATION

This dissertation organized into three sections. Section 2 presents three published journal papers and two under review journal papers.

In paper I, using standard two-source method and the simple non-paralyzing model assumption GM counter's dead-time dependence on applied voltage, operating temperature, and fatigue was calculated. Both ^{60}Co and ^{137}Cs sources were used for dead-time measurements. The results suggest plateau region is the best region for operating with a minimum dead-time which is not sensitive to the applied voltage. The results examined in this study indicate that there is no universally acceptable generalized dead-time model and make such generalized model questionable.

In paper II, a computation method was used to compare the traditional dead-time correction models with recently proposed hybrid dead-time models. A computational algorithm based on a decay source method was used to study the behavior of various dead-time models. Validation of the code was performed for the hybrid model behavior by confirming that the predictions lie between the two ideal dead-time models. It was interesting to see that two seemingly similar hybrid dead-time models produced significantly different results.

In paper III, both non-paralyzing and paralyzing dead-time calculations were obtained for fast neutron detector which was used for spent fuel interrogations. The dead-time for another neutron detector (^{3}He) was also calculated using subcritical assembly

experiment. MCNP (Monte Carlo N-Particle) code was developed for subcritical assembly to compare with experimental results.

In paper IV, a multitude of fission products identified as candidates have been scrutinized for their suitability of burnup analysis and spent fuel analysis. Best isotopes obtained for analysis by investigating half-life, fission yield, branching ratios, production modes, thermal neutron absorption cross section and fuel matrix diffusivity.

In paper V, using NDA method and MS&T research reactor spent fuel analysis performed. Four different fuel element's fast delayed neutron energy spectra taken for detailed analysis. Spent fuel investigations were performed using delayed thermal neutrons using BF_3 detector in literature. However, no study performed using fast delayed neutron energy spectrum. In this paper, burnup values of spent fuel elements were obtained. U and Pu conversions were also calculated using NDA method.

Section 3 summarizes the findings and conclusions of this study and proposes future research.

REFERENCES

[1] A. Patil, "Dead time and Count Loss Determination in Radiation Detection System in High Count Rate Applications" PhD Thesis, Missouri University of Science & Technology, Rolla, MO, USA. (2010).

[2] G.F. Knoll, "Radiation Detection and Measurement". (4th Edition, 2010). New York: John Willey and Sons, Inc. USA.

[3] N. Tsoulfanidis and S. Landsberger, "Measurement and Detection of Radiation", (3rd Edition, 2012), CRC Press, New York, NY, 10016 USA.

[4] W. Feller, "On probability problems in the theory of counters". in R. Courant Anniversary volume. Studies and Essays. Interscience. New York. 105-115. (1948).

[5] A. Patil and S. Usman, "Measurement and Application of Paralysis Factor for Improved Detector Dead Time Characterization", Nuclear Technology, Volume. 165, (2009).

[6] S. H. Lee and R. P. Gardner, "A new GM Counter Dead Time Model", Appl. Rad. Isot, 53, 731- 737, (2000).

[7] P. B. Moon, "Recent developments in Geiger-Muller counters". J. Sci. Instr. 14, 189. (1937).

[8] A. F. Reid, "Preparations and Measurement of Isotropic Tracers". Edward Brothers, Ann Arbor. (1946).

[9] H. G. Stever, "The discharge mechanism of fast G-M counters from the dead-time experiment". Phys. Rev. 61, 38-52. (1942).

[10] T. Akyurek and et. al., "Characterization of Best Candidate Isotopes for Burnup Analysis and Monitoring of Irradiated Fuel", Annals of Nuclear Energy, 69, 278-291, (2014).

[11] United States Enrichment Corporation, Megatons to Megawatts Program, http://www.usec.com/news/megatons-megawatts-program-recycles-450-metric-tons-weapons-grade-uranium-commercial-nuclear-fu, accessed on 13 April, 2013, created on 9 July 2012.

[12] A. Håkansson, and et. al., "Results of spent-fuel NDA with HRGS". In: Proceedings of the 15th Annual Esarda meeting, Rome, Italy. (1993).

[13] C. Willman, and et al., "A nondestructive method for discriminating MOX fuel from LEU fuel for safeguards purpose", Annals of Nuclear Energy 33, 766-773, (2006).

[14] M. L. Dennis, S. Usman, "Feasibility of 106Ru peak measurement for MOX fuel burnup analysis". Nuclear Engineering and Design, 240, 3687-3696, (2010).

[15] K.A. Jordan, G. Perret, “A delayed neutron technique for measuring induced fission rates in fresh and burnt LWR fuel”, Nuclear Instruments and Methods in Physics Research A 634, 91-100, (2011).

[16] K. Inoue and et al., “Burnup determination of Nuclear Fuel”, Mass Spectroscopy, 17, 830-842, (1969).

PAPER

I. GM COUNTER DEAD-TIME DEPENDENCE ON APPLIED VOLTAGE, OPERATING TEMPERATURE AND FATIGUE

T. Akyurek, M. Yousaf, X. Liu and S. Usman

Department of Mining and Nuclear Engineering, Missouri University of Science & Technology, Rolla, MO, 65401, USA

Abstract

This paper utilized standard two-source method and the simple non-paralyzing model assumption to examine a GM counter's dead-time dependence on applied voltage, operating temperature, and fatigue. Both ^{60}Co and ^{137}Cs sources were used for dead-time measurements. The results gathered suggest the presence of three distinct regions of dead-time behavior. At low voltages, the dead-time decreases as the voltage increases (Region I) followed by a region of stable dead-time plateau (Region II) and finally a region of increasing dead-time with increasing voltage. Region II is the best region for operating with a minimum dead-time which is not sensitive to the applied voltage. Typical dead-time values for GM counters were between 100 and 300 μs; the dead-time values in Region II were within this range. The results examined in this study also indicate a strong temperature dependence of dead-time, with a correlation coefficient of 0.93.The GM counter dead-time for various fatigues (ageing) were investigated for three fatigue levels with a correlation coefficient of 0.48. The experimental results confirm that dead-time increases as both temperature and fatigue increase. The fundamental nature of dead-time seems to be

different for voltages lower than the stable dead-time plateau (Region II) and for voltages higher than the plateau.

1. Introduction

Researchers have been examining the dead-time phenomenon in radiation detectors since the early 1940s. In detector systems, a minimum time of separation must occur between two events before they can be recorded as independent. This minimum separation time is referred to as the counting system's dead-time [1, 2]. This dead-time depends on the detector's properties and the pulse processing circuitry's characteristics. Researchers have been interested in developing a detector dead-time model that can implicitly characterize a detector system's behavior while reducing the counting errors [3, 4].

Moon [5] developed a two-source method that is commonly used to measure a detecting system's total dead-time. This method has been integrated into a number of other works [6, 7]. It is based on measuring the counting rate from two sources, both individually and in combination. The measured counting rate of combined sources will be less than the sum of individual sources counting rates because the observed counting losses are non-linear. The dead-time can be calculated from the difference between the two sources. However, several assumptions must be made regarding the system's intrinsic characteristics after the data is collected, before the dead-time can be calculated.

Another method commonly used to measure a system's total dead-time is the decaying source method [6]. This technique, essentially, requires a short-lived isotope; it is based on that isotope's decaying behavior. This method has several advantages for measuring the dead-time and ability to validate assumption of system being paralyzable or

non-paralyzable. Unfortunately, for this method a large amount of time is needed to determine the dead-time.

In a Geiger-Muller (GM) counter, an electron-ion pair is produced when an ionizing radiation interacts with the detector. Both an electron and a positive ion are accelerated to their respective electrodes as a result of the high voltage. The accelerated electron creates a cascade of secondary ionization, leading to an avalanche [8]. This avalanche propagates through the anode wire's length at a velocity of approximately 2-4 cm/μs until the entire wire is involved. The pulse comprises all of the negative charges produced and collected, lasting a few microseconds. The charge collecting time varies according to the type of gas, temperature, pressure, and applied voltage used. The pulse's duration likely depends on the initial ionization's location, the detector's geometry, and the applied voltage. The drift velocity for ions in a gas is defined as

$$\upsilon = \frac{\mu \varepsilon}{\mathrm{p}} \tag{1}$$

where υ is the drift velocity, ε is the electric field's strength, and p is the gas pressure [9]. The mobility (μ) remains constant over a wide range of applied electric field and pressure for a given gas filled detector, regardless of either positive or negative ions. Typical values lie within the range of 1 and 1.5x10-4 m2 atm/V.sec for gases with a medium atomic number [9]. Therefore, either an increase or a decrease in the charge collection time will affect the number of counts or pulses collected by the detection system. Free electrons and positive ions behave quiet differently because of their mobility in a collection system. Free electrons are 1000 times more mobile because of their lower mass than ions, therefore their collection time is approximately in micro-seconds (μs) which is much smaller than the ion

collection time. Randomness occurs in the paralysis due to the random nature of the initial ionization's location, [10]. The drift velocity for an ion is also altered by temperature; ion mobility is proportionally altered by temperature. It is proposed that the ions drift velocity is inversely proportional to temperature [11].

Although, electrons are collected at the anode very quickly, positive ions tend to linger around the anode longer because of their low mobility before being collected at the cathode which results in severe distortion of electric field. While the electric field is distorted, any subsequent pulse generated before the positive charge is completely removed will be reduced in amplitude. If the field distortion is strong, the subsequent radiation interaction in the detector may produce an undetectable pulse. Counts are thus lost in the GM counter as a result of the dead-time effect. The dead-time duration depends on the detector's geometry, filled gas properties, temperature, pressure, and most importantly the operating voltage [12].

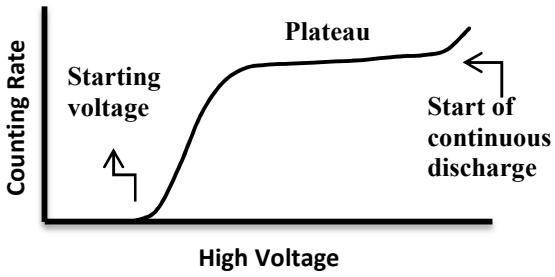

Figure 1. Illustration of the counting rate-voltage dependence of GM counters.

Fig. (1) illustrates the counting rate versus the applied voltage behavior on a GM counter. The applied voltage at which pulses are first recorded by the counting system is known as the "starting voltage". Until the voltage is increased to this minimum voltage, most of the charge created by radiation will be combined, producing only a small,

undetectable pulse. If the voltage is increased, the counting curve becomes a nearly flat plateau above a certain voltage. In this plateau region, detector operating voltage would be stable; any minor fluctuation in the voltage will not result in count rate fluctuation. This operation voltage varies among different GM tubes produced by different manufacturers. If the voltage is increased to a sufficiently high voltage, the plateau region ends and then continuous discharge mechanism starts in the GM tube since discharges initiates from sharp irregularities on the anode wire or multiple pulsing by quenching mechanism failure. There are two idealized models used to determine detector's dead-time; "Paralyzing" and the "Non-paralyzing" models. No detector fits any one of these ideal models perfectly; the reality is between these two extremes [13]. A paralyzable model assumes that each event during the dead-time will reset the dead-time to a fixed duration, thereby extending the dead-time. The dead-time extension will depend on the count rate. Mathematically,

$$m = ne^{-n\tau} \tag{2}$$

where m is the measured count rate, n is the true count rate and τ is the dead-time. A non-paralyzable model is unaffected by events that occur during its dead-time. Therefore, the dead-time is fixed after each recorded event. During this dead-time, all events are completely lost. The fraction of time during which an apparatus is sensitive is $1\text{-}m\tau$. Therefore, the fraction of the true number of events can be recorded as [13]

$$m = \frac{n}{1+n\tau} \tag{3}$$

A better representation of the dead-time phenomenon is by a hybrid model. There are two approaches for hybrid dead-time models; by using two separate dead-time as

proposed by Lee and Gardner or single dead-time with a paralysis factor as proposed by Patil and Usman. Lee and Gardner combined the two idealized models and produced an equation that depends on both paralyzing and non-paralyzing dead-times. The decaying source method, with a ^{56}Mn isotope, was used to assess the hybrid GM dead-time model's validity. Both the observed and the estimated true counting rates were analyzed, and the paralysis factor for the GM counter was found to be 5% or lower. This result supports the common assumption of non-paralayzing behavior for GM counter. Their equation for a recorded count rate in terms of the two dead-times is [14]

$$m = \frac{ne^{-n\tau_P}}{1 + n\tau_N} \tag{4}$$

Recently, Patil and Usman used paralysis factor in their equation which is slightly different approach from Eq. (4) [15]

$$m = \frac{ne^{-n\tau f}}{1 + n\tau(1 - f)} \tag{5}$$

Rather than using two separate dead-times (both a paralyzing and non-paralyzing dead-time), they used a total dead-time and a paralysis factor "*f*" (the measure of a paralyzing probability).

The alteration of a GM counter's dead-time was examined in this study at various voltages, different operating temperatures, and the GM counter's several levels of fatigue (ageing). While fatigue is not a significant factor in most applications, it can be quite significant for high intensity applications for example nuclear reactors where gas filled detectors (both fission chambers and BF_3 proportional counters) are commonly used.

Therefore basic understanding of the changes in detector response as it ages due to fatigue is important. Previous discussions suggest that the non-paralyzing model offers a reasonably good approximation for a GM counter [14, 15]. Therefore, this ideal, non-paralyzing, two-source method was used in this study to calculate dead-times. The results indicate a GM's dead-time is dependent on applied voltages, operating temperatures, and fatigue.

2. Experimental Design

Fig. (2a) illustrates the experimental set-up of system to measure counts for both sources, while Fig. (2b) shows the arrangement for electrically heating (using heating pads) to allow the dead-time data to be collected at different operating temperatures and fatigues. Fig. (2c) shows both the GM counter and the Cobalt sources in dead-time dependence on temperature and fatigue measurements. Caution was exercised to ensure identical source-detector geometry. During the experiments, the GM counter [16], the preamplifier [17] (Ortec 142, 2014), the amplifier [18] (Ortec 570, 2014), the high voltage power supply [19] (Ortec 556, 2014) and the timer/counter [20] (Ortec 996, 2014) were used as experimental instruments. Two ^{60}Co sources (half-life 5.62 yrs.) and two ^{137}Cs (half-life 30 yrs.) sources were used to calculate the deadtime-voltage relationship and the deadtime-temperaute relationship respectively. The activities of the sources were 5 μCi at the time of their production in February 1994 for deadtime-voltage measurements. For temperature dependence and fatigue dependence newer sources of ^{137}Cs (produced in May 2013) with an initial activity of 5 μCi were used.

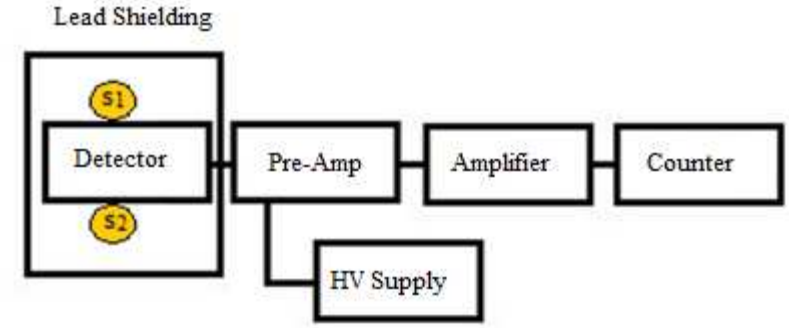

a.

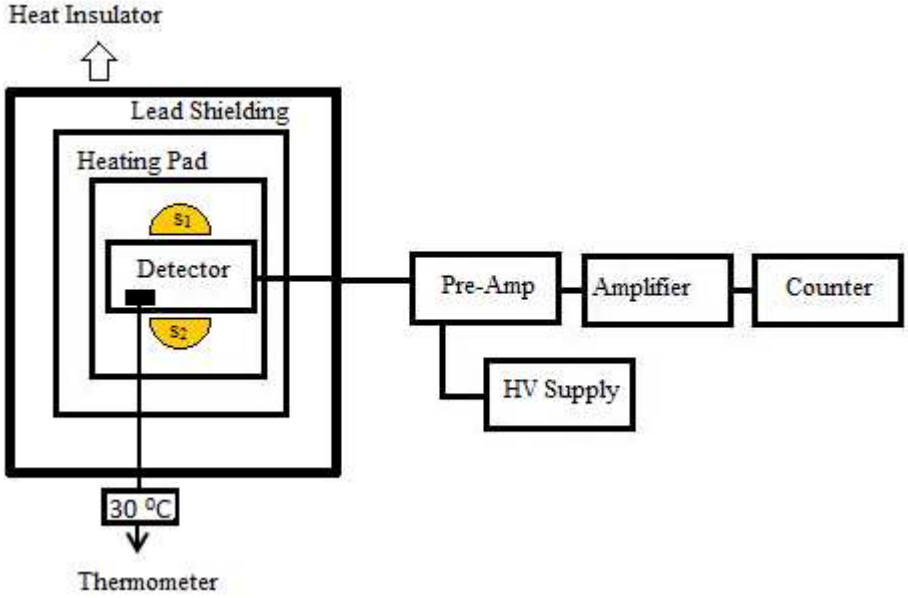

b.

c.

Figure 2 a) Basic experimental setup for study of deadtime-voltage dependence of GM detector. **b**) Experimental setup for study of deadtime-temperature, and fatigue dependence of GM detector. **c)** GM counter and Co sources used in deadtime-voltage dependence experiment.

Lee and Gardner [14] reported a GM counter paralysis factor of 5% or less which justifies our use of non-paralyzing assumption. Therefore, both a standard two source method and a simple non-paralyzing dead-time model were used to measure GM counter's dead-time. The procedure for dead-time measurement is outlined in Knoll's [21]) textbook which was closely followed.

$$X = s_1 s_2 - b s_{12} \tag{6}$$

$$Y = s_1 s_2 . (s_{12} + b) - b . s_{12} . (s_1 + s_2) \tag{7}$$

$$Z = \frac{Y(s_1 + s_2 - s_{12} - b)}{X^2} \tag{8}$$

$$\tau = \frac{X(1 - \sqrt{1 - Z})}{Y} \tag{9}$$

The unshielded background in the lab for dead-time-voltage dependence measurements was 2.56 per second for a GM operated at 1100 volt. However, using lead shielding chamber the background counts dropped to 0.44 per second. A two hours long background measurement was taken for each voltage step. The ^{60}Co source placed near the middle of the detector individually and in combined after all background radiation measurements were completed. Care was exercised to ensure that the same geometry was used for all of the repeated experiments. A one hour count was taken for each of the individual as well as the combined source measurements; that is s_1,s_2, and s_{12} respectively. Eqs. (6), (7), (8), and (9) were used to calculate the system's dead-time at each operating voltage condition. The same method was repeated for the ^{137}Cs sources. Using the standard error propagation method in dead-time measurements, uncertainty were calculated and are shown in the respective plots.

Subsequently, the GM counter was surrounded by a heating pad so that the temperature could be altered and deadtime-temperature dependence could be measured. The counter, the heating pad, and the lead shielding were all enclosed in an aluminum covered cubic box. The box was then placed in a thermostatically controlled cabinet. The detector's operating temperature was varied between 0 ^{0}C and 70 ^{0}C. Thus, the deadtime-temperature and fatigue dependence experiments were performed within these ranges increasing by 10 degree for each step. Applied voltage on detector was fixed during the temperature dependence experiment. This experiment was repeated at different applied voltages between 1100 V and 1150 V for each 10 V step in the area of a GM plateau region. One hour long background measurements were taken for each temperature step. The ^{137}Cs source was placed near the middle of the detector individually and combined after all background radiation measurements were completed. A one hour count was taken for each of the individual as well as the combined source measurements; that is s_1,s_2, and s_{12} respectively. Unlike the voltage-deadtime dependence measurements, only half disk ^{137}Cs sources were used to collect temperature measurements shown in Fig. (3).

Equations 6-9 were used to calculate the system's dead-time at each operating temperature-fatigue (ageing) condition. The experiment was repeated to examine fatigue dependence after completing all dead-time measurements of GM counter with different temperatures. For fatigue the detector was exposed to high intensity radiation. After exposure to the desire 3.0x10^{10} counts the temperature dependence experiment was repeated. Three fatigue levels were used; almost new detector (that is less than 3x10^{10}counts), 6x10^{10} count fatigue and 9x10^{10} count fatigue level.

Figure 3. The ^{137}Cs source used in the deadtime – temperature and fatigue dependence measurements.

3. Results

Equations 6 - 9 were used to calculate the dead-time for each voltage step. The results for the ^{60}Co sources are shown in Table 1. The count rate for both the individual and the combined source measurements were calculated as counts/hour for each step. The tabulated version of counting rate unit was converted to count/sec for convenience. The s_1,s_2, and s_{12} counting rates increased up to 1150 V. Beyond this point, the detector's behavior was stable up to 1200 V. Then count rates jump to discharge region beyond that voltage. Dead-time of the detector system decreased until it reached the plateau region; and it increased thereafter.

The same method was used to measure the dead-time of detector system using ^{137}Cs source. The results gathered for the ^{137}Cs sources are listed in Table 2. The detector system shows the same behavior for the ^{137}Cs sources as it had for the ^{60}Co sources. Additionally, the s_1,s_2, and s_{12} counting rates increased up to 1050 V. Beyond this point, the detector's behavior was stable until 1150 V. Then counting rates jump to discharge region beyond 1150 V.

Table 1. Calculated dead-time with observed data and uncertainty values for all cases using ^{60}Co sources

Voltage (V)	S1 (count/sec)	S12 (count/sec)	S2 (count/sec)	BKG (count/sec)	Dead Time (sec)
1100	5.5506 ± 0.0277	9.6367 ± 0.0365	4.5644 ± 0.0251	0.4411 ± 0.0078	0.0008867 ±0.000305
1110	5.2218 ± 0.0269	9.0057 ± 0.0353	4.2594 ± 0.0243	0.4539 ± 0.0079	0.0005984 ±0.000335
1120	5.4911 ± 0.0276	9.5157 ± 0.0363	4.5161 ± 0.0250	0.4715 ± 0.0080	0.0004935 ±0.000309
1130	6.1725 ± 0.0292	11.0378 ± 0.0391	5.3661 ± 0.0273	0.4763 ± 0.0081	0.0004422 ± 0.000248
1140	8.3089 ± 0.0339	14.9371± 0.0455	7.2288 ± 0.0316	0.5706 ± 0.0089	0.0002917 ± 0.000158
1150	9.6388 ±0.0365	17.0044 ± 0.0485	8.0975 ± 0.0355	0.7115 ± 0.0094	0.0001539 ±0.000130
1160	9.5811 ± 0.0364	17.3272 ± 0.0490	8.5272 ± 0.0344	0.7624 ± 0.0102	0.0001370 ±0.000125
1170	10.2140 ± 0.0376	17.9879 ± 0.0499	8.6093 ± 0.0345	0.8113 ± 0.0106	0.0001650 ±0.000119
1180	10.0783 ± 0.0374	17.8158 ± 0.0497	8.6185 ± 0.0345	0.8538 ± 0.0108	0.0001903 ±0.000120
1190	10.0117 ± 0.0372	17.6086 ± 0.0494	8.5222 ± 0.0344	0.8969 ± 0.0111	0.0002041 ±0.000122
1200	10.3946 ± 0.0380	17.8847 ± 0.0498	8.4581 ± 0.0342	0.9421 ± 0.0114	0.0001821 ±0.000119
1210	13.9213 ± 0.0439	25.1728 ± 0.0591	12.3394 ± 0.0413	0.9864 ± 0.0117	0.0003470 ±0.00007

Fig. (4) shows the counting rate versus the applied voltage behavior for the GM counter. The statistical uncertainties were calculated and one standard deviation (1σ) error bars are added to the data. When ^{60}Co source was used the initial counts were observed at the operating voltage of 900 V, therefore 900V is recognized as the starting voltage. The counting curve becomes a nearly flat plateau between 1150 V and 1200 V for this particular counter with ^{60}Co sources and the system is stable for this voltage range. After 1200 volts, the plateau region ends and the continuous discharge region begins in the GM tube since

discharges start from irregularities on the anode wire or multiple pulsing by quenching mechanism failure.

Table 2. Calculated dead-time with observed data for all cases using ^{137}Cs sources

Voltage (V)	S1 (count/sec)	S12 (count/sec)	S2 (count/sec)	BKG (count/sec)	Dead Time (sec)
1010	10.7820 ± 0.0847	18.7227 ± 0.1117	9.1493 ± 0.0780	0.0640 ± 0.00298	0.0062383 ± 0.000937
1020	15.7067 ± 0.1023	27.8340 ± 0.1362	13.8500 ± 0.0960	0.2124 ± 0.00543	0.0037670 ± 0.000519
1030	23.8720 ± 0.1261	41.3487 ± 0.1660	19.8480 ± 0.1150	0.2968 ± 0.00642	0.0023636 ± 0.000487
1040	34.7080 ± 0.1521	59.4973 ± 0.1991	26.4980 ± 0.1329	0.3343 ± 0.00681	0.0007820 ± 0.000466
1050	41.1740 ± 0.1656	75.4180 ± 0.2242	35.1753 ± 0.1531	0.3764 ± 0.00723	0.0001969 ± 0.000314
1060	44.9927 ± 0.1731	83.0980 ± 0.2353	39.7233 ± 0.1627	0.3940 ± 0.00739	0.0003540 ± 0.000498
1070	48.0247 ± 0.1789	88.5940 ± 0.2430	44.2887 ± 0.1718	0.4183 ± 0.00762	0.0008196 ± 0.00059
1080	54.1907 ± 0.1900	99.7227 ± 0.2578	47.5167 ± 0.1779	0.4361 ± 0.00778	0.0003107 ± 0.000575
1090	57.6027 ± 0.1959	107.8787 ± 0.2681	55.2853 ± 0.1919	0.4410 ± 0.00782	0.0007593 ± 0.000567
1100	56.3107 ± 0.1937	106.7833 ± 0.2668	53.8467 ± 0.1894	0.4432 ± 0.00784	0.0005046 ± 0.000568
1110	51.4027 ± 0.1851	99.7340 ± 0.2578	49.5747 ± 0.1817	0.4546 ± 0.00794	0.0001588 ± 0.000554
1120	52.5920 ± 0.1872	100.7813 ± 0.2592	48.9167 ± 0.1805	0.4710 ± 0.00808	0.0000509 ± 0.000573
1130	52.2687 ± 0.1866	99.5507 ± 0.2576	47.8713 ± 0.1786	0.4775 ± 0.00814	0.0000228 ± 0.000575
1140	53.2287 ± 0.1883	101.1080 ± 0.2596	48.5813 ± 0.1799	0.5732 ± 0.00892	0.0000255 ± 0.000573
1150	80.9333 ± 0.2322	140.3260 ± 0.3058	71.0400 ± 0.2176	0.7108 ± 0.00993	0.0010447 ± 0.000446
1160	90.3620 ± 0.2454	146.9927 ± 0.3130	77.2047 ± 0.2268	0.7607 ± 0.01027	0.0016419 ± 0.000445
1170	113.2667 ± 0.2747	172.1387 ± 0.3387	94.2360 ± 0.2506	0.8124 ± 0.01062	0.0019772 ± 0.000437
1180	126.7533 ± 0.2906	180.4740 ± 0.3468	125.8200 ± 0.2896	0.8553 ± 0.01089	0.0031538 ± 0.000441

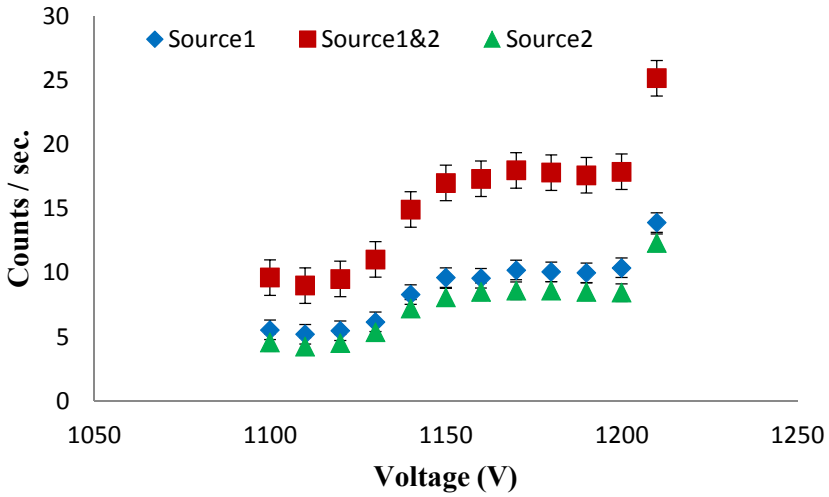

Figure 4. The counting rate as a function of voltage for a GM counter using Co sources.

Fig. (5) shows the counting rate's slope for the detector with respect to the applied voltage using ^{137}Cs sources (with one standard deviation error bars). The detector's plateau region was observed between 1050 and 1250 V as indicated by the manufacturer. The data plotted in Fig. (4). and Fig. (5) indicate that the slope regions for the ^{60}Co and ^{137}Cs sources were slightly different. The plateau for the ^{60}Co sources was between 1150 and 1200 Volt; while for ^{137}Cs these values were between 1050 and 1140 V. This slight difference is likely due to difference in gamma energies. Additional research is needed to further investigate this observation.

The dead-time and the applied voltage dependence are shown in Figs. (6). and (7). for ^{60}Co and ^{137}Cs respectively. The GM region for the ^{60}Co was between 1100 V and 1210 V; and for the ^{137}Cs the range was between 1010 V and 1180 V. This data indicates that increasing the applied voltage leads to decrease in dead-time until the region of plateau and increases thereafter. The plateau region for the ^{60}Co was between 1150 V and 1200 V, while for ^{137}Cs the plateau was between 1050 V and 1140 V. Although the observed

plateau regions for the ^{60}Co and ^{137}Cs sources were different from each other, the results were within the range of the manufacturer's reported plateau regions. It is however important to notice the non-overlapping low dead-time plateau regions for the two sources which may be significant for certain applications and use of energy compensated GM would be required [22].

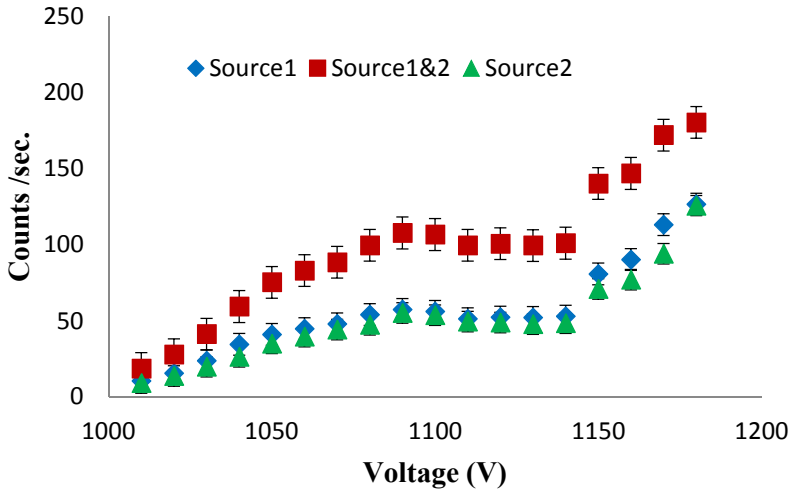

Figure 5. The counting rate as a function of voltage for a GM counter using Cs sources.

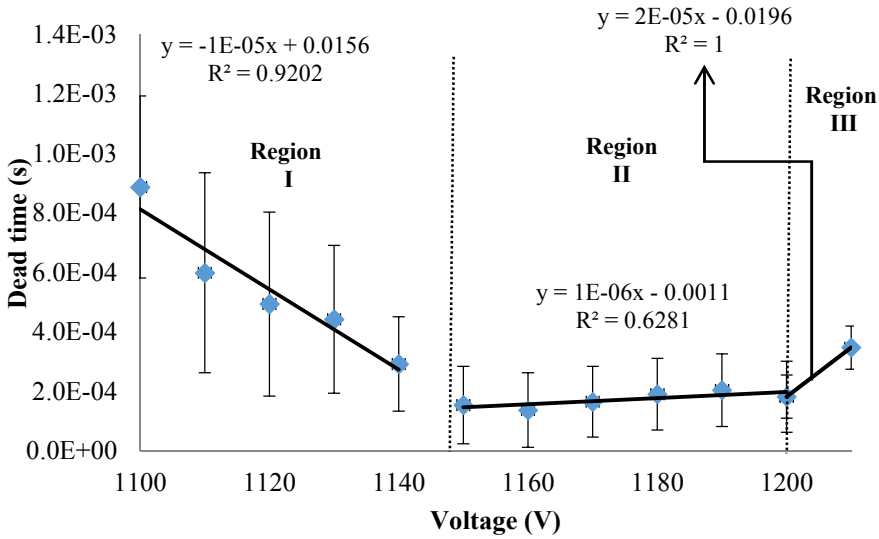

Figure 6. Deadtime-voltage dependence for GM counters using ^{60}Co sources.

For most Geiger tubes, the dead-time is between 50 and100s μs [23]. Typical dead-time values for in GM counters are between 100 and 300 μs [8]. Dead-time values in plateau region (operating region) are between 153 μs and 205 μs for the ^{60}Co sources and 25 μs and 819 μs for the ^{137}Cs sources. The dead-time measurements in the plateau region for the ^{60}Co sources examined in this study were within the range reported in the literature. For the case of ^{137}Cs only dead-time values of 819 μs and 759 μs, with corresponding voltages of 1070 V and 1090 V, did not agree with range suggested in the literature. A 5% loss count will occur if the dead-time is 100 μs and the counting rate is 500 counts/sec. Data from this study indicated that the lost counts due to dead-time were less than 1%. This value may be higher for other type of detector (e.g., HPGe detector or scintillation detector) because they are known to be paralyzing in nature.

Three distinct dead-time regions are observed in both of Fig. (6) and Fig. (7.). Initially when the applied voltage is low, the positive ions take longer to move to the cathode. Consequently, the GM counter does not recover from the dead-time for much longer. However, during this time any increase in the operating voltage results in both a faster charge collection and a faster dead-time recovery as discussed further in the discussion and conclusion section. The middle region shows a rather flat plateau. In this region the dead-time is not strongly affected by the voltage. If the operating voltage is increased further, an increase in dead-time is observed most likely due to the increase velocity with which the ion collides with the cathode wall. This higher velocity seems to be responsible for secondary emission and hence dead-time extension. Based on these results it is recommended that GM tube should be used in the dead-time plateau region (Region-II) with a minimum dead-time and without any operating voltage dependence.

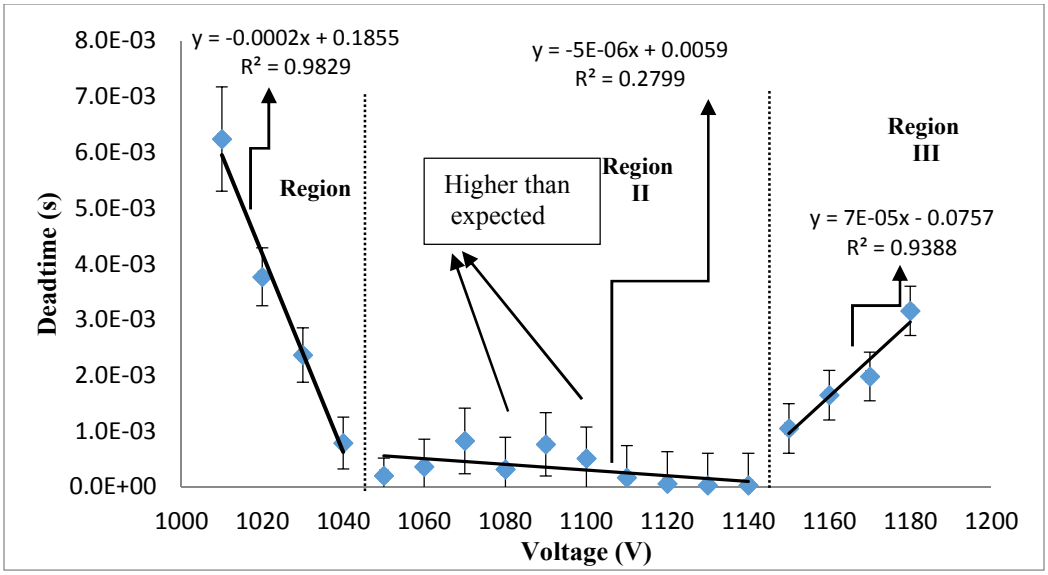

Figure. 7. Deadtime-Voltage dependence for GM counters using ^{137}Cs sources.

In the case of operating temperature and fatigue dependent dead-time calculations, a wide range of operating conditions were covered with a matrix which included six different voltages within the GM counter's plateau region, eight temperatures between 0 ^{0}C to 70 ^{0}C with a step of 10 ^{0}C and three different fatigues (new GM with less than $3x10^{10}$ counts, $6x10^{10}$ counts and $9x10^{10}$ counts). The GM detector has been sparsely used in the radiation laboratory over the years. While there is no precise record of detector ageing at starting point of measurements but the assumption of initial fatigue of less than $3x10^{10}$ counts seems reasonable. For the initial ageing step, the detector was exposed to ~$3x10^{10}$ counts and the fatigue was raised to $6x10^{10}$ counts level. For the last set of experiment the detector was exposed to an additional $3x10^{10}$ counts (total fatigue of approximately $9x10^{10}$ counts). Again, based on Eqs. (6), (7), (8), and (9) dead-time for each temperature step, voltage and fatigue were calculated. As example only the case of less than $3x10^{10}$ counts ageing and at 1100 V and 1110V results are tabulated in table 3 and table 4 respectively. Dead-time operating temperature dependence for various voltages and the fatigue levels

are shown in Fig. (8). Peeva and Guleva [24] used the oscilloscope method to obtain dead-time temperature and fatigue dependence measurements. They found that the dead-time increased as the operating temperature and fatigue level increased. Their data was however limited to a fixed 60 Volt operating conditions.

Table 3. Dead-time values with varying temperatures and uncertainty values, aged $3x10^{10}$ counts at 1100 V

Temp (^{0}C)	S1 (count/sec)	S12 (count/sec)	S2 (count/sec)	BKG (count/sec)	Dead Time (sec)
0	219.8700 ± 0.24713	399.5933 ± 0.33316	205.4033 ± 0.23886	0.0861 ± 0.00489	0.0003018 ± 0.00000214
10	223.9567 ± 0.24942	447.2378 ± 0.35247	253.9600 ± 0.2656	0.0867 ± 0.00491	0.0002876 ± 0.00000183
20	257.3617 ± 0.26737	473.7783 ± 0.36277	264.0778 ± 0.27084	0.0922 ± 0.00506	0.0003854 ± 0.00000180
30	288.1900 ± 0.28294	516.8772 ± 0.37892	303.2783 ± 0.29025	0.0919 ± 0.00505	0.0004880 ± 0.00000175
40	293.1950 ± 0.28538	544.4256 ± 0.38888	364.5678 ± 0.31823	0.0964 ± 0.00517	0.0006423 ± 0.00000189
50	301.7033 ± 0.28949	609.2933 ± 0.4114	489.2333 ± 0.36864	0.0981 ± 0.00522	0.0008202 ± 0.00000212
60	462.8300 ± 0.35856	612.1200 ± 0.41235	464.3750 ± 0.35916	0.0992 ± 0.00525	0.0011103 ± 0.00000274
70	571.1289 ± 0.39831	729.6728 ± 0.45021	693.3844 ± 0.43887	0.1008 ± 0.00529	0.0012053 ± 0.00000476

For each voltage, the detector dead-time increased as the detector's fatigue/ageing increased. The GM counter's dead-time seems to be increasing exponentially with temperature. The fatigue results in dissociation of the gas molecules and hence reducing its quenching capability. This reduced quenching capability results is longer duration of

detector unavailability and hence prolong dead-time. As the detector ages (fatigues) the fill gas degrades (dissociates) leading to prolong dead-time as the data suggest. At higher temperatures due to increased random motion of the gas molecules the ion travel time and hence the dead-time is increased. This increase in dead-time is more pronounced with higher fatigue (more dissociated gas molecules). Hence more positive ions and slower travel time. Consequently, the dead-time increased as the fatigue increased.

Table 4. Dead-time values with varying temperatures and uncertainty values, aged $3x10^{10}$ counts at 1110 V

Temp (^{0}C)	S1 (count/sec)	S12 (count/sec)	S2 (count/sec)	BKG (count/sec)	Dead Time (sec)
0	239.1933 ± 0.2577	441.7400 ± 0.3502	222.6933 ± 0.2487	0.0872 ± 0.00492	0.00019700 ± 0.00000139
10	265.8267 ± 0.2717	509.6333 ± 0.3762	265.8267 ± 0.2717	0.0878 ± 0.00492	0.00016197 ± 0.00000102
20	278.2383 ± 0.2780	502.5183 ± 0.3736	277.8167 ± 0.2778	0.0908 ± 0.00502	0.00038272 ± 0.00000183
30	306.7883 ± 0.2919	568.6050 ± 0.3973	336.5683 ± 0.3057	0.0942 ± 0.00511	0.00040935 ± 0.00000144
40	342.6900 ± 0.3085	707.9622 ± 0.4434	522.8372 ± 0.3810	0.0939 ± 0.00511	0.00054460 ± 0.00000171
50	387.5144 ± 0.3280	749.0483 ± 0.4561	553.4231 ± 0.3920	0.0953 ± 0.00514	0.00056825 ± 0.00000130
60	604.3250 ± 0.4097	756.4783 ± 0.4584	563.1267 ± 0.3955	0.0964 ± 0.00517	0.00093322 ± 0.00000250
70	556.2500 ± 0.3930	793.4733 ± 0.4694	706.4267 ± 0.4429	0.1003 ± 0.00528	0.00097136 ± 0.00000219

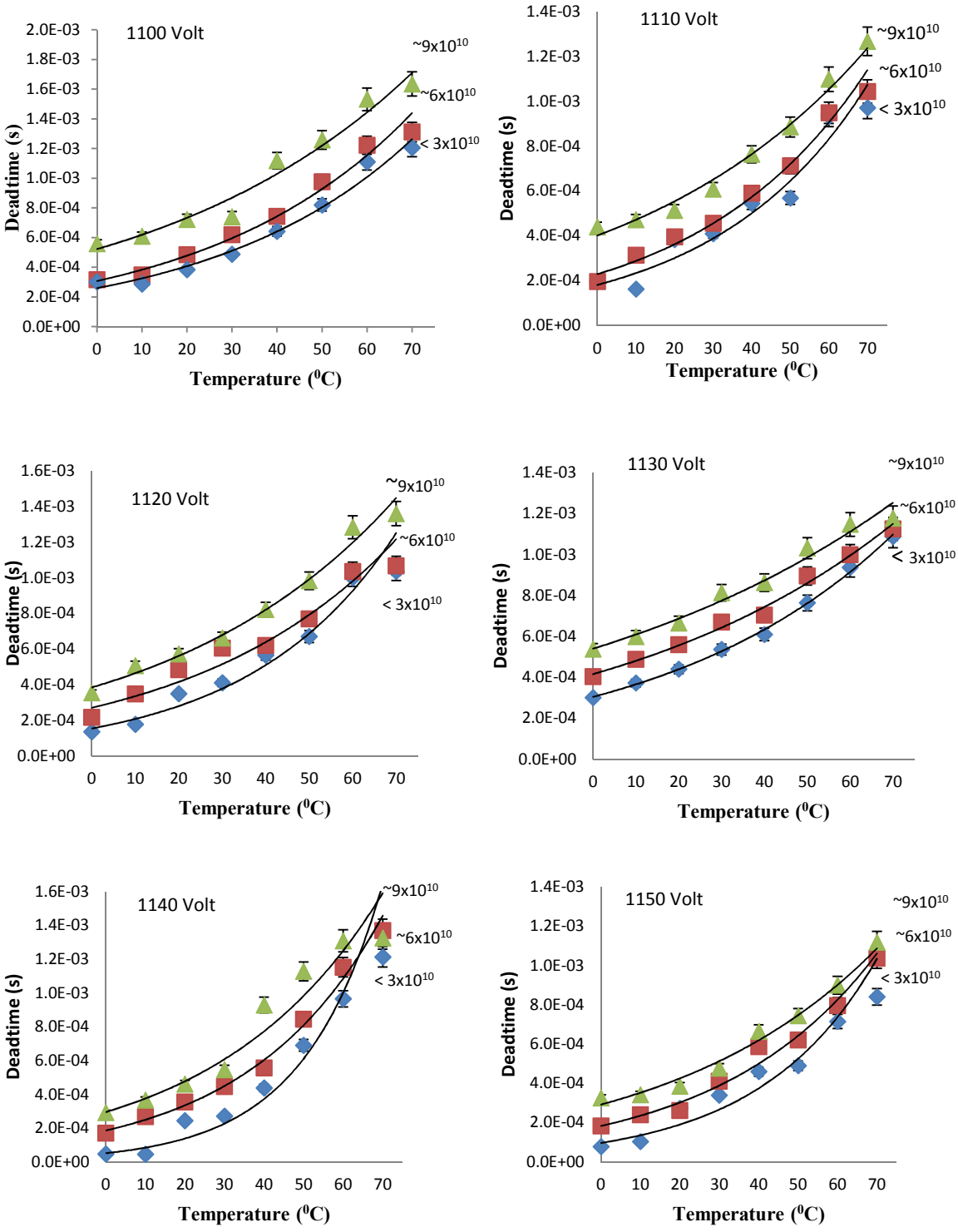

Figure 8. Deadtime-temperature and fatigue dependence for GM counter using ^{137}Cs sources at different applied voltages.

4. Discussion and Conclusion

Both a standard two source method and a simple non-paralyzing model were used to calculate GM counter's dead-time. It is observed that dead-time depend strongly on applied voltage, operating temperature, and fatigue. Pair of ^{60}Co and ^{137}Cs sources with 5 μCi strength were used for dead-time-voltage dependence measurements. In both cases, the plateau regions' dead-time values are in agreement with previously reported values. Dead-time values for ^{60}Co source were between 153 and 205 μs in the plateau region (Region II); they were much higher than referenced values in other regions (Regions I and III). The dead-time values were between 25 and 819 μs in the plateau region for the ^{137}Cs sources. The plateau region (Region II) is stable for dead-time. Thus, this region is more suitable for operation while regions I and III should be avoided for operation of detection. It is also interesting to observe that the uncertainty in the calculated dead-time in much higher in the region I (see Fig. 6 and 7) than in the region II of relatively constant and smaller dead-time uncertainty.

The same method used to study voltage dependence was also used to study both temperature fatigue dependence. For this set of experiments, the dead-time was 13 μs at 0 ^{0}C and 1120 volts. Puri has found the dead-time to be 15 μs at 0 ^{0}C [25]. Peeva and Guleva used the oscilloscope method to determine the GM counter's dead-time with regard to temperature dependence. They found that the dead-time was 80 μs at a 2.2×10^8 counts fatigue level GM counter, a fixed 40 V, and a 20 ^{0}C temperature [24]. The dead-time in this study was 72 μs at 20 ^{0}C, 1100 Volt, and 9×10^{10} counts fatigue level GM counter. For all fixed voltages and fatigue levels dead-time was found to be an exponential function of operating temperature.

The GM counter's temperature and fatigue results in increased dead-time, thus producing a higher count rate loss. A simple statistical analysis was performed on the detector's dead-time to calculate the correlation coefficient of various operating parameters. This analysis revealed strong temperature dependence, with a correlation coefficient of 0.93. In the plateau region, the voltage dependence was weak, with a correlation coefficient of only 0.16. Only three fatigue points were available for which the correlation coefficient was found to be 0.48. This rather weak correlation between fatigue and dead-time is probably due to the small data size of only three fatigue levels.

Fatigue dependence of dead-time is important for other applications of gas filled detectors. For example in reactor application BF_3 proportional counter and fission chamber etc. are exposed to high count rate and we expect to see similar behavior of increased dead-time and count rate loss. Therefore some type of fatigue compensation may be needed to correct the count rates as the detector ages. Likewise, for current mode application (ion chamber) we also expect a current loss due to aging as well. Temperature dependence is also found to be exponential, therefore for high temperature application proper calibration would need to be done at the temperature of the measurements. These effects would require additional investigations.

To validate our hypothesis that the dead-time decreases with increasing voltage at the low voltage range is due to the fast collection of charge with increasing voltage, we wanted to examine the individual pulses generated by the detector without any pulse processing. Unfortunately the detector being tested got damaged perhaps either due to excessive fatigue as it went through during the earlier aging test or poor handling during some teaching sections. Nevertheless, a different detector (Centronic-N204/BNC) was

used for this pulse examination and analysis. We expected to see similar qualitative behavior but different values for voltages etc. A typical pulse at low voltage (1250V for this detector) using ^{60}Co source is shown in Fig. (9).

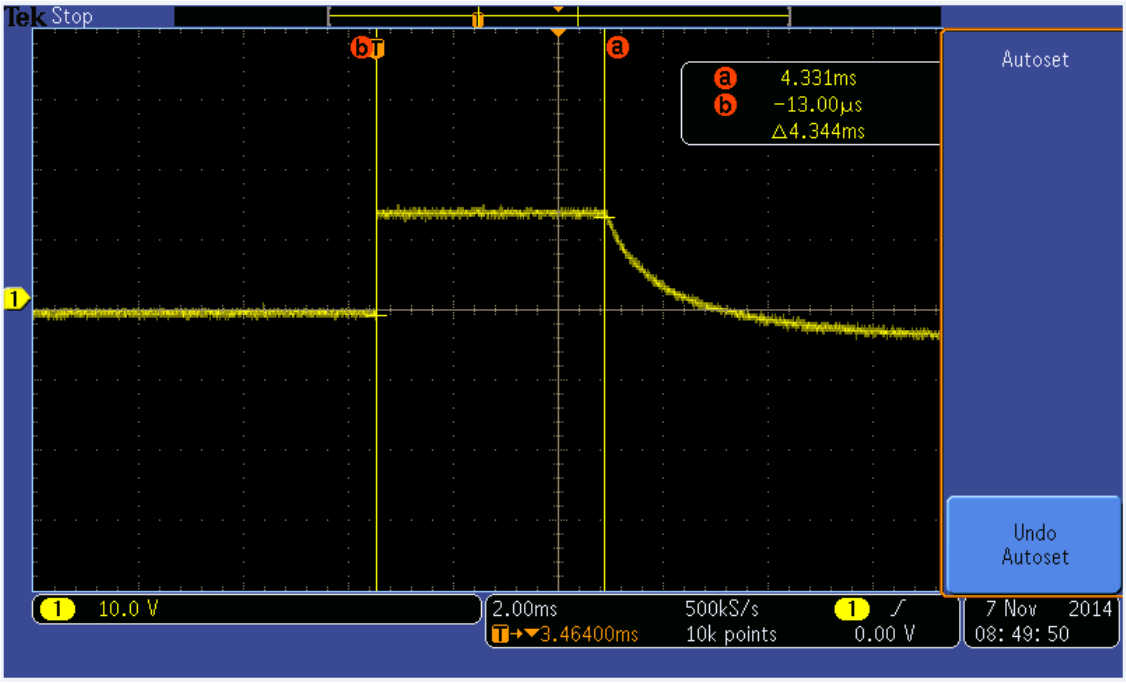

Figure 9. GM- N204/BNC Pulse at 1250V using ^{60}Co.

There is a full voltage part of the pulse between marker (a) and (b) and a tail. Time duration of the full pulse (D) and the tail duration were recorded for various operating voltages. As per our hypothesis both the duration of the pulse and the tail length were observed to be decreasing with increasing operating voltage. On the other hand, when these pulses were observed at the high voltage side of the low dead-time plateau the pulses were devoid of the tail and the duration of the full pulse started to increase with increasing voltage. The other interesting observation was that the subsequent pulses were of much smaller duration if they arrived shortly after the first pulse. If the gap between the two pulses were sufficiently long the second pulse was observed to be of full duration. Fig. (10)

shows a full duration pulse followed by a second incomplete pulse. It is suggested that the pulse duration is measure of the non-paralyzable dead-time length. The full pulse duration was recorded at various voltages and plotted to investigate the effect of operating voltage on the pulse duration.

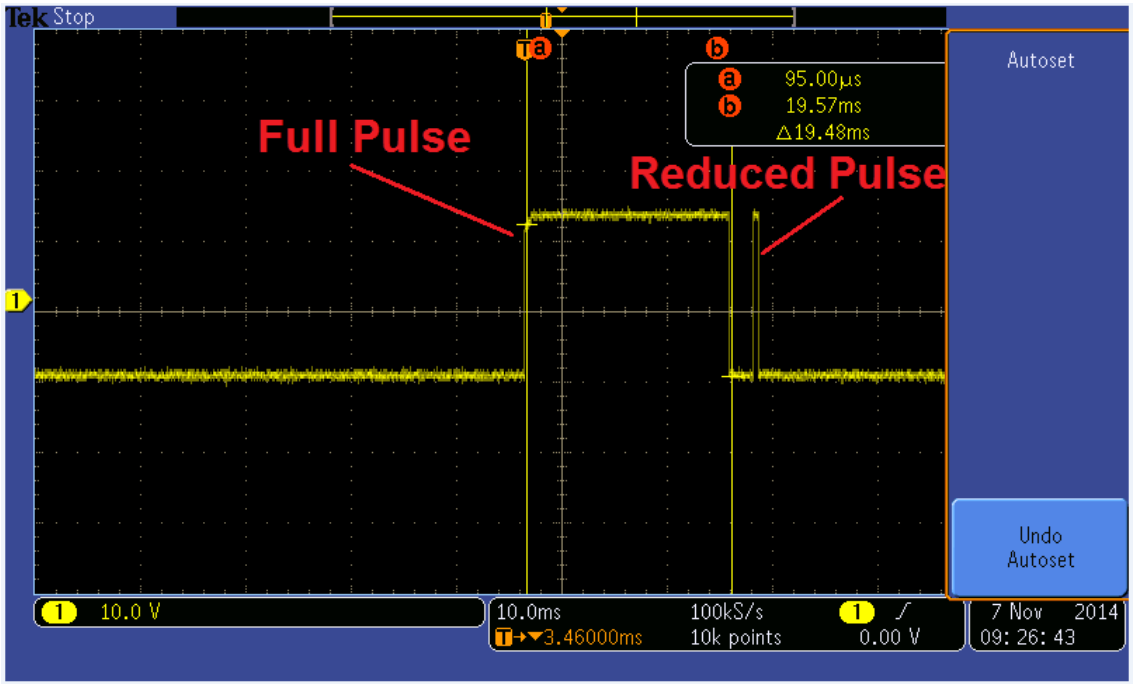

Figure 10. GM- N204/BNC Pulse at 1850V using ^{60}Co.

Fig. (11) shows the pulse duration (D+T for low voltage and D for high voltage as T=0 for high voltages) as a function of operating voltage for two different radiation sources. As one can notice, the duration of the pulse reduces with increasing voltage till a minimum is reached and then it starts to increase. The data demonstrate that the pulse loss mechanism at the high voltage side is due to reduced pulse formation which is perhaps not recorded in the counting system. As the voltage increases the duration of the pulse increases resulting in a prolonged dead-time. On the other hand, on the low voltage side when the voltage

increases both the full pulse duration and the tail duration decreases suggesting faster charge collection and reduced dead-time. The plateau region for this detector did not match with the plateau region of the detector used for earlier temperature and fatigue data collection therefore no detailed analysis was possible.

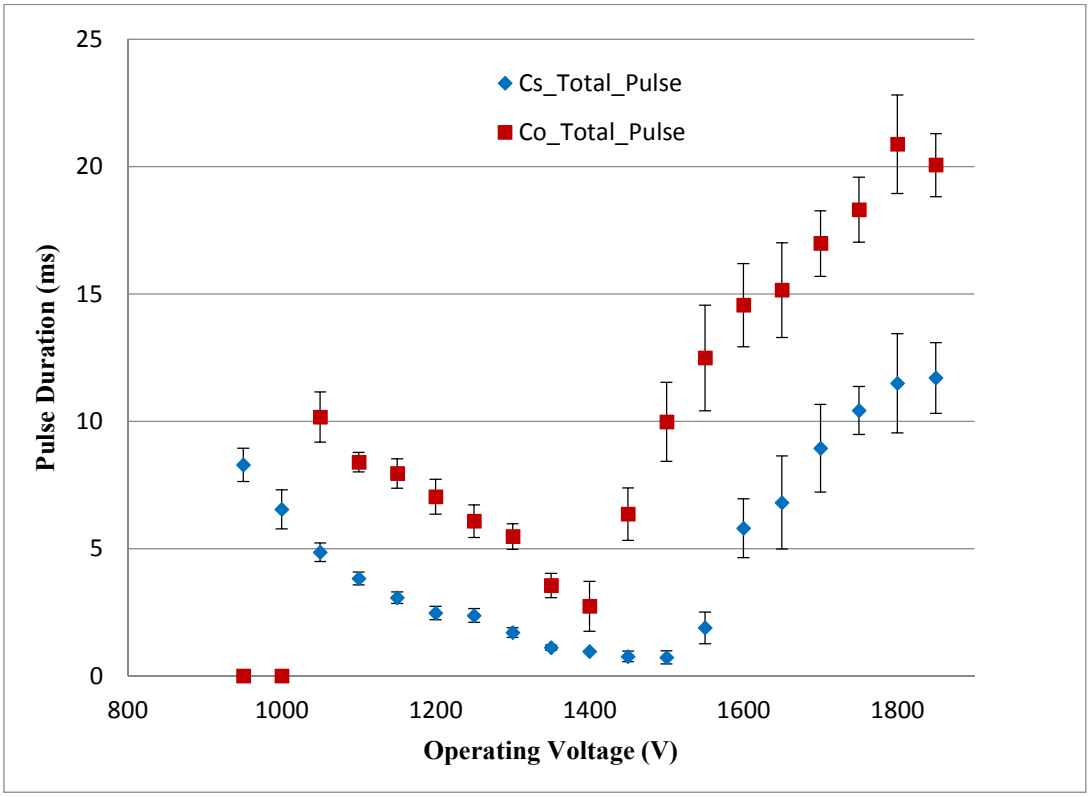

Figure 11. GM- N204/BNC Pulse analysis using ^{60}Co.

To investigate the effect of time gap between two successive pulses and the duration of the second reduced pulse, we manually collected data using ^{60}Co source at GM operating voltage of 1850 V. The counts were collected for 10 second duration and second pulse duration showed "Gap" dependence as exhibited in Fig. (12). As the gap increases the second pulse approaches the full pulse duration supporting our hypothesis that at high

voltages the loss mechanism is due to the reduced duration second pulses which cannot be recorded by the counter.

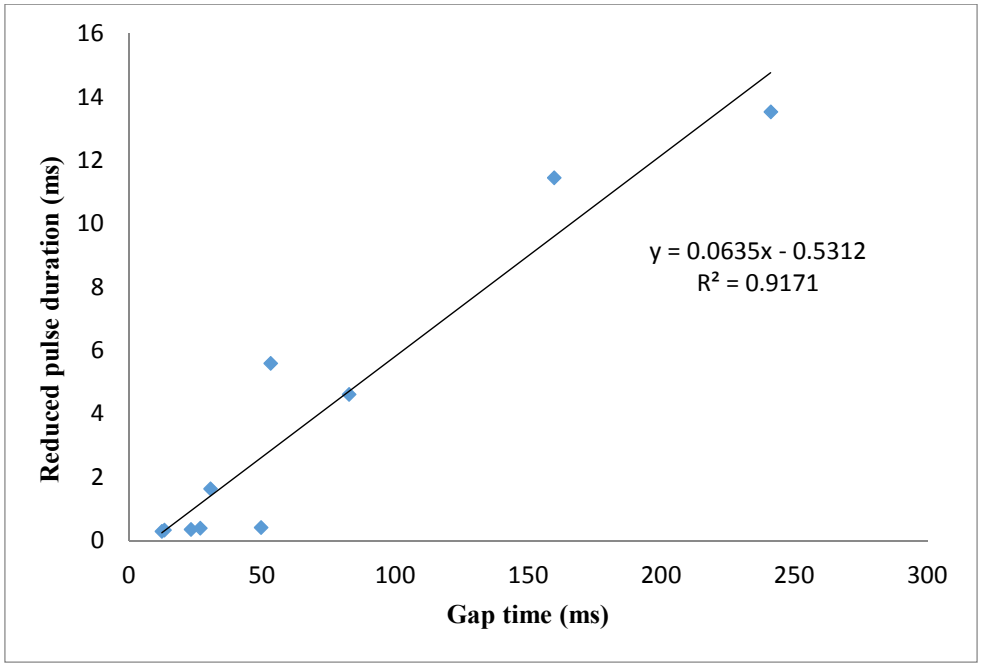

Figure 12. Gap Time vs. reduced pulse duration for GM at 1850 V using ^{60}Co.

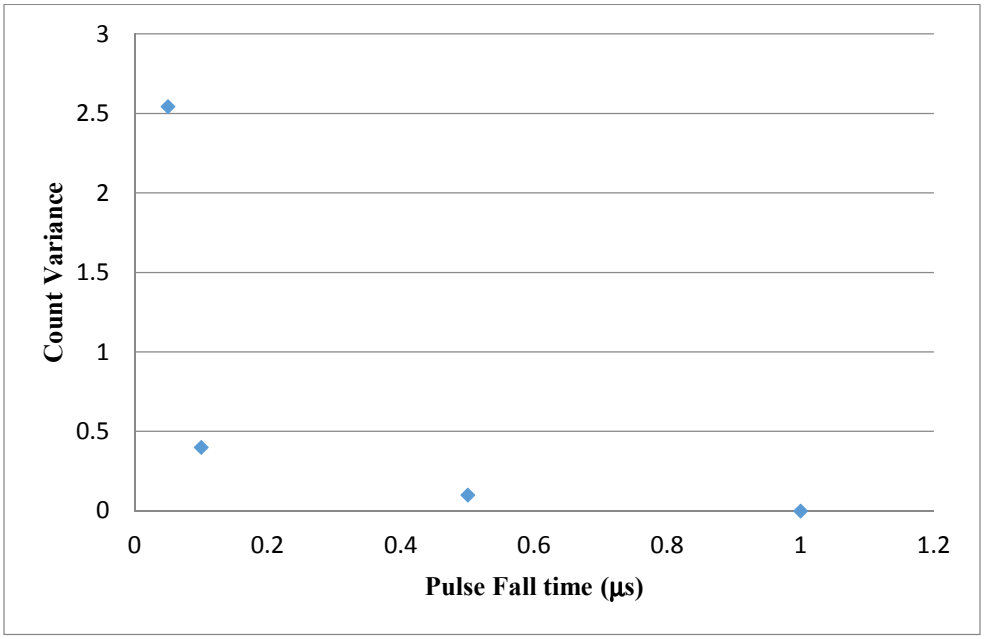

Figure 13. Count variance vs. pulse fall time for GM at 1850 V using ^{60}Co.

To test the hypothesis that the short duration pulses are not recorded by the counter, pulse generator was used to collect data for four different pulses with sharp rise time of 0.05 μs (1 V pulse with 0.1 μs Fall time; 0.268 V pulse with 1 μs Fall time; 0.102 V pulse with 0.5 μs Fall time and 0.252 V pulse with 0.05 μs Fall time). The data showed (see Fig. 13) that the variance of count recorded is an exponential function of pulse duration/fall time. For long duration pulses above 1 μs all pulses were recorded with zero variance.

REFERENCES

[1] G. F. Knoll, "Radiation Detection and Measurement". 4th Edition, p.121, John Willey & Sons Inc, USA, (2010a).

[2] J. W. Muller, "Dead-time problems". Nuclear Instruments and Methods. 112, 47-57. (1973).

[3] J. W. Muller, "Generalized Dead Times". Nuclear Instruments and Methods. 301, 543-551, (1991).

[4] H. G. Stever, "The discharge mechanism of fast G-M counters from the dead- time experiment". Phys. Rev. 61, 38-52, (1942).

[5] P. B. Moon, "Recent developments in Geiger-Muller counters". J. Sci. Instr. 14, 189, (1937).

[6] Y. Beers, "Precision method of measuring Geiger counter resolving times". Rev. Sci. Instr. 13, 72-76, (1942).

[7] A. F. Reid, "Preparations and Measurement of Isotropic Tracers". Edward Brothers, Ann Arbor, (1946).

[8] N. Tsoulfanidis, S. Landsberger, "Measurement and Detection of Radiation". 3th Edition. p. 159-160. CRC Press. Taylor & Francis Group. New York, (2011).

[9] G. F. Knoll, "Radiation Detection and Measurement". 4th Edition, p.135, John Willey & Sons Inc, USA. (2010b).

[10] D. H. Wilkinson, Ionization Chambers and Counters, Cambridge University Press. Cambridge, (1950).

[11] J. C. May, D. H. Russell, A Mass-Selective Variable-Temperature Drift Tube Ion Mobility-Mass Spectrometer for Temperature Dependent Ion Mobility Studies. J. Am. Soc. Mass Spectrom. 22. 1134-1145, (2011).

[12] A. Patil, "Dead time and count loss determination for radiation detection systems in high count rate applications". p. 11. PhD Thesis. Missouri University of Science & Technology. Rolla. (2010).

[13] W. Feller, "On probability problems in the theory of counters". in R. Courant Anniversary volume. Studies and Essays. Interscience. New York. 105-115. (1948).

[14] S. Lee, R. P. Gardner, "A new G-M counter dead time model". Applied Radiation and Isotopes. 53. 731-737, (2000).

[15] A. Patil, S. Usman, "Measurement and Application of Paralysis Factor for Improved Detector Dead Time Characterization". Nuclear Technology. 165. 249-256, (2009).

[16] N. Wood, N. Wood Counter Laboratory, Chicago, Ill., 41/2 in. active length, 1 in. diameter.

[17] http://www.ortec-online.com/Solutions/modular-electronic-instruments.aspx, Accessed on 14, Jan. 2014.

[18] http://www.ortec-online.com/download/570.pdf, Accessed on 14, Jan. 2014.

[19] http://www.ortec-online.com/download/556-556H.pdf, Accessed on 14, Jan. 2014.

[20] http://www.ortec-online.com/download/996.pdf, Accessed on 14, Jan. 2014.

[21] G. F. Knoll, "Radiation Detection and Measurement". 4th Edition, p.124 John Willey & Sons Inc, USA. (2010c).

[22] LND Inc. Oceanside, New York, USA, http://www.lndinc.com/products/category/10/ Accessed on Dec. 18, 2014.

[23] G. F. Knoll, "Radiation Detection and Measurement". 4th Edition, p.213. John Willey & Sons Inc, USA. (2010d).

[24] A. Peeva, D. Guleva, "Dead Time and Fatigue in Self-Quenching G.M. Counters at Different Temperatures". Nuclear Instruments and Methods. 44. 314-316. (1966).

[25] S. P. Puri, "A Study of the Operation of GM Counters at Low Temperature". Ind. J. Phys. 22. 214-219, (1956).

II. A COMPARISON OF TRADITIONAL AND HYBRID RADIATION DETECTOR DEAD-TIME MODELS AND DETECTOR BEHAVIOR

T. Akyurek, M. Yousaf, and S. Usman

Department of Mining and Nuclear Engineering, Missouri University of Science & Technology, Rolla, MO, 65401, USA

Abstract

High intensity radiation measurements are confounded by detector dead-time and pulse pile-up problems. A computational method was used to compare the traditional dead-time models with recently proposed hybrid dead-time models. A computational algorithm based on a decay source method was used to study the behavior of various dead-time models. Validation of the code was performed for the hybrid models by confirming that the predictions lie between the two ideal dead-time models; the paralyzing and the non-paralyzing model. It was interesting to note see that two seemingly similar hybrid dead-time models produced significant different results. Lee and Gardner's model based on two dead-times and Patil and Usman paralysis factor based model are inherently different in their logic as well as results. For Lee and Gardner's model altering the orders of dead-times produced significantly different response. These hybrid models should be studied further to investigate both the dependence and the variation of model parameters on detector design and operating conditions. It is well accepted that one dead-time does not apply to all detectors and even for the same detector applicability of the same model under all operating condition is questionable. Therefore, dead-time model should be chosen carefully for the specific detector, operating conditions and radiation to be measured to correctly represent the physical measurement phenomenon.

1. Introduction

Radiation detection is a process starting from interaction of radiation in detector producing pulses which then pass through various signal processing modules (pre-amplifier, amplifier, discriminator, and counter) and finally recorded by the counter or Multichannel Analyzer as shown in Fig. (1). Every pulse processing device needs a minimum amount of time to process the signal. Thus, the device is unavailable for some duration of time. The amount of time for which a device is unable to process a new signal or the minimum time that must separate two detectable events [1] is known as dead-time. Detector dead-time has been an area of active research since the inception of radiation detection.

Dead-time phenomenon is significant in radiation detection, particularly at high intensity radiation (e.g., spent fuel monitoring and spectroscopy, medical application etc.). Researchers have been working for decades to formulate a generalized mathematical relation for dead-time that could be used to correct the measured counts. Akyurek et al [2] recently reported GM counter's dead-time depends on the operating voltage, temperature and even the age of the detector. Therefore, the efforts for a generalized model to fit all detectors under all operating conditions may not have good scientific foundation.

A radiation detection system contains two types of elements that contribute to total dead-time; the detector's physical dead-time and the system's pulse processing dead–time. For gas filled detectors, the largest dead-time contribution comes from the detector itself [3]. For GM counter, a pulse is generated due to radiation interaction and ionization of the gas. The pulse must now pass through a series of instrument before being recorded. Every individual instrument has its own characteristics dead-time to process these pulses but the

value of the electronic dead-time is negligible as compared to the GM dead-time and hence can be neglected.

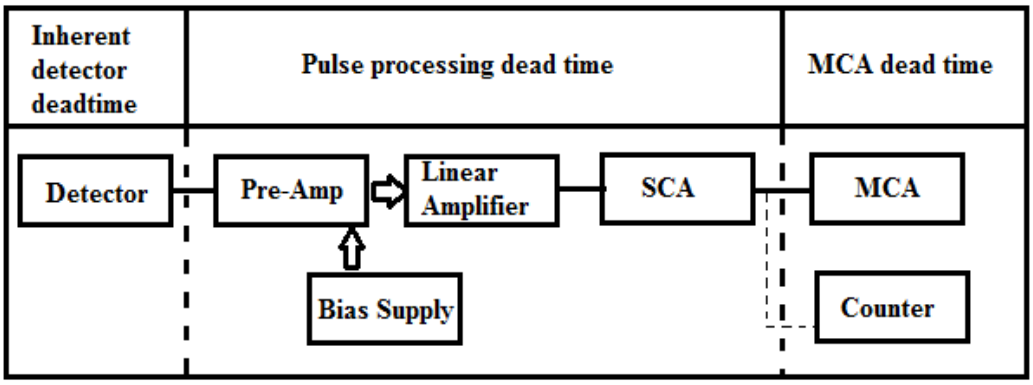

Figure 1. Radiation detection system showing all instruments in an NIM

The Nuclear Instrumentation Modules (NIM) can typically be used to obtain two types of information; the count rate, or the pulse's height distribution information (spectroscopy application). Pulse pile-up also plays a significant role in count losses, where the collected charge is the partial sum of the two individual events rather than the second pulse being lost with no impact on the shape and/or size of the recorded pulse. Pomme [4] provided a detailed explanation of the phenomenon of pulse pile-up in radiation detection.

First mathematical relation for dead-time was formulated by Feller [5] and Evans [6] which is known as non-extending or non-paralyzable dead-time model. For non-paralyzable dead-time model, the observed count rate is;

$$m = \frac{n}{1 + n\tau} \tag{1}$$

Feller [5] and Evans [6] derived a type II formula for extendable or paralyzable model which is based on the assumption that any, event occurred during the dead-time will

extend dead-time, the dead-time is extended. For this case, a relationship between the true and measured count rate is given by;

$$m = ne^{-n\tau} \tag{2}$$

No real world detector exactly follows any one of these ideal models. The reality is always somewhere in between these two extremes [7]. These ideal models should be considered as a mathematical convenience rather than a phenomenological representation of dead-time.

Dead-time correction methods are proposed to extend the useful range of operation of radiation detector as suggested by Lee and Gardner [7]. Albert and Nelson [8] proposed a probability-based model to estimate the dead-time losses. They assumed that the dead-time would be extended within a probability of p. Gardner and Liu [9] derived a modified dead-time model which was introduced for a paralyzable model;

$$\tau = an^{b} \tag{3}$$

where *a* and *b* are either constants or fitting parameters that are specific for a given GM counting system. All of these models successfully extended the GM detector's counting range of GM detector but only to some extent [9].

Müller [10] proposed several dead-time models by combining the two dead-times and using different permutation of their orders. Lee and Gardner [7] recently attempted to extend further GM detector's counting range by using a hybrid dead-time model that combines two idealized models into one mathematical relation;

$$m = \frac{ne^{-n\tau_P}}{1 + n\tau_{np}} \tag{4}$$

This expression is similar to the one given by Müller [10]. This hybrid formulation combines paralyzing and non-paralyzing dead-time models into a single analytical expression [7]. Lee and Gardner assumed a non-paralyzing dead-time as a physical dead-time of detector which depends on physical characteristics of detector. This almost constant non-paralyzing dead-time is followed by a paralyzable dead-time till the point when a pulse of recordable amplitude is produced. Thus paralyzable dead-time depends on the detection system's discriminator level setting (see Fig. 2). Any pulse generated in the detector below a certain discrimination level will not be detected unless the amplitude of the pulse is higher than the discriminator setting. The paralyzing portion of the dead-time depends on both the discrimination level and the pulse processing electronics.

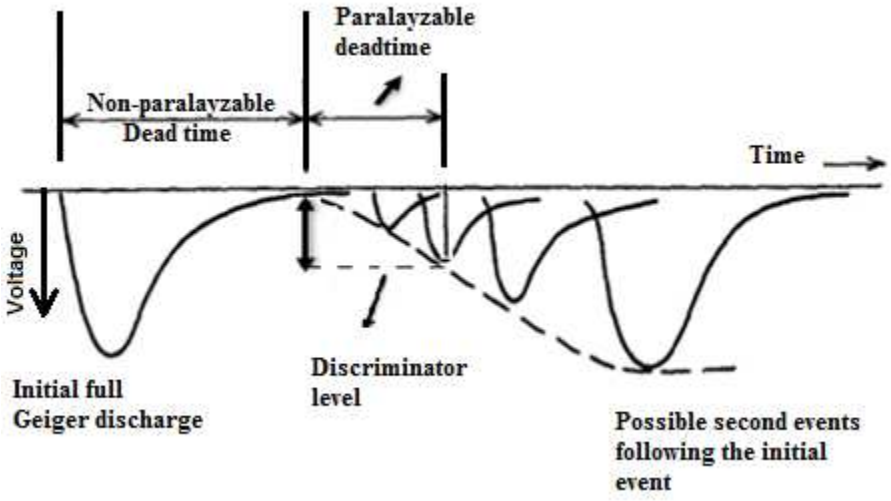

Figure 2. Lee and Gardner's hybrid dead-time model

Lee and Gardner [7] used the decay source method to validate their model. They reported an agreement within 5% of the true count rate up to a count rate of $3x10^4$ counts per second. They however did not justify their choice of the dead-time orders (putting a non–paralyzable dead-time before a paralyzable dead-time). A modified two-source

method was required because the traditional two-source method can only provide one parameter; that is, dead-time (either paralyzable or non-paralyzable) [11].

Patil and Usman [12] recently proposed another hybrid dead-time model, which is essentially a modified form of Müller's model [10]. They proposed a probability-based paralysis factor *f*. They also claimed better accuracy with their approach of using a single dead-time and a paralysis factor. This paralysis factor is defined as the probability of paralyzing a detector system. The probability lies between 0 and 1 therefore, the model also satisfies the two idealized dead-time models as the asymptotic cases. For example, if a paralysis factor is zero (no paralysis), their hybrid equation reduces to non-paralyzing model [12]. Mathematically, the measured count rate is given by;

$$m = \frac{ne^{-n\tau f}}{1+n\tau\left(1-f\right)} \tag{5}$$

where τ represents the total dead-time, and *f* is the paralysis factor. Patil and Usman [12] also developed a modified decaying source method to measure both the dead-time and the paralysis factor. This method does not require any presumption regarding the detection system's nature (either paralyzable or non-paralyzable) for data collection and analysis. The modified decay source method can be used at high counting rates to calculate not only the total dead-time but also the paralysis factor [13]. Müller [14] proposed another dead-time model by assuming Poisson input for the detection system. Pomme [4] subsequently discussed the limitation of this approach. Levert and Sheen [15] illustrated that frequency distribution is not necessarily Poisson; it is also dependent on the resolving time.

Müller [10] provided a detailed analysis of various possible dead-time combinations. He also discussed the impact of the choice on the overall system

performance. The best combination of these two dead-time parameters is expected to be obtained from experimental data and through an error reduction method. The fundamental question of the order of the dead-time must, however, be answered first based on the physical reasoning and the process of pulse formation and processing. Because the same combination of two dead-times (paralyzing and non-paralyzing) produces significantly different results if only their order is changed.

Patil and Usman [12] proposed a hybrid model that uses one paralysis factor and one dead-time. Their model does not use the two dead-times as proposed by Lee and Gardner [7]. Patil and Usman [12] did not offer sufficient justification or explanation of the paralysis factor and its dependence on the detection system's physical parameters and the count rate.

Since 1940's significant effort have been made to formulate an accurate generalized detector dead-time correction method which would cover all detectors for all operating conditions [14]; a goal which has not been realized till today. There is no universally acceptable generalized model and the recent work by Akyurek et al. [2] makes the concept of such generalized model questionable. Feller [5] and Evans' [6] idealized models are useful as upper and lower limits for a given situation. Lee and Gardner [7] provided a useful hybrid model but did not provide any justification for the order of these two dead-times. Likewise, Patil and Usman [12] did not provide either any physical meaning for the paralysis factor or any justification for using a fixed paralysis factor.

Present study was conducted in an attempt to compare ideal models to recently proposed hybrid models to provide insight into these models and their limitations. This comparison is important for high count rate applications because the selection of a dead-

time correction method has pronounced effects on the corrected counts. Section 1 includes a detailed discussion of both classical and recently proposed hybrid dead-time models and their limitations. A brief overview of decay source methods for dead-time measurements is given in section 2. The simulation algorithm for this study is summarized in section 3. The results are presented in section 4, and the paper concludes with discussion of the results in section 5.

2. Decay Source Method

The decay source method is commonly used to calculate the radiation detection system's dead-time. This method is based on known exponential decay behavior of a radioactive source [1];

$$n = n_0 e^{-\lambda t} + n_b \tag{6}$$

where n_b is the background count rate, and n_o is the count rate at t=0. Considering very low background counts (n_b =0), and using non-paralyzing assumption, the decay source equation (6) yields;

$$me^{\lambda t} = -n_0 \tau m + n_0 \tag{7}$$

If $me^{\lambda t}$ is plotted as a function of measured counts "m", the slope of line would be $n_o\tau$, hence dead-time can be calculated from the ratio of slope to intercept value. The intercept can be calculated by fitting best straight line for the data to obtain n_o. Using paralyzing assumption, the decay source equation (6) becomes;

$$\lambda t + ln\, m = -n_0 \tau e^{-\lambda t} + ln \tag{8}$$

The dead-time can be calculated by plotting $e^{-\lambda t}$as abscissa $\lambda t + \ln(m)$ on the ordinate (see Fig. 3).

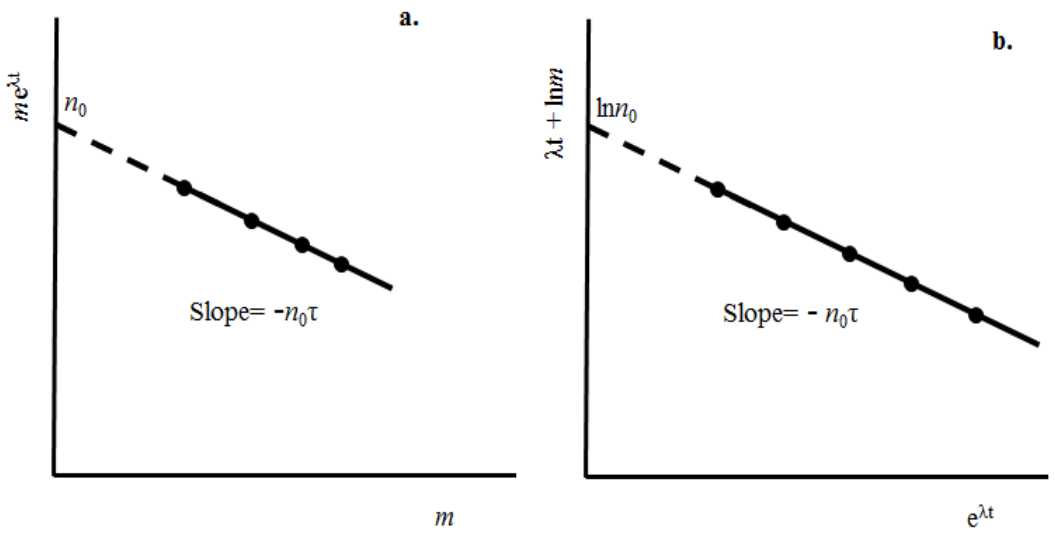

Figure 3. Graphical representation of decay source method

The decaying source method is useful not only when calculating the dead-time but also to verify the assumption of paralyzing or non-paralyzing detector [12]. Care should be taken when selecting a suitable radioactive source because this method requires a pure source with only a single half-life [1]. This standard decay source method can only be used for a single dead-time measurement. It is not suitable for a hybrid model with more than one parameters. Patil and Usman [12] proposed a modified decay source method that can be used to measure both the dead-time and the paralysis factor, requiring no presumption regarding the paralyzing nature of the detector.

3. Theory

Four dead-time models are currently available in the literature; the ideal paralyzing and the ideal non-paralyzing models, the hybrid model with two dead-times, and a paralysis factor-based hybrid model. The difference that exists between the two ideal models is well-known, however, the difference between the two hybrid models is not discussed in the literature. The present study was conducted as an attempt to investigate the two hybrid

approaches, providing the users with a better tool when selecting the best model for their application.

The time interval between successive decay events is random due to statistical nature of radioactive decay which can be modeled by a random number generator. The response of different models, as well as the extension of dead-time in various models, is illustrated in Fig. (4). In case 1, which is a non-paralyzing model, if a second event occurs during the dead-time, it will not be detected and detector dead-time will not be extended. All subsequent events during dead-time will be lost without any dead-time extension. For case 2, the paralyzable model, any event during the dead-time will not be detected and the event will reset the dead-time of detector for the same duration as the original dead-time. All subsequent events during the extended dead-time will be lost, as illustrated in Fig. (4).

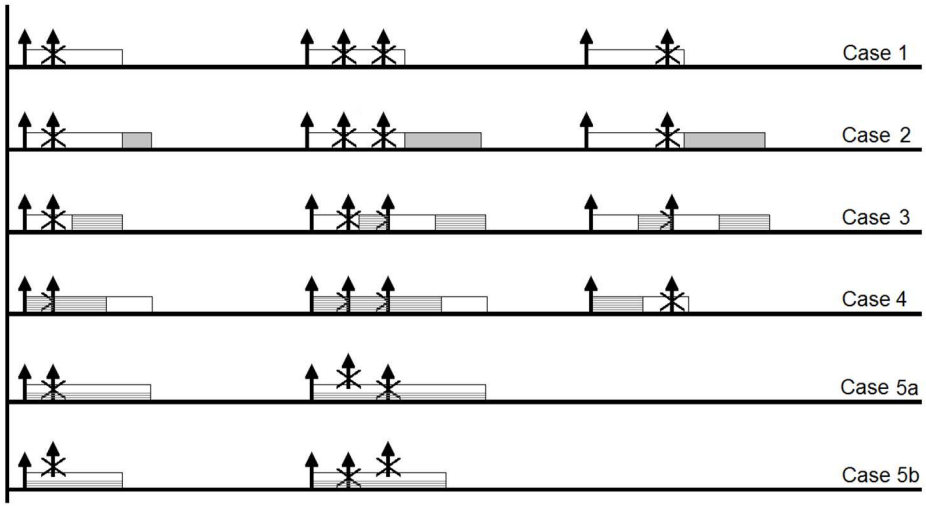

Figure 4. Algorithm of different dead-time models

Two cases of hybrid model proposed by Lee and Gardner [7] were examined in cases 3 and 4. For case 3, the non-paralyzing dead-time is before the paralyzing dead-time as proposed by Lee and Gardner [7]. They did not provide any justification for this order,

therefore a reverse order was also studied. The paralyzing dead-time is represented by the hashed area, and the non-paralyzing dead-time is represented by a non-hashed area. Any subsequent event that occurs during the first half of case 3 (a non-paralyzing portion of dead-time), it is lost without any dead-time extension. However, if an event occurs during the second (paralyzing) portion of dead-time, the event is lost and the dead-time is reset.

The order of the two dead-times is altered in case 4, the paralyzing dead-time is placed before the non-paralyzing dead-time. Finally, the model proposed by Patil-Usman is shown in case 5. The dead-time is indicated by a combination of hashed and unhashed portions throughout the dead-time. During the entire dead-time, there is a fixed probability that a subsequent event will result in the paralysis of the system. A fixed paralysis factor of 50% was assumed in cases 5a and 5b. The lower hashed part had a paralysis probability of 50%. The upper non-hashed part was non-paralyzing part. If an event occurs during the dead-time, it was not detected. The likelihood of this event paralyzing or not paralyzing would be depend on the paralysis factor of the system. As shown in the Fig. (4), based on the probability of paralysis the lost event may or may not extend the dead-time. This scheme is schematically shown by an event in the hashed part of dead-time is extending the dead-time while others are not extending the dead-time. It can be argued that the paralysis factor is not fixed, instead, it must vary during the dead-time.

Numerical simulations for GM counter dead-time required a random time interval generation between two successive events. A detailed discussion of the probability of emission and time interval between two events is given by Knoll [1]. This time interval is a function of the source intensity and was calculated by;

$$\Delta t = -\frac{\ln(N_{random})}{I(t)} \tag{9}$$

A FORTRAN's RAN() function was used to generate the random number. A seed was used as the function's argument. A similar simulation strategy with identical time interval function was recently implemented by Akani and Raisali [16]. The code continuously updated the true count rate and hence the intensity *I(t)* thereby simulating the radioactive decay;

$$I(t) = ne^{-\lambda t} \tag{10}$$

Where λ is radioactive decay constant. This random interval was used to simulate the successive events, if the second event was within the dead-time of the detector it was not recorded. The event was counted only if it was outside the dead-time. It was also treated as the first count, and the process was repeated. If it was within the dead-time for the paralyzing model, the dead-time was reset to zero. For the two possible cases of Lee and Gardner model, if the second event was in the paralyzing portion of the dead-time the second event resulted in resetting the dead-time otherwise only the event was lost.

For the Patil-Usman model, a second random number was generated between 0 and 1. The dead-time was reset only if this random number was equal to or larger than the paralysis factor. If the second random number was smaller, the count was lost but the dead-time was not reset. This logic was programed into Sim-Pulse, a computer code that was used to produce the results presented in the following sections.

4. Simulation Results

A Compaq Visual FORTRAN Professional Edition 6.5.0 was used to develop a "Sim-Pulse V1.1" code. This code was then used to simulate dead-time models according to the decaying source method. A Pentium IV processor with 3.2 GHz and 2.0 GB of memory was used to run the simulations. Intensity *I(t)* was made a function of time;

allowing simulation of a decaying source with a desired half-life. Changes in '*I*' modified the distribution of random numbers and, thus, the time interval. The code offered flexibility in modeling any decaying source by specifying a half-life. Any type of detector dead-time model; paralyzing, non-paralyzing, hybrid with two dead-time or with one dead-time and paralysis factor can be simulated. Validation of code was performed by the well-known behavior of the two ideal models and the fact that they are the limiting cases for the hybrid models [7, 13].

It is recognized that all actual detectors would have its own dead-times (paralyzing and non-paralyzing) for the Lee and Gardner model or a fix total dead-time and a paralysis factor as per Patil and Usman model. These parameters should be determined by collecting experimental data and finding the values which would give the minimum error. These values will depend on the operating conditions as reported by Akyurek [2, 17], Peeva and Guleva [18] and Puri [19]. Simulations were performed using Sim-Pulse to test the hypothetical cases to examine the behavior of various dead-time models. These results were then used to examine the behavior of the all dead-time model.

A source of initial activity (between 10^4 and 10^6 counts per second for a total fixed dead-time of 1μsecond) was used to perform each simulation. Both the paralyzing and the non-paralyzing models had one dead-time, while for Lee and Gardner model the total dead-time was divided into two parts based on the paralysis factor as shown in Table 1. The total dead-time for the Patil-Usman model was fixed but the paralysis factor was varied between 10% and 90%. The modified decay source method was used to simulate Vanadium (^{52}Vn) decay with a half-life of 225.6 second. A small bin size of 1 s was modeled to collect the counts.

Table 1. Simulation parameters for all cases

Case 1 (f=50%)					**Case 2 (f=50%)**			
Model	**NP**	**P**	**L+G**	**P+U**	**NP**	**P**	**L+G**	**P+U**
CPS	10^4	10^4	10^4	10^4	10^6	10^6	10^6	10^6
Bin Size(s)	1	1	1	1	1	1	1	1
Total Dead-time(µs)	1.0	1.0	0.5+0.5	0.5+0.5	1.0	1.0	0.5+0.5	0.5+0.5
Half Life(s)	225.6	225.6	225.6	225.6	225.6	225.6	225.6	225.6
Case 3 (f=50%)					**Case 4 (f=50%)**			
CPS	10^4	10^4	10^4	10^4	10^6	10^6	10^6	10^6
Bin Size(s)	1	1	1	1	1	1	1	1
Total Dead-time(µs)	300	300	150+150	150+150	300	300	150+150	150+150
Half Life(s)	225.6	225.6	225.6	225.6	225.6	225.6	225.6	225.6
Case 5 (f=10%)					**Case 6 (f=10%)**			
CPS	10^6	10^6	10^6	10^6	10^4	10^4	10^4	10^4
Bin Size(s)	1	1	1	1	1	1	1	1
Total Dead-time(µs)	1	1	0.9+0.1	0.9+0.1	300	300	270+30	270+30
Half Life(s)	225.6	225.6	225.6	225.6	225.6	225.6	225.6	225.6
Case 7 (f=10%)					**Case 8 (f=25%)**			
CPS	10^6	10^6	10^6	10^6	10^6	10^6	10^6	10^6
Bin Size(s)	1	1	1	1	1	1	1	1
Total Dead-time(µs)	300	300	270+30	270+30	1	1	0.75+0.25	0.75+0.25
Half Life(s)	225.6	225.6	225.6	225.6	225.6	225.6	225.6	225.6

Table 1. continued

	Case 9 (f=90%)				Case 10 (f=25%)			
CPS	10^6	10^6	10^6	10^6	10^6	10^6	10^6	10^6
Bin Size(s)	1	1	1	1	1	1	1	1
Total Dead-time(μs)	1	1	0.1+0.9	0.1+0.9	300	300	225+75	225+75
Half Life(s)	225.6	225.6	225.6	225.6	225.6	225.6	225.6	225.6

Two dead-times were simulated; the small value of 1μs and the large value of 300 μs. A wide range of parameters were tested to compare each model's performance as listed in Table 1. As the first case, dead-time behavior of each model with a low count rate of 10^4 counts per second and a dead-time of 1μs, with a paralysis probability of 50% was simulated. Fig. (5) show that all models exhibit similar linear behavior at small count rates.

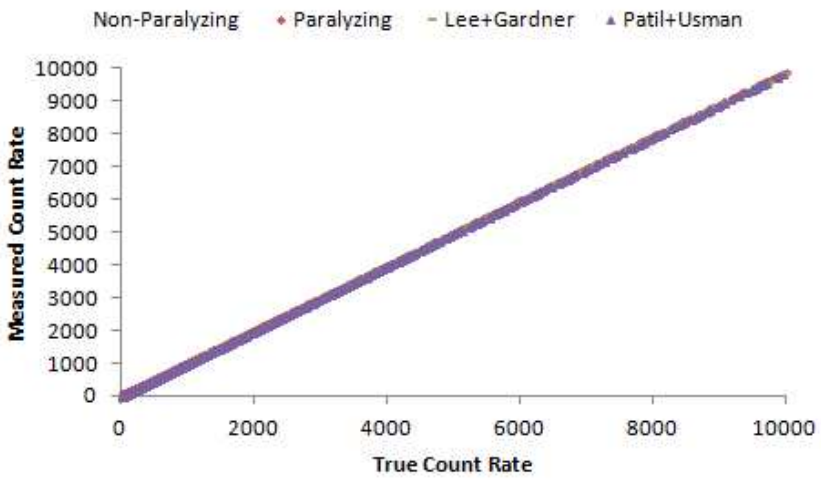

Figure 5. Simulation results for the input parameters in case 1

Various dead-time models began to depart from one another at an initial count rate of 10^6 (see Fig. 6). As expected, both hybrid models were between the two idealized

models. The Patil-Usman model began to approach the ideally non-paralyzing model, recording more counts than the Lee and Gardner model. For this hypothetical case of 1μs dead-time and 50% paralysis factor there is slight difference in Patil-Usman and Lee-Gardner models' maximum recorded counts even though both have same total dead-time and same paralysis factor demonstrating the significance of the model assumptions.

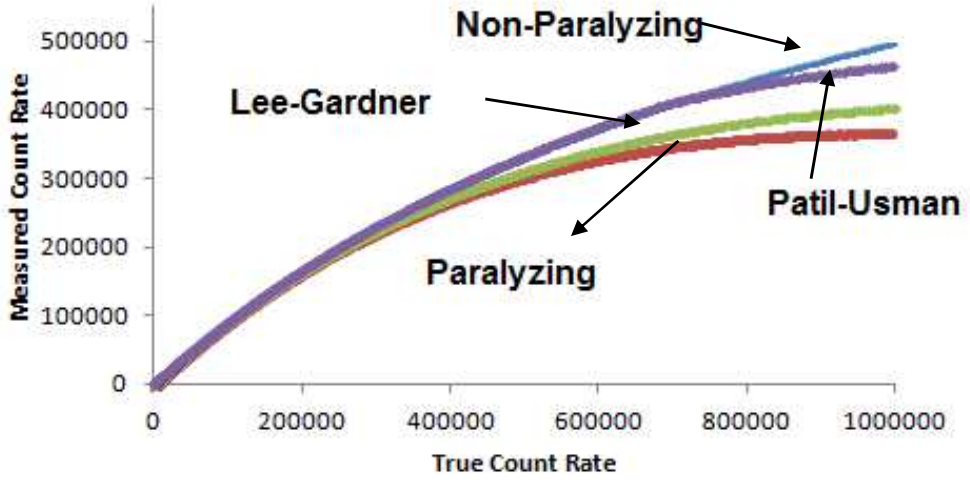

Figure 6. Simulation results for the input parameters in case 2

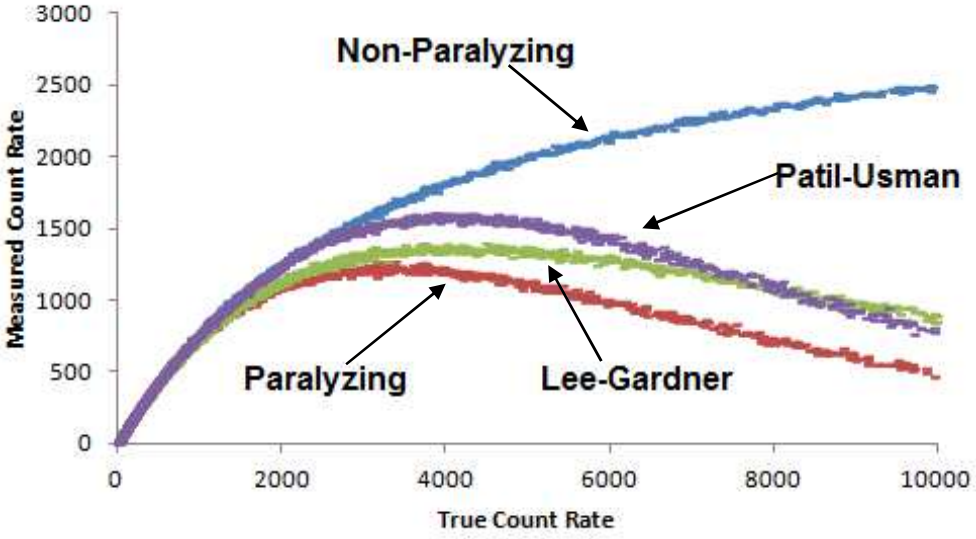

Figure 7. Simulation results for the input parameters in case 3

Each model's response was quite different from the other as the total dead-time was increased to 300 μs for an initial count rate of 10^4 counts per second, as illustrated in Fig. (7). The difference was more pronounced for higher count rate of 10^6 counts per second as shown in Fig. (8). Again as expected, both hybrid models were between the two ideal cases. An obvious maxima was observed for the paralyzing model as well as in the two hybrid models. For this case of 50% paralysis factor, the peaking or maxima of Patil-Usman model is higher than Lee and Gardner model while both hybrid models' maxima is higher than the ideal paralyzing model.

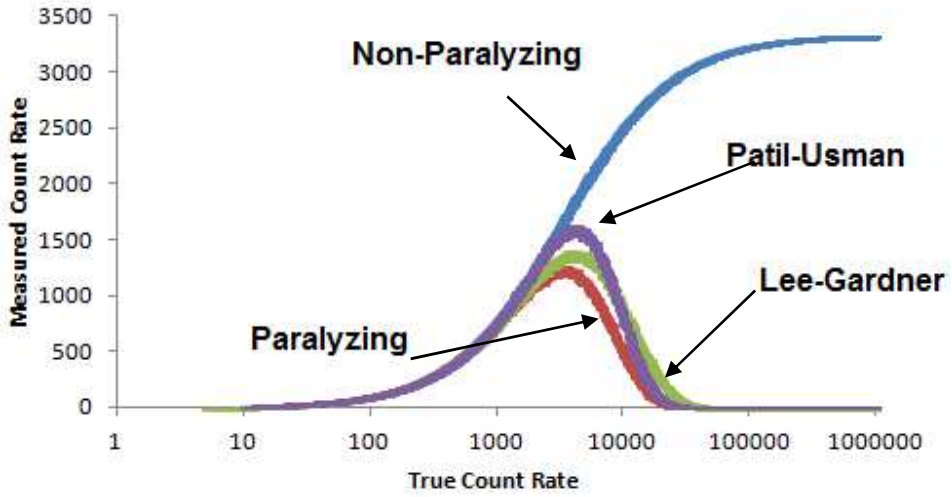

Figure 8. Simulation results for the input parameters in case 4

In contrast, the measured count rate in the paralysis factor model decreased faster than either the Lee-Gardner model or the Patil-Usman model. The two seemingly similar hybrid models did not produce the same results. Constant paralysis probability in the Patil-Usman model produced higher recorded counts for low counts rate while at high count rate constant paralysis probability leads to a lower any recorded count rate. Neither the paralyzing nor any of the hybrid models had recorded counts at high count rates (100,000

cnt/s). Only the non-paralyzing model showed a positive asymptotic value at high count rate (the saturation value).

For case 5, all the to the input parameters were same as those for case 2 except the paralysis factor was reduced to 10% instead of 50%. For this case, the two hybrid models tend to approach the non-paralyzing model at a high initial count rate of 10^6 count per second because of the low paralysis probability (10%). The Patil-Usman model was nearly identical to the non-paralyzing model but Lee and Gardner is distinctly different (see Fig. 9).

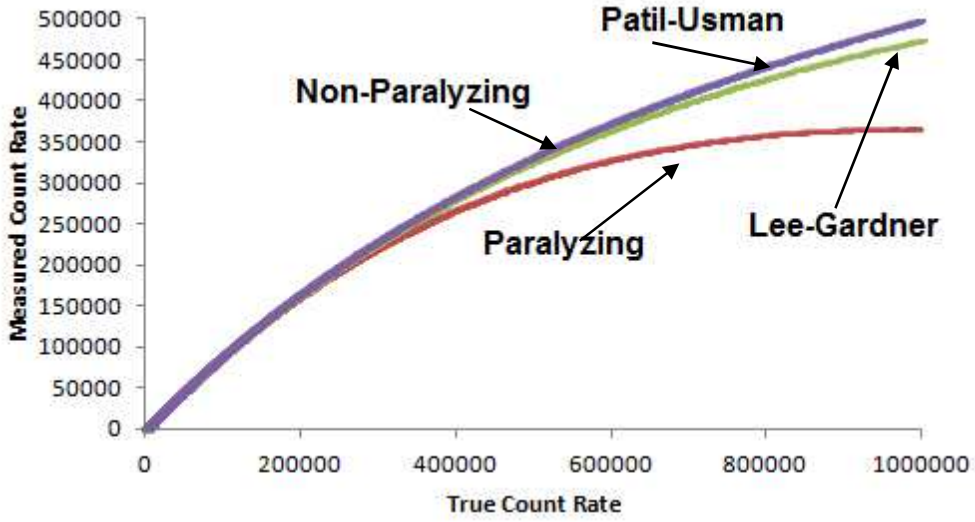

Figure 9. Simulation results for the input parameters in case 5

For case 6 and 7, simulations were performed with same input parameters as case 3 and 4, except paralysis factor was now reduced to 10% instead of 50%. For small count rate of 10^4 counts per second and the larger dead-time, the behavior of the two hybrid models is entirely different. Patil-Usman model is approaching the ideal non-paralyzing model and starts deviating from the ideal model only after count rate of $8x10^3$. On the other hand, Lee-Gardner model behaves similar to the paralyzing model and started to deviate

from the ideal paralyzing model at approximately $2x10^3$ counts per second. These results are quite significant as they reveal that these seemingly similar hybrid models are quite different in their behavior (see Fig. 10).

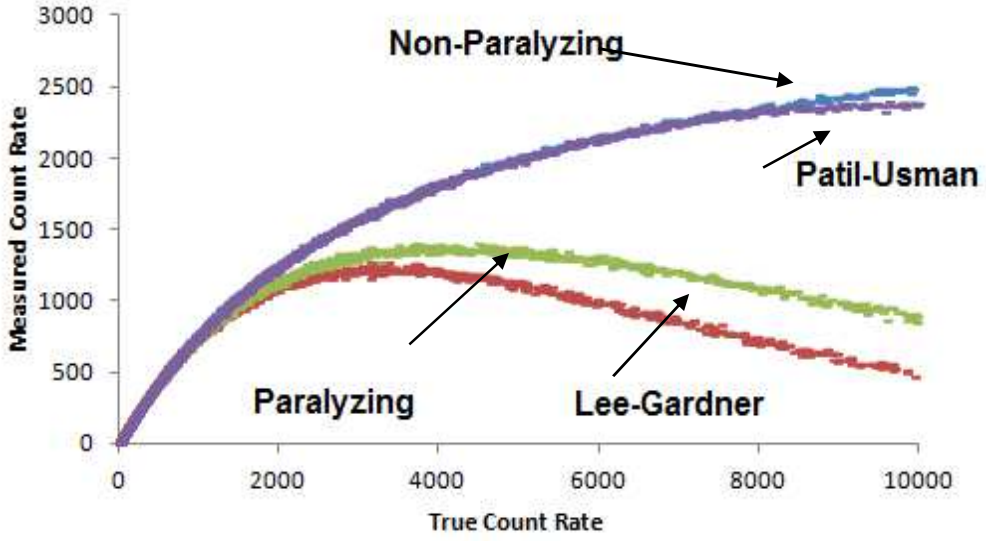

Figure 10. Simulation results for the input parameters in case 6

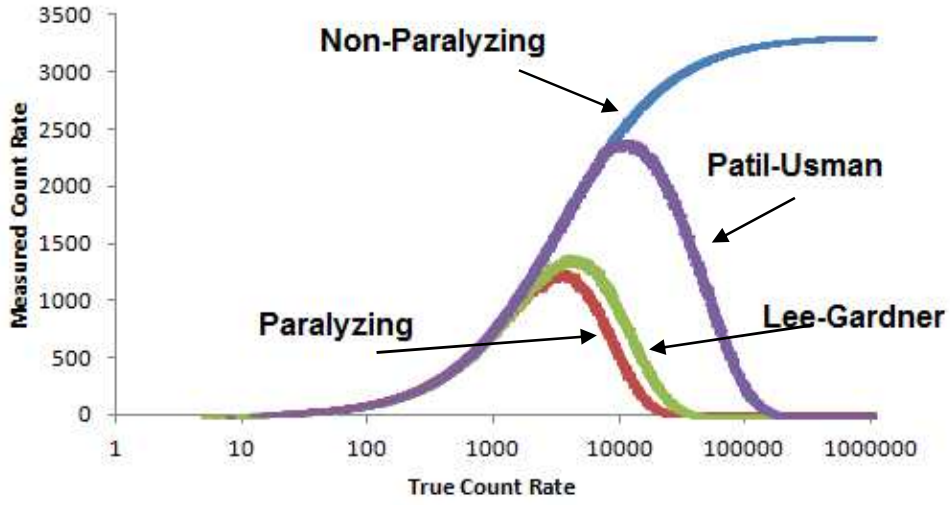

Figure 11. Simulation results for the input parameters in case 7

The effect of the 300 μs dead-time for high count rate of 10^6 is illustrated in Fig. (11). The recorded count rate approached zero at high count rates as it did for larger dead-

time. The difference between the two hybrid models is however quite prominent at the larger dead-time. The Patil-Usman model's peaking value was at a higher true count rate, producing much higher recorded count rate.

Both the dead-time and the paralysis factor played significant role in the model behavior. Thus additional simulations were conducted for a moderate paralysis factor of 25% and a high paralysis factor of 90%.

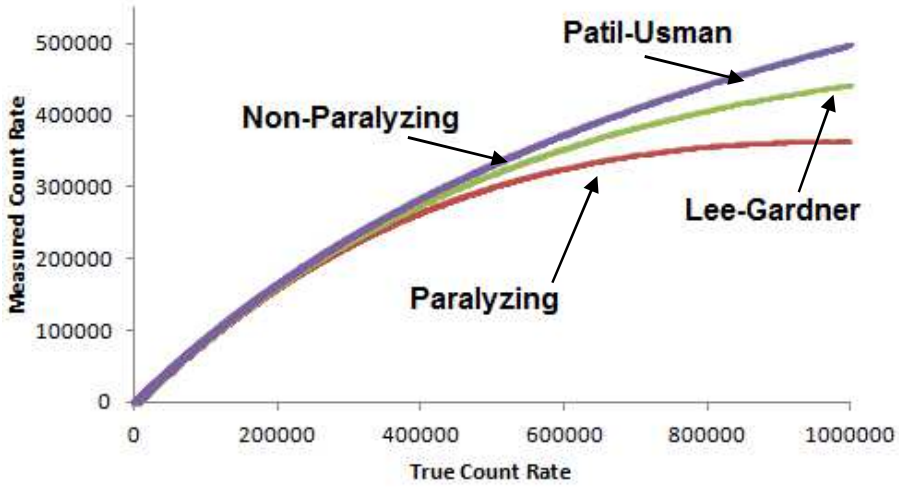

Figure 12. Simulation results for the input parameters in case 8

Hybrid models' behaviors during all simulations were between the two idealized models. It is important to compare case 2, 5, 8 & 9, (see Figs. 6, 9, 12 and 13) for an increase of paralysis factor from 10% to 90%, with total dead-time in both cases being 1 μs. Both of the hybrid models approached the ideal paralyzing model at a paralysis factor of 90%. The two hybrid models were close to a non-paralyzing model at a paralysis factor of 10% (see Fig. 9). Lee-Gardner model, however, produced a lower count rate than did either the Patil-Usman model or the ideal non-paralyzing model. The results were quite interesting at a paralysis factor of 50% (case 2). The Lee-Gardner model was closer to the

paralyzing model, and the Patil-Usman model was closer to the non-paralyzing model. These results thus indicate that the two hybrid models are quite different.

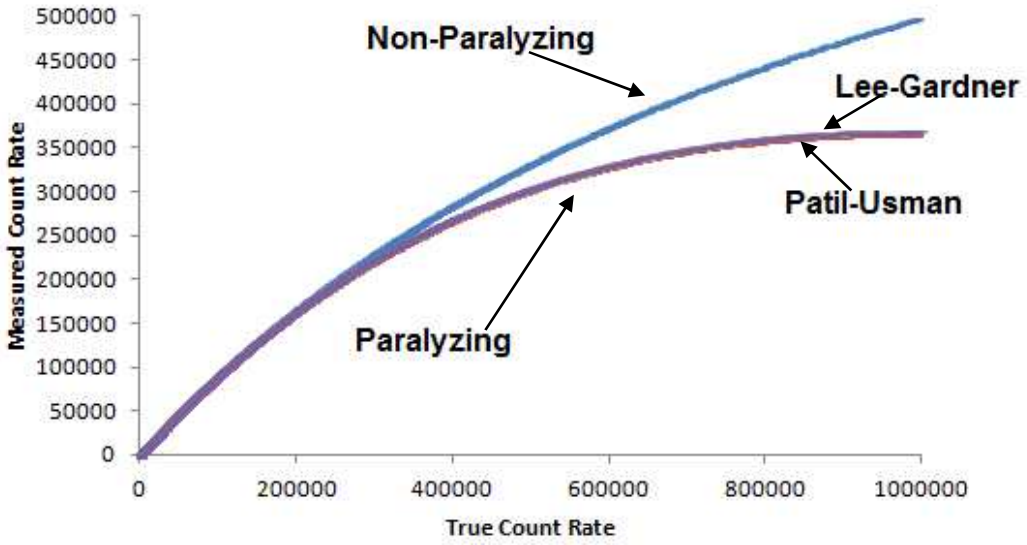

Figure 13. Simulation results for the input parameters in case 9

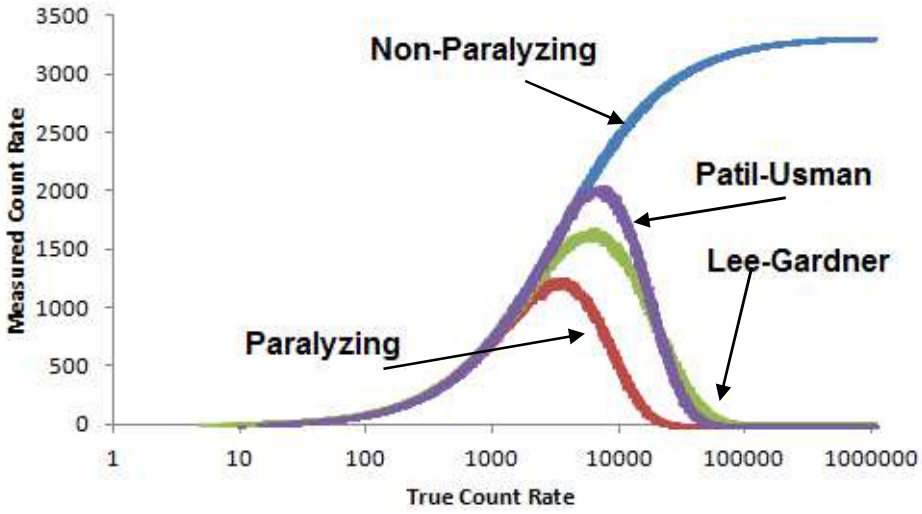

Figure 14. Simulation results for the input parameters in case 10

A comparison between cases 8 and 10 demonstrates the effect of a large dead-time. The dead-time in case 8 was 1 μs, while for case 10 (Fig. 14) the dead-time is 300 μs all

other simulation parameters unchanged (i.e., initial count rate of 10^6, bin size of a second and paralysis factor of 25%). The change in dead-time from 1 μs to 300 μs was profound (see Figs. (12) and (14), respectively). Neither the paralyzing model nor the two hybrid models recorded any counts for a large dead-time when the true count rate was over 100,000 per second. The ideal paralysis model reached complete paralysis much sooner than the hybrid models.

Finally, after validation of code and initial model testing behavior of Lee-Gardner [7] model was further investigated to see if the order of the two dead-times would have any effect on the model prediction. Lee-Gardner suggested that the non-paralyzing dead-time should be placed before the paralyzing dead-time (NP+P). Simulations were also conducted with a reverse dead-time order (P+NP). A decaying source method with a high initial activity of 10^7 counts per second was used for simulation with a short half-life of 10 sec. A Multichannel Scalar with a bin size of 1 second was simulated. The simulation's set-up is listed in Table 2. Patil-Usman model with a fixed paralysis factor of 50% was also simulated for comparison.

Table 2. Simulation parameters for the dead-time models

S #	Description	Value
1	Activity (counts/second)	$1*10^7$
2	Half Life (second)	10
3	MCA Binsize (second)	1
4	Paralyzing Dead-time (second)	$0.5*10^{-6}$
5	Non-paralyzing dead-time (second)	$0.5*10^{-6}$
6	Paralysis factor	50% fixed

Lee and Gardner [6] suggested that the non-paralyzing dead-time be placed before paralyzing dead-time (NP+P) which produces results quite similar to Patil-Usman. But by

switching the order of dead-times i.e., paralyzing dead-time placed before non-paralyzing dead-time (P+NP) the results are quite different as shown in Fig. (15). Both cases showed not only difference in peak counts but NP+P model approaches the total paralysis (zero count rate recorded) much faster than the P+NP case. Difference in response clearly shows that dead-time order is very important for Lee and Gardner's hybrid model [7].

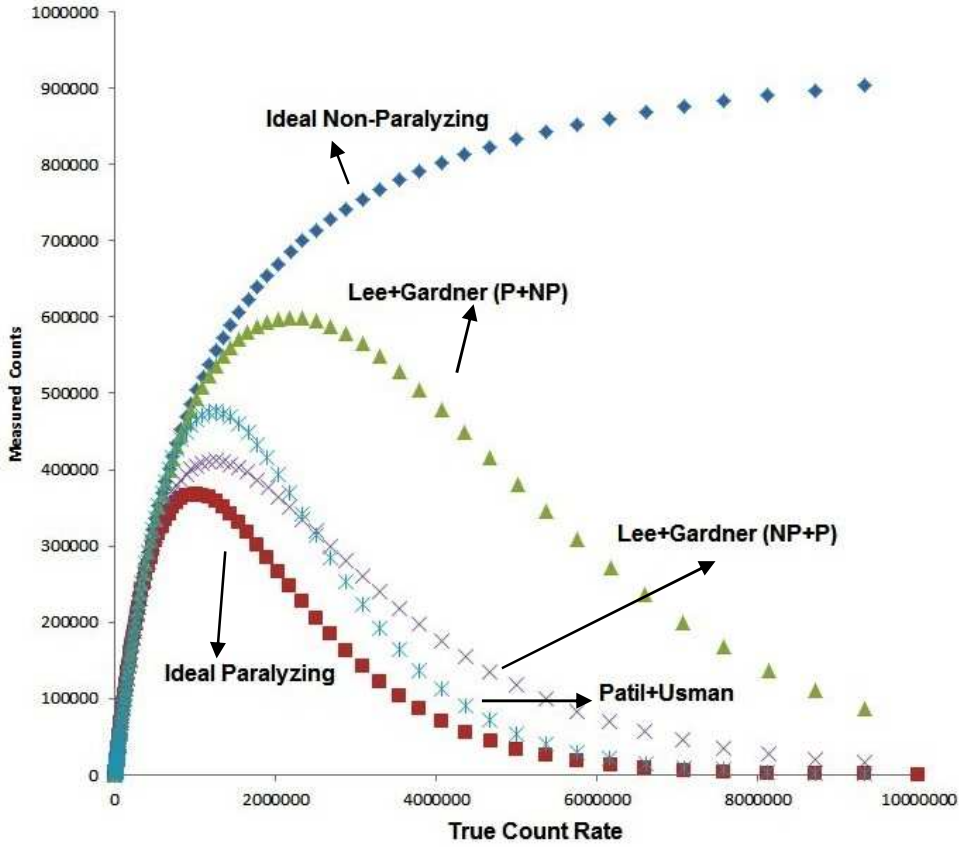

Figure 15. Traditional and hybrid dead-time model simulation results

The peak counts collected throughout this study were larger for Patil-Usman model than for Lee and Gardner model, regardless of the paralysis factor. It is only once we modified the Lee and Gardner [6] model by placing paralyzing before non-paralyzing dead-time, the peak counts of modified Lee-Gardner dead-time model were higher than Patil-Usman dead-time model.

Likewise, the peak counts for every model was different. The non-paralyzing model had maximum peak counts at the asymptote (as expected), and the paralyzing model set the minimum peak count limit. The simulation results taken from these hypothetical examples indicate that hybrid models produced significantly different results. The users should not assume that all hybrid models with same dead-time and paralysis factor will produce same result; dead-time order is important [20].

5. Conclusion

The decay source method was used to conduct numerical simulations to compare the ideal dead-time models with the hybrid models. Hypothetical cases were studied to investigate the impact of paralysis factor, total dead-time, initial count rate, and model choice. Experimental data was used to determine suitable values for the parameters (both total dead-time and paralysis factor), under the expected operating conditions for a given detector [15-19].

Validation of code was performed by using dead-times as low as 1μs to as high as 300μs, paralysis factor from 10% to 90%, and with initial count rates of 10^4 to 10^6 counts per second. All newly proposed hybrid models were between the two extreme ideal cases (the paralyzing model and the non-paralyzing model). The two hybrid models, which are seemingly similar, exhibited different behavior for a different amount of dead-time and paralysis factors. Several interesting observations were made during the simulations.

Finally, the dead-time order was altered to investigate two different cases of Lee-Gardner dead-time model. An initial count rate of 10^7 counts per second with a total dead-time of 1μs and a paralysis probability of 50% was used. The Lee-Gardner model exhibited an entirely different behavior during these simulations with reversed dead-time order. A

smaller peak count rate was observed in the NP+P case. This rate converged to zero much faster than the P+NP case.

Behavior of Patil-Usman model has been investigated using different initial count rates and fixed paralysis probability. However, based on the comparison of these results, one may question the validity of the approach of these hybrid models. Patil and Usman used a constant paralysis factor for the entire dead-time, while Lee and Gardner use a step change from zero to one during their dead-time by dividing the dead-time into two distinct portions. These results indicate that there is need for further investigation of this problem which must be based on physical reasoning. Dependence of paralysis probability on detection system parameters must be based on reasoning founded in physics not on mathematical convenience. As experimental data from Akyurek et al. [2] showed, for the same GM counter dead-time behavior is highly dependent on the operating conditions, namely; bias voltage, temperature, and detector age. Not only that the value of dead-time changes with the operating conditions but the very nature of the phenomenon changes resulting in pulse shape alteration (Fig. (9) and (10) of their publication [2]).

Observation made in this study further reinforced the finding; as shown in Fig. (16), pulse generated by a NaI(Tl) changes in both shape and the amplitude with operating voltage. For high energy (^{60}Co) the pulse showed sharp edges (Fig. 16 a) due to high gamma energy vs (Fig. 16 d) where the edges were not as sharp. Similarly, there was an obvious pulse shape change for ^{60}Co when the operating voltage was increase from 600 V to 700 V. These results are consistent with Akyurek et al. [2], therefore it would not be advisable to propose a single dead-time model for a given detector under all operating conditions. From these simulations, it is concluded that a careful selection of dead-time

model is required to appropriately correct the measured count rates taking into considerations the operating conditions. Model selection must consider the physical nature of the phenomenon not only the ease of mathematics.

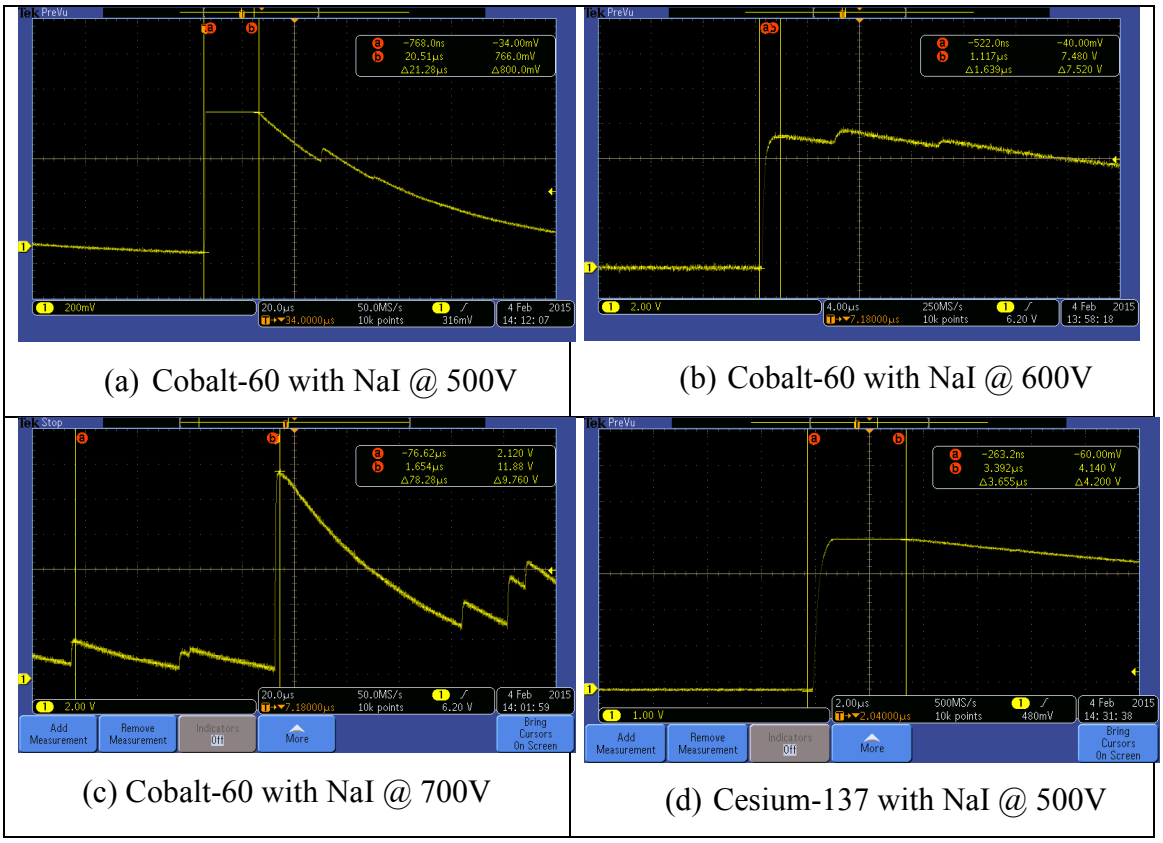

Figure 16. Pulse shape for NaI(Tl) detector under various operating conditions

REFERENCES

[1] G. F. Knoll, (4th Edition, 2010). "Radiation Detection and Measurement". New York: John Willey and Sons, Inc. USA.

[2] T. Akyurek, M. Yousaf, X. Liu and S. Usman, "GM Counter Deadtime Dependence on Applied Voltage, Operating Temperature and Fatigue", Radiation Measurements, 73, 26-35, 2015.

[3] N.Tsoulfanidis and S. Landsberger (3rd Edition, 2012) Measurement and Detection of Radiation, CRC Press, New York, NY, 10016 USA.

[4] S. Pomme, "Dead-time, pile-up, and counting statistics," ACS Symposium Series, 945, 218-233, 2007.

[5] W. Feller, “On probability problems in the theory of counters,” in R. Courant Anniversary volume, Studies and Essays, Interscience, New York, 105-115, 1948.

[6] R. D. Evans, “The Atomic Nucleus,” McGraw-Hill, New York, 1955.

[7] S. H. Lee and R. P. Gardner, “A new GM Counter Dead Time Model”, Appl. Rad. Isot, 53, 731- 737, 2000.

[8] G. E. Alber and L. Nelson. “Contribution to Statistical Theory of Counter Data”, Ann. Math. Stat., 24, 9-22, 1953.

[9] R.P. Gardner and L.Liu, “On Extending the Accurate and Useful Counting rate range of GM Counter Detector System”, Appl. Radiation Isot. Vol. 48, 1605-1615, 1997.

[10] Müller, J.W. “Dead time problems”, Nuclear Inst. And meth. Vol. 112, 47-57, 1973

[11] S.H. Lee, R.P. Gardner and Moosung JAE, “Determination of Dead Times in the Recently Hybrid G-M Counter Dead Time Model”, Nucl. Sci and Tech. Supplement 4, 156-159, 2004

[12] A. Patil and S. Usman, “Measurement and Application of Paralysis Factor for Improved Detector Dead Time Characterization”, Nuclear Technology, Volume. 165, 249-256 2009.

[13] A. Patil, “Dead time and Count Loss Determination in Radiation Detection System in High Count Rate Applications” PhD Thesis, 2010, Missouri University of Science & Technology, Rolla, MO, USA

[14] Müller, J.W. “Generalized Dead times”, Nuclear Inst. And meth. Physics Research, A 301, 543-551, 1991

[15] C. Levert and W. Scheen “Probability fluctuations of discharges in a Geiger-Müller counter produced by cosmic radiation”, Physica 10, 225–238, 1943.

[16] M. Arkani and G. Raisali, “Measurement of deadtime by time interval distribution method”, Nuclear Instruments and Methods in Physics Research A 774,151–158, 2015.

[17] T. Akyurek, M. Yousaf, and S. Usman, “Operating voltage dependence of detector deadtime - GM counter”, Transactions of the American Nuclear Society, Vol. 107, 331-332, 2012.

[18] A. Peeva and D. Guleva, “Dead Time and Fatigue in Self-Quenching G.M. Counters at Different Temperatures”, Nuclear Instruments and Methods, 44, 314-316, 1966.

[19] S. P. Puri, “A Study of the Operation of GM Counters at Low Temperature”, Ind. J. Phys., 22, 214-219, 1956.

[20] M. Yousaf & S. Usman, “Comparison of Traditional and Hybrid Dead Time Model of Radiation Detector” Transactions of the American Nuclear Society, Vol. 106, Chicago, Illinois, June 24–28, 2012, USA.

III. PORTABLE SPECTROSCOPIC FAST NEUTRON PROBE AND ^{3}He DETECTOR DEAD-TIME MEASUREMENTS

T. Akyurek, L. P. Tucker, X. Liu, S. Usman

Department of Mining and Nuclear Engineering, Missouri University of Science & Technology, Rolla, MO, 65401, USA

Abstract

This paper presents dead-time calculations for the Portable Spectroscopic Fast Neutron Probe (N-Probe) using a combination of the attenuation law and paralyzing and non-paralyzing dead-time models. The N-Probe contains an NE-213 liquid scintillator detector and a spherical ^{3}He detector. For the fast neutron probe, non-paralyzing dead-time values were higher than paralyzing dead-time values, as expected. Average paralyzing dead-time was calculated to be 101.2 μs and non-paralyzing dead-time was calculated to be 254.8 μs for the N-Probe liquid scintillator detector. A Canberra ^{3}He neutron detector's dead-time value was estimated using a combination of subcritical assembly measurements and MCNP simulations. The paralyzing dead-time was estimated to be 14.5 μs, and the non-paralyzing dead-time was estimated to be 16.4 μs for ^{3}He gas filled detector.

1. Introduction

Many techniques have been developed for detecting and measuring the uncharged neutron since its discovery in 1932. One of the most prevalent neutron detectors is the organic liquid scintillation detector (e.g., NE-213). These detectors are frequently used in nuclear experiments for their good energy resolution and high detection efficiency for neutrons and photons [1,2]. Using pulse shape discrimination (PSD) techniques, liquid scintillation detectors allow for the separation of the neutron and photon signals. The

techniques are based on the difference in scintillator response to neutron and photon events [3]. Since the neutron is not a charged particle, it does not ionize the scintillation material directly. It can be generally detected through nuclear interactions that produce energetic charged particles. Fast neutron detection relies on the production and detection of protons from (*n,p*) reactions within the detector. Therefore, hydrogen-rich materials are typically used as the detector material [4]. The most commonly used scintillator for fast neutron detection and spectroscopy is the NE-213 liquid scintillator produced by Nuclear Enterprises Limited. The most significant advantage of this scintillator is its excellent pulse-shape discrimination properties compared to other scintillators [5].

^{3}He gas proportional counters are common neutron detectors best suited for the detection of thermal neutrons since the $^{3}He(n, p)$ reaction is attractive for thermal neutron detection. ^{3}He counters are not suitable for operation in the Geiger-Müller region since there is no capability to discriminate the pulses produced by photon interactions [6]. The neutrons are captured by the $^{3}He(n, p)^{3}H$ reaction, producing a proton and a triton with a reaction *Q*-value of 764 keV. The energy dependent cross section of this reaction is one of the well-known standards in neutron measurements. Since the proton and triton are charged ions, both will usually be registered by the proportional counter [7]. Another widely used detector for thermal neutrons is the BF_3 proportional detector. Boron trifluoride behaves as a proportional gas and the target for thermal neutron conversion into secondary particles. Enriching the ^{10}B in the gas can make the detector up to five times more efficient [8].

Bubble Technology Industries (BTI) has manufactured a portable neutron scintillation spectrometer (N-Probe) with potential applications at nuclear reactor facilities, spent fuel storage areas, and waste processing operations [9]. Fig. (1) shows the N-Probe

spectrometer which contains a 5 cm by 5 cm NE-213 liquid scintillator detector to measure fast neutrons between 800 keV and 20 MeV, as well as a spherical ^{3}He detector to measure low energy neutrons from 0 to 1.5 MeV [10]. Sophisticated pulse-shape discrimination was used to remove undesirable photon counts for the NE-213 liquid scintillator detector. These two detectors work simultaneously and pulse-height distributions from both are shown during the measurements. The detector's software merges information from the two detectors to generate a single neutron energy spectrum. One of the significant advantages of the N-Probe is that it provides both the neutron energy spectrum and the total neutron counts for fast neutrons and thermal neutrons.

Figure 1. N-Probe fast and thermal neutron spectrometer [9].

Scientists have been working on dead-time problems for radiation detectors since the 1940s. In any detector system, a minimum amount of time must separate two events before they can be measured independently. This minimum separation time is referred to as the counting system's dead-time [11]. The properties of the detector and the pulse processing circuitry's characteristics are the sources of dead-time. Researchers have been

working on improving a detector dead-time model that can implicitly characterize a detection system's behavior while reducing counting errors [12, 13].

There are two commonly known dead-time models: the "Paralyzing" and the "Non-paralyzing" models. In reality, detection systems fit neither of these idealized models perfectly, instead falling somewhere between the two models [14]. The paralyzing model is mathematically expressed by Equation (1), where m is the measured count rate, n is the true count rate and τ is dead-time. This model assumes that each event during the dead-time will reset it to a fixed duration, thus extending the dead-time. The extension depends on the count rate.

$$m = ne^{-n\tau} \tag{1}$$

According to the non-paralyzing model, dead-time is fixed after each detected event, and all events occurring during dead-time are lost. The fraction of time during which an apparatus is sensitive is $1-m\tau$. Therefore, the fraction of the true number of events can be recorded as seen in Equation (2) [14]

$$m = \frac{n}{1+n\tau} \tag{2}$$

The dead-time of the N-Probe detector is not provided by BTI, and there is no other dead-time study published on the N-Probe detector. In this study, the dead-time of the BTI N-Probe (NE-213 Liquid scintillation) was examined using different thicknesses of Plexiglas at the Missouri University of Science and Technology Research Reactor (MSTR). Furthermore, the dead-time of the Canberra 10 mm diameter ^{3}He tube detector [15] was calculated by comparing measured counts from different locations in the subcritical assembly at MSTR with MCNP simulations. The dead-time calculations are

provided for both the paralyzing and non-paralyzing models for the fast neutron detector (N-Probe) and the Canberra 10 mm diameter ^{3}He tube detector.

During the all experiments, the reactor operated at 5 kW power for a standardized neutron flux from the beam port. The macroscopic cross section of Plexiglas was calculated for fast neutrons with both non-paralyzing and paralyzing dead-time models using the fast neutron detector (N-Probe). The neutrons were attenuated by different thicknesses of Plexiglas and counted by the detector in front of MSTR beam port.

2. Experimental Design

2.1 Dead-time Experiment for N-Probe Fast Neutron Detector

The Missouri S&T Research Reactor is a swimming pool type reactor licensed to operate at 200 kW [16]. A special 2-cm-diameter collimator was used for the neutron beam from the beam port to the Plexiglas. During the experiment, the operation of the detector and measurement was controlled remotely by a computer to avoid any radiation exposure. Fig. (2) shows the experimental set-up of the system to measure fast neutrons with N-Probe detector in the beam port room of the MSTR.

Fast neutron measurements were first taken with no plexiglass. A 0.5-cm-thick layer of plexiglass was then placed between the detector and collimator. The neutron measurements were taken from 0 to 3.0-cm-thick layers of plexiglass using thickness intervals of 0.5 cm. Measurements with and without plexiglass were taken for ten minutes with a constant flux at 5 kW power. With the reactor still at 5 kW, the beam port was closed to replace the plexiglass after each measurement.

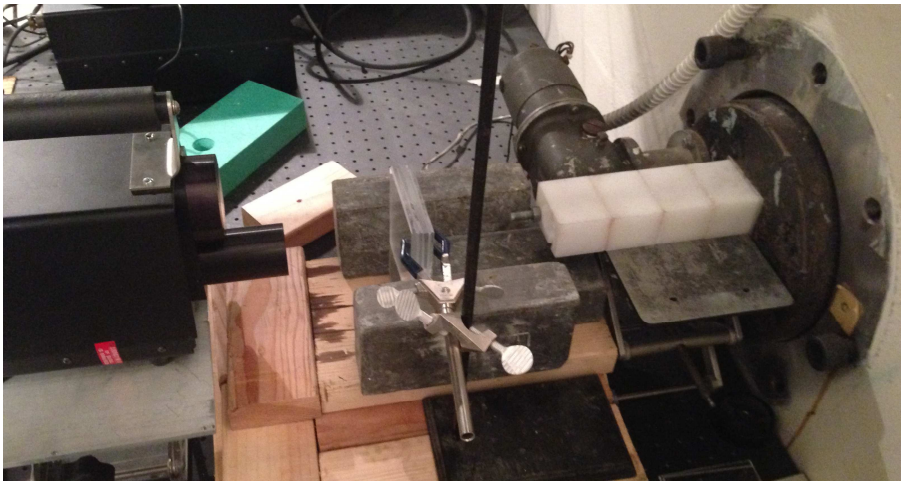

Figure 2. Illistration of experimental setup

Since neutrons are neutral particles, they interact weakly with matter; it is for this reason that they have the potential to penetrate deeply. Light atoms (e.g, hydrogen, oxygen) can interact with neutrons with a high interaction probability. If a narrow beam attenuation experiment is implimented for neutrons, as shown in Fig. (2), the number of neutrons will decrease exponentially with absorber thickness. The relationship between incoming neutron beam and transmitted beam is given as

$$I = I_0 . e^{-\Sigma_{TOT} . x} \tag{3}$$

where Σ_{TOT} is the total macroscobic cross section which is the probability per unit path length that any interaction type will take place and x is the thickness of the absorber [17]. The total macroscopic cross section is given as

$$\Sigma_{TOT} = \Sigma_a + \Sigma_s + .. \tag{4}$$

where Σ_a is absorbtion cross section and Σ_s is the scattered cross section. Fig. (3) illustrates the neutron capture and scattering interaction probabilities in the matter and assumes that

only those neutrons do not interact with matter will arrive to the detector. Assuming the incident number of true neutrons (n_0) is equal to the intensity of incident neutrons (I_0), then the transmitted number of true neutrons (n_1) can be expressed as

$$n_1 = n_0 . e^{-\Sigma_{TOT} . x} \tag{5}$$

The total macroscopic cross section can be calculated for neutrons as the following:

$$\Sigma_{TOT} = -\frac{1}{x} \ln(\frac{n_1}{n_0}) \tag{6}$$

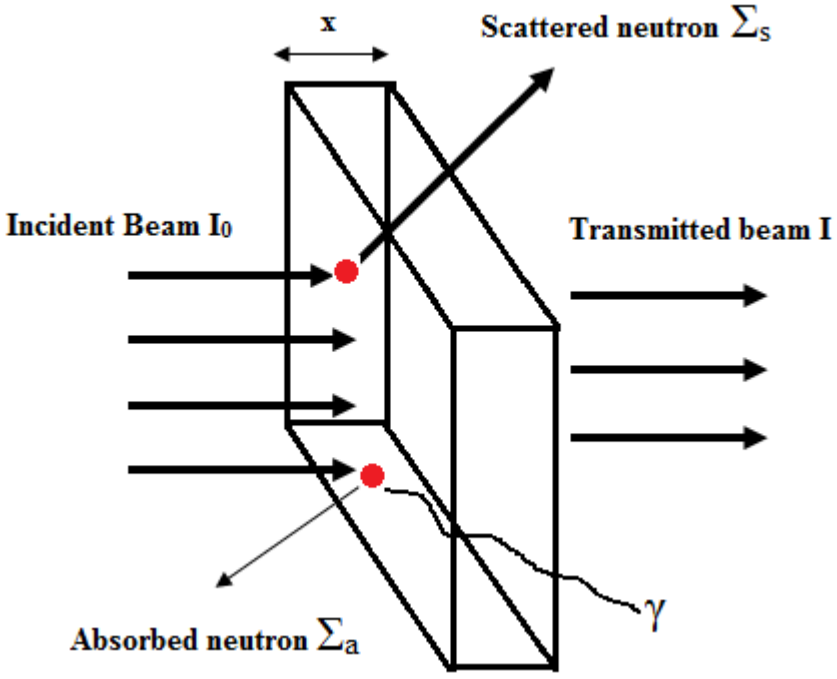

Figure 3. Neutron capture and scrattering interaction probabilities

With no Plexiglas between the detector and collimator, the non-paralyzing measured count rate can be written as the following:

$$m_0 = \frac{n_0}{1+n_0\tau} \tag{7}$$

where m_0 is the measured count rate and n_0 is the true count rate with no shielding or absorber between the detector and collimator. With the addition of shielding and/or absorber between the detector and collimator, the non-paralyzing model becomes

$$m_1 = \frac{n_1}{1+n_1\tau} \tag{8}$$

If another layer of shielding and/or absorber were added between the detector and collimator, then m_1 and n_1 would become m_2 and n_2, respectively. The ratio between m_0 and m_1 is given as

$$\frac{m_0}{m_1} = \left(\frac{n_0}{1+n_0\tau}\right).\left(\frac{1+n_1\tau}{n_1}\right) \tag{9}$$

where n1 is shown in Eq. (5). Substituting this into Eq. (9) provides the following ratio:

$$\frac{m_0}{m_1} = \left[\frac{1+n_0\tau e^{-\Sigma_{TOT}.x}}{(1+n_0\tau).e^{-\Sigma_{TOT}.x}}\right] \tag{10}$$

If there was a second shielding layer, Eq. (10) would become;

$$\frac{m_0}{m_2} = \left[\frac{1+n_0\tau e^{-\Sigma_{TOT}.2x}}{(1+n_0\tau).e^{-\Sigma_{TOT}.2x}}\right] \tag{11}$$

From Eq. (10) and (11), it is evident that the $n_0\tau$ parameters are the same for both equations. The $n_0\tau$ parameter from Eq. (10) is;

$$n_0\tau = \left[\frac{\frac{m_0}{m_1} e^{-\Sigma_{TOT}.x} - 1}{e^{-\Sigma_{TOT}.x} - \frac{m_0}{m_1} e^{-\Sigma_{TOT}.x}} \right] \tag{12}$$

The $n_0\tau$ parameter from Eq. (11) is;

$$n_0\tau = \left[\frac{\frac{m_0}{m_2} e^{-\Sigma_{TOT}.2x} - 1}{e^{-\Sigma_{TOT}.2x} - \frac{m_0}{m_2} e^{-\Sigma_{TOT}.2x}} \right] \tag{13}$$

Therefore, Eqs. (12) and (13) are equal

$$\left[\frac{\frac{m_0}{m_1} e^{-\Sigma_{TOT}.x} - 1}{e^{-\Sigma_{TOT}.x} - \frac{m_0}{m_1} e^{-\Sigma_{TOT}.x}} \right] = \left[\frac{\frac{m_0}{m_2} e^{-\Sigma_{TOT}.2x} - 1}{e^{-\Sigma_{TOT}.2x} - \frac{m_0}{m_2} e^{-\Sigma_{TOT}.2x}} \right] \tag{14}$$

The only unknown in Eq. (14) is the total macroscopic cross section (Σ_{TOT}) of Plexiglas. Plugging all known parameters into Eq. (14) will give total macroscopic cross section. Once the total macroscopic cross section is found, Eq. (12) can be used to find the $n_0\tau$ parameter, which in turn can be used in Eq. (7) to find the true count rate (n_0) for non-paralyzing model. Using the true count rate (n_0) and measured count rate (m_0) in Eq. (7) will give the detector's dead-time for non-paralyzing model. This same methodology can be applied for any thickness, so that dead-time of the detector can be determined for all thicknesses. Using the same ratio technique demonstrated with non-paralyzing method

equations, the ratio between m_0 and m_1 can be calculated for the paralyzing model. This ratio is shown in Eq. (15)

$$\ln\left(\frac{m_0}{m_1}\right) = -n_0\tau + \Sigma_{TOT}.x + n_0\tau.e^{-\Sigma_{TOT}.x} \tag{15}$$

If there was second shielding layer, Eq. (15) would become the following:

$$\ln\left(\frac{m_0}{m_2}\right) = -n_0\tau + \Sigma_{TOT}.2x + n_0\tau.e^{-\Sigma_{TOT}.2x} \tag{16}$$

As evidenced by from Eqs. (15) and (16) the $n_0\tau$ parameters are the same for both equations. The $n_0\tau$ parameter from Eq. (15) is;

$$n_0\tau = \frac{\ln\left(\frac{m_0}{m_1}\right) - \Sigma_{TOT}.x}{e^{-\Sigma_{TOT}.x} - 1} \tag{17}$$

The $n_0\tau$ parameter from Eq. (16) is;

$$n_0\tau = \frac{\ln\left(\frac{m_0}{m_2}\right) - \Sigma_{TOT}.2x}{e^{-\Sigma_{TOT}.2x} - 1} \tag{18}$$

Therefore, Eqs (17) and (18) are equal

$$\frac{\ln\left(\frac{m_0}{m_1}\right) - \Sigma_{TOT}.x}{e^{-\Sigma_{TOT}.x} - 1} = \frac{\ln\left(\frac{m_0}{m_2}\right) - \Sigma_{TOT}.2x}{e^{-\Sigma_{TOT}.2x} - 1} \tag{19}$$

As in the non-paralyzing model case, there is only one unknown in Eq. (19): the total total macroscopic cross section (Σ_{TOT}) of Plexiglas. Plugging all known parameters into Eq. (19) gives the total macroscopic cross section. Once the total macroscopic cross section is obtained, Eq. (17) can be used to find the $n_0\tau$ parameter, which can then be used in Eq. (20) to find the true count rate (n_0) for paralyzing model. Using the true count rate (n_0) and measured count rate (m_0) in Eq. (20) will provide the detector's dead-time for the paralyzing model. This same methodology can be applied for any thickness, thus dead-time of the detector can be obtain for all thicknesses.

$$m_0 = n_0 e^{-n_0\tau} \tag{20}$$

2.2 Dead-time Experiment for Canberra ^{3}He Detector

The following procedure used to calculate the dead-time of a gas filled Canberra ^{3}He detector. The Missouri University of Science and Technology (MS&T) Subcritical Assembly was filled with water and its plutonium-beryllium (PuBe) neutron source was placed in the center position (see Fig. 4). The Canberra ^{3}He detector was suspended inside an acrylic tube (to protect it from the water) and placed in the grid plate position A1 (5.08 cm center-to-center). A five minute count was taken and the detector was moved to the second position, A2, 10.16 cm from the source. This process was repeated for the remaining seven positions on the A axis and again along each of the five other axes – B, C, D, E, and F. This layout, which was also used for the MCNP simulations, can be seen in Fig. (5). The Canberra Lynx Digital Signal Analyzer was used to supply power to the detector and record counts [18].

An MCNP model of the Missouri S&T Subcritical Assembly was used to simulate the measurements. The model was developed by Tucker [15] and it was experimentally validated. Nine simulations were performed with the detector modeled in each of the nine detector locations along axis A. The water-filled cells between the source and the detector were give higher importance to ensure usable statistics. One hundred million histories were used for detector locations A1 through A6. One hundred fifty million histories were used for locations A7 through A9. Cell-averaged neutron flux (neutrons per square centimeter per source particle) was tallied over the detector gas portion of the modeled detector.

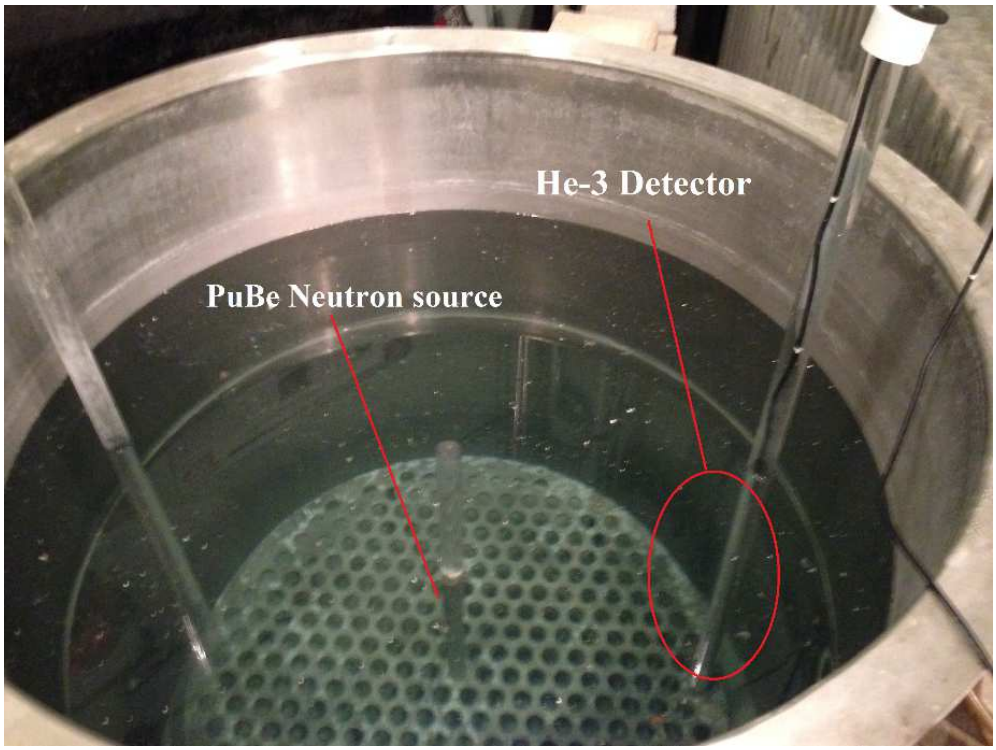

Figure 4. Picture of ^{3}He detector neutron measurements in subcritical assembly

Measurements of a plutonium-beryllium (Pu-Be) neutron source were taken from nine distances with the Canberra ^{3}He Detector in the Missouri University of Science and Technology (Missouri S&T) Subcritical Assembly. These measurements were compared

to the results from MCNP simulations. The difference between the measured and simulated values was used to estimate the detector's dead time.

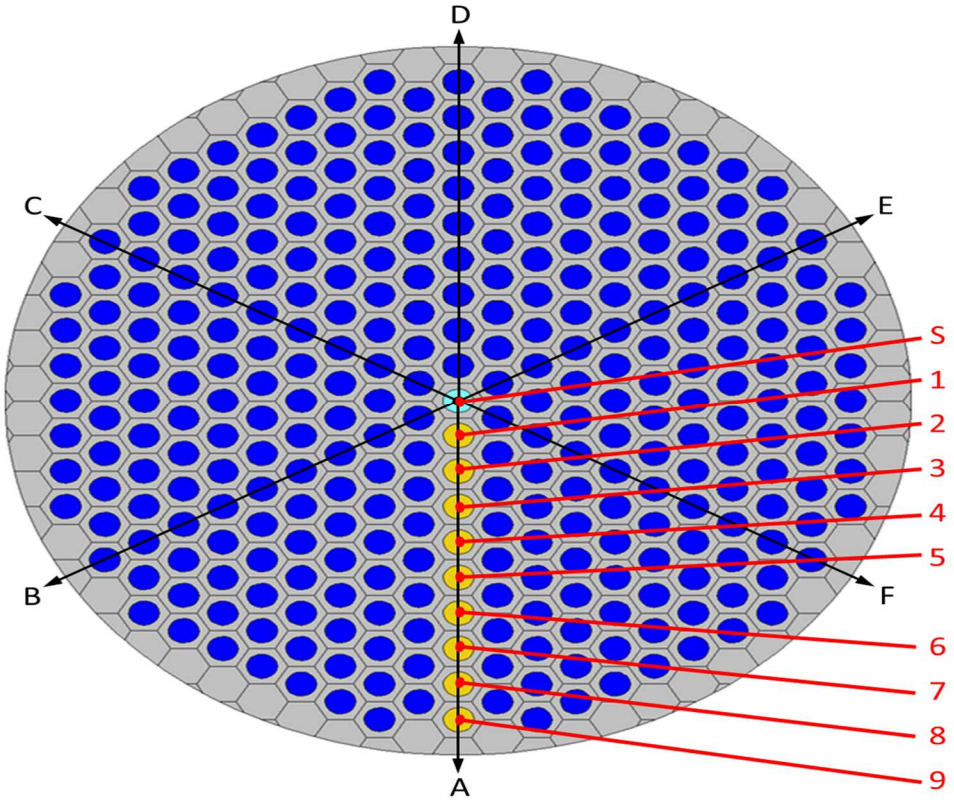

Figure 5. MCNP simulation layout. The Pu-Be neutron source (S) was placed in the center-most position of the subcritical assembly. Nine MCNP simulations and nine measurements were performed in the numbered locations on axis A. Five more sets of measurements, repeating those made on axis A were made on the five remaining axes.

3. Results

The fast neutron measurements were first taken without layer and six different thickness of Plexiglas layers. Data collection for each step was 10 minutes. The Plexiglas thickness changed from 0.5 cm to 3 cm with increment of 0.5 cm. The measurements are tabulated in Table 1 at 5 kW constant power for each thickness.

Fig. (4) shows the graph of neutron count rate with different thickness of Plexiglas. Errors propagations were calculated based on one standard deviation (1σ) and are included on the graphs. The first count without any Plexiglas for fast neutrons using the N-Probe spectrometer was 3463.09 per second and the counts decreased with increment of Plexiglas thickness. The last count for fast neutron measurement with 3 cm thickness of Plexiglas was 2995.82 per second.

Table 1. The fast neutron measurements using N-Probe at 5 kW power

Plexiglas thickness (cm)	N-Probe Fast Neutrons counts	Count rates
0	2077857	3463.09 ± 58.85
0.5	2035029	3391.71 ± 58.24
1	1986735	3311.22 ± 57.54
1.5	1938566	3230.94 ± 56.84
2	1893107	3155.17 ± 56.17
2.5	1842570	3070.95 ± 55.42
3	1797494	2995.82 ± 54.73

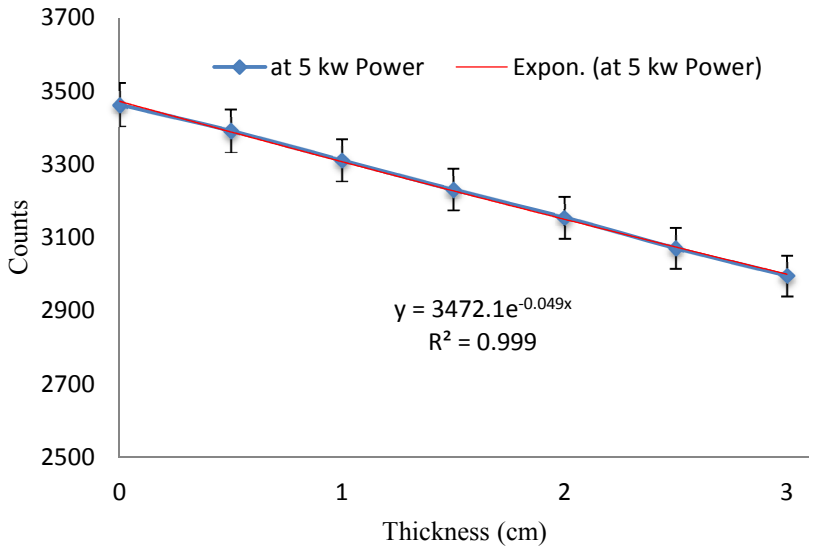

Figure 6. Fast neutron count rates with different thickness of Plexiglass at 5 kw power.

Eqs. (14) and (19) were used to calculate the non-paralyzing total macroscopic cross section and paralyzing total macroscopic cross section, respectively, for Plexiglas. The results for the total macroscopic cross section for average neutrons are tabulated in Table 2. The total macroscopic cross sections were calculated based on total counts of fast neutrons (fast neutrons vary from 800 keV to 20 MeV) for the N-Probe. The total absorption cross section of a Plexiglas can be calculated for a specific neutron energy using the same method. Since the fast neutron energies are widely distributed in a constant beam flux, calculations of total macroscopic cross sections were complete for all counts.

Table 2. Total macroscopic cross section (Σ_{TOT}) for Plexiglas using all counts

Plexiglas Thickness (cm)	Σ_{TOT} (1/cm) Non-Paralyzing Method	Σ_{TOT} (1/cm) Paralyzing Method
0.5	0.329919	0.137613

The average macroscopic cross section of Plexiglas using the N-Probe liquid scintillator (Fast probe) was calculated to be 0.329919 cm^{-1} for the non-paralyzing model and 0.137613 cm^{-1} for the paralyzing model.

Based on a combination of the attenuation law and non-paralyzing and paralyzing dead-time models, the dead-time of the fast probe (N-Probe detector) was calculated. Eqs. (7), (13) and (14) were used to calculate dead-time for the non-paralyzing model while Eqs. (17), (19) and (20) were used to calculate dead-time for the paralyzing model. Table 3 shows all the dead-time calculations for the N-Probe detector. Non-paralyzing average dead-time of the detector was found to be 254.8 μs with an error of ± 4.91 and paralyzing average dead-time of the detector was found to be 101.2 μs with an error of ± 2.43. As expected non-paralyzing dead-time of the detector was higher than paralyzing dead-time.

Error propagations (S_τ) of dead-time measurements for both idealized models were calculated using Eq. (21). s_m and s_n are individual errors of measured counts and true counts.

$$S_\tau^2 = (s_m \frac{\partial \tau}{\partial m})^2 + (s_n \frac{\partial \tau}{\partial n})^2 \quad (21)$$

Table 3. Dead-time calculations of N-Probe for two ideal models

Plexiglas thickness (cm)	Non-Paralyzing Dead-time (μs)	Errors	Paralyzing Dead-time (μs)	Errors
0	254.8	± 4.91	101.2	± 2.43

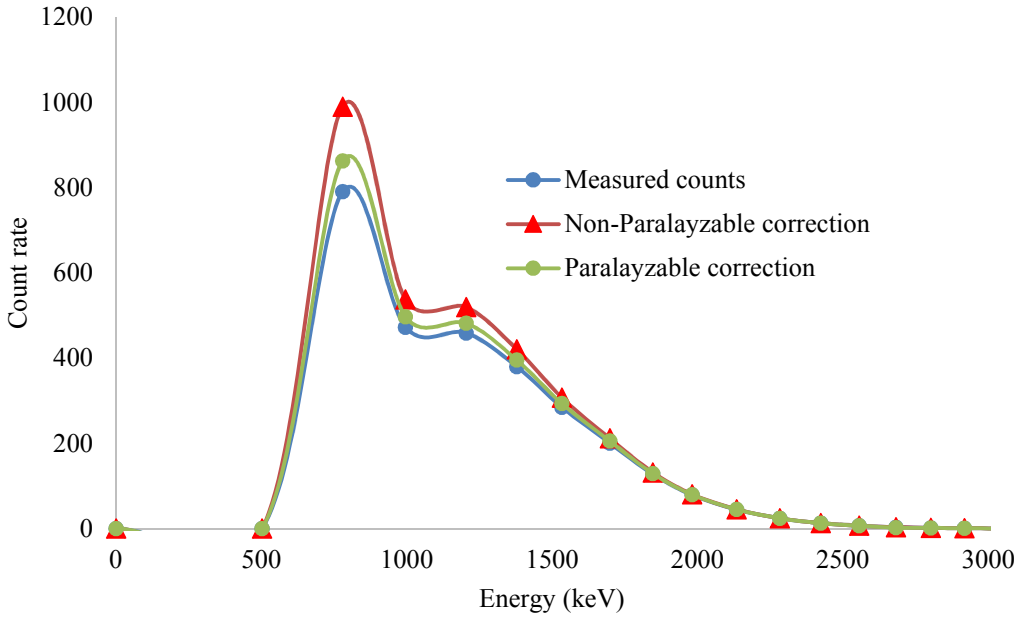

Figure 7. High count rate fast measurement and corrected count rates.

After calculating the dead-time of the detector, a high count rate experiment was conducted and the count rates were corrected using non-paralyzing and paralyzing dead-times (see Fig. 7). As count rate increases, the dead-time effect of the detector increases.

The dead-time effect is almost negligible at low count rates. In the experiment, fast neutron counts were high at around 900 keV and the dead-time effect can be separable.

Measurements of a plutonium-beryllium (PuBe) neutron source were taken from nine distances with the Canberra ^{3}He detector in the Missouri University of Science and Technology (MS&T) Subcritical Assembly. These measurements were compared to results from the MCNP simulations. The difference between the measured and simulated values was used to estimate the detector's dead-time. The results of the measurements are provided in Table 4.

The results of the measurements (counts per second) and simulations (n cm^{-2} sp^{-1}) cannot be directly compared so both sets of data were normalized to their smallest value (see Fig. 8). In order to calculate detector dead time, the true and measured count rates must be known. The collection of the measured count rate has already been discussed. The MCNP results were used to generate the true count rate. To do this, each tally result generated by MCNP was divided by the tally result for the ninth detector position (45.72 cm from the source) and multiplied by the measured value at the ninth detector position as seen in Eq. (22).

$$True\ Count\ Rate = \frac{S_i}{S_9} M_9 \tag{22}$$

Where S represents the tally result from MCNP and M represents the measured value. Eq. (22) was applied to the results for the eight closest detector distances and the dead-time at each location was calculated according to both the paralyzing and non-paralyzing models. The ninth location was excluded because the normalization process made it impossible to calculate a dead-time using Eq. (22). The results of the simulations

Table 4. Neutron measurements from the Canberra ^{3}He Detector in the Subcritical Assembly

Distance from PuBe neutron source (cm)	**Count rate (counts s^{-1})**
5.08	12661.98 ± 156.32
10.16	7522.19 ± 53.33
15.24	2935.79 ± 56.30
20.32	1101.94 ± 26.70
25.40	439.10 ± 30.23
30.48	174.85 ± 5.29
35.56	74.17 ± 2.06
40.64	33.18 ± 0.68
45.72	15.44 ± 0.52

Table 5. Results of MCNP simulations of Canberra ^{3}He neutron detector in the Subcritical Assembly

Distance from PuBe neutron source (cm)	**Cell-averaged Flux Tally Result (n cm^{-2} sp^{-1})**
5.08	2.40851E-03 ± 4.09447E-06
10.16	1.43884E-03 ± 3.02156E-06
15.24	5.57542E-04 ± 1.95140E-06
20.32	2.01799E-04 ± 1.10989E-06
25.40	7.43707E-05 ± 6.76773E-07
30.48	2.98034E-05 ± 4.26189E-07
35.56	1.21184E-05 ± 2.13284E-07
40.64	5.59834E-06 ± 1.45557E-07
45.72	2.32741E-06 ± 9.12345E-08

are provided in Table 5. The paralyzing dead-time was calculated to be 14.5 μs, and the non-paralyzing dead-time was calculated to be 16.4 μs.

Eq. (22) was applied to the results for the eight closest detector distances and the dead-time at each location was calculated according to both the paralying and non-paralyzing models. The ninth location was excluded because the normalization process made it impossible to calculate a dead-time using Eq. (22). The results of the simulations are provided in Table 5. The paralyzing dead-time was calculated to be 14.5 μs, and the non-paralyzing dead-time was calculated to be 16.4 μs.

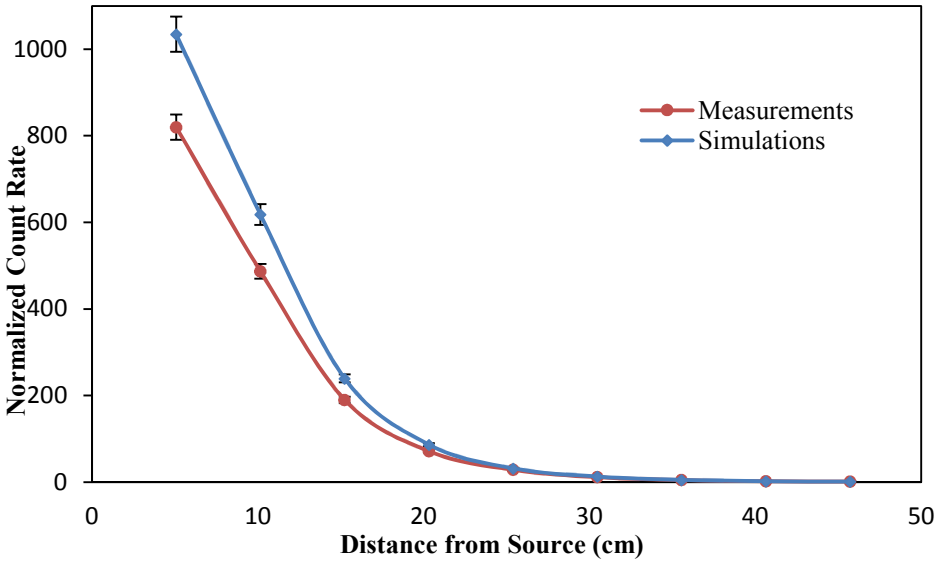

Figure 8. The results of the measurements and simulations, normalized to their lowest values for comparison.

4. Conclusion

The N-Probe utilizes two different spectroscopic techniques for providing neutron spectrum. From 800 keV to 20 MeV, the fast neutron energy region is measured by a liquid scintillator combined with a photon discriminator (fast probe). From 0 to 800 keV the

thermal neutron energy region is measured by a spherical ^{3}He detector. The dead-time of the fast probe was determined via the combination of the attenuation law and idealized dead-time models. All measurements were taken in front of the beam port at the Missouri S&T Research Reactor while at 5 kW constant power. Average paralyzing dead-time value was found to be 101.2 ± 2.43 μs, while the average non-paralyzing dead-time value was found to be 254.8 ± 4.91 μs. Dead-time values for the fast probe were higher than expected since average liquid scintillator dead-time is 1 to 5 μs [6]. The total macroscopic cross sections of Plexiglas were also calculated with all counts for both idealized dead-time models. The same method was used to calculate the dead-time of the N-Probe thermal neutron probe at 5 kW power (constant flux). However, some fast neutrons thermalize when the layers of Plexiglas is placed in front of detector. These thermalized neutrons affect the dead-time calculations and result in negative dead-time values.

The dead-time of a tube-type Canberra ^{3}He gas-filled detector was calculated for both non-paralyzing and paralyzing dead-time models using subcritical assembly measurements and MCNP simulations. The paralyzing dead-time was calculated to be 14.5 μs, and the non-paralyzing dead-time was calculated to be 16.4 μs for ^{3}He gas filled detector. The dead-time of gas-filled proportional (especially GM counters) detectors generally lies between 100 and 300 μs [6]. However, Loaiza [19] used a two source model to calculate the dead-time of a ^{3}He proportional counter and its dead-time was found to be 0.46 μs. We have not used two source method to determine the dead-time of the detector since no neutron source available.

REFERENCES

[1] V. V. Verbinski, and et. al., Calibration of an organic scintillator for neutron spectrometry. Nucl. Instrum. Methods 65, 8–25, (1968)

[2] J. A. Harvey, and N. W/ Hill, Scintillation detectors for fast neutron physics, Nucl. Instrum. Meth. 162, 507, (1979).

[3] I. Yousuke, and et. al., "Deterioration of pulse-shape discrimination in liquid organic scintillator at high energies". Nuclear Science Symposium Conference Record, 1,219–221, (2000).

[4] G. F. Knoll, Radiation Detection and Measurement. 4th Edition, p.573, 2010, John Willey & Sons Inc, USA.

[5] M. Karlsson, Absolute efficiency calibration of NE-213 liquid scintillator using a 252Cf source, The Department of Nuclear Physics in Lund University, Sweden, 1997

[6] N. Tsoulfanidis, S. Landsberger, Measurement and Detection of Radiation. 3th Edition, 2011, CRC Press. Taylor & Francis Group. New York.

[7] T. W. Krane, and M. N. Baker, Neutron Detectors Chapter 13, http://www.lanl.gov/orgs/n/n1/panda/00326408.pdf (Accessed, September 2014).

[8] G. F. Knoll, Radiation Detection and Measurement. 4th Edition, p.523, 2010, John Willey & Sons Inc, USA.

[9] H. Ing, and et. al., Portable Spectroscopic Neutron Probe, Radiation Protection Dosimetry, 126, 238-243, (2007).

[10] Mobile Microspec Operational Manual, Bubble Technology Industries Inc (BTI), Revised: October 30, 2009.

[11] J.W. Muller, Dead-time problems. Nuclear Instruments and Methods. 112, 47-57, (1973)

[12] J.W. Muller, Generalized Dead Times, Nuclear Instruments and Methods, 301,543-551, (1991)

[13] H. G. Stever, The discharge mechanism of fast G-M counters from the dead-time experiment, Phys. Rev. 61, 38-52, (1942).

[14] W. Feller, On probability problems in the theory of counters, in R. Courant Anniversary volume, Studies and Essays. Interscience. New York. 105-115, (1948).

[15] L. P. Tucker, Upgrade and simulation of the subcritical assembly at Missouri University of Science and Technology, Master's Thesis, Missouri University of Science and Technology. Rolla, MO. 2011.

[16] http://nuclear.mst.edu/research/reactor/

[17] J. R. Lamarsh, Introduction to Nuclear Engineering, 3rd Edition, p. 57, 2001, Prentice Hall, New Jersey, USA

[18] Canberra Industries, Inc., Lynx Digital Signal Analyzer Data Sheet, Meriden, Conn., 2012.

[19] D. J. Loaiza, High-efficiency 3He proportional counter for detection of delayed neutrons, Nuclear Instuments and Methods in Physics Research A, 422, (1999), 43-46.

IV. CHARACTERIZATION OF BEST CANDIDATE ISOTOPES FOR BURNUP ANALYSIS AND MONITORING OF IRRADIATED FUEL

T. Akyurek, L.P. Tucker, and S. Usman
Department of Mining and Nuclear Engineering, Missouri University of Science & Technology, Rolla, MO 65409, USA

Abstract

This research is an extension of feasibility study of MOX fuel online burnup analysis. A multitude of fission products identified as candidates have been scrutinized for their suitability of burnup analysis and spent fuel analysis. Best isotopes obtained for analysis by investigating half-life, fission yield, branching ratios, production modes, thermal neutron absorption cross section and fuel matrix diffusivity. ^{132}I and ^{97}Nb are identified as good isotope candidates for on-line burnup analysis. ^{132}I is also a good candidate for plutonium/uranium discrimination due to the large difference in the fission yield of the isotope. For interim storage monitoring the well-established cesium isotopes appears to be the best choices unless the data gaps are addressed. Only alternate for cesium for interim monitoring is ^{131}I at the present time. For the long-term storage monitoring ^{94}Nb is the most attractive candidate. It has a low diffusion rate of ~10^{-11} cm^2/s, an almost zero neutron absorption cross section making it burnup history independent and decent gamma yield of 1.44E-09. In addition, the paper also identifies the data gaps for developing a robust burnup analysis tool using gamma spectroscopy.

1. Introduction

Between 1977 and 1981 commercial reprocessing was banned by the United States government, interrupting the U.S. reprocessing industry. The U.S. moratorium on

reprocessing did not, however, discourage European countries such as France from developing the technology and incorporating Mixed OXide (MOX) fuel into their nuclear fuel cycle. While other nations pursued reprocessing, the U.S. chose to invest in the Yucca Mountain Nuclear Waste Repository. However, with Yucca Mountain no longer under consideration, the U.S. is reconsidering its fuel cycle options, and taking a second look at reprocessing and MOX fuel [1, 2].

Decades of operation in France have demonstrated that MOX fuel can be incorporated into a UO_2 fueled core without risking the safety of the plant or increasing the risk of proliferation [3]. Now the U.S. power industry is investigating the fuel. In 2005, Duke Energy commissioned AREVA to build four MOX fuel assemblies for the Catawba Nuclear Station. The Megatons to Megawatts program is another major commitment by the U.S to incorporate MOX into the fuel cycle. This program is an agreement between the United States and Russia to dispose of approximately 35 metric tons (MT) of weapons-grade plutonium by converting it into MOX fuel to be burned in commercial nuclear power plants. The MOX fuel assemblies will be manufactured at the Department of Energy's Savannah River Site through a contract with Duke COGEMA Stone & Webster. As of July 2012, this program has converted 450 MT of weapons-grade uranium to low-enriched fuel for power reactors [4].

Thorium fueled reactors are also under consideration because of the advantages of the thorium fuel cycle. Thorium is abundant in the earth's crust. With roughly four times the concentration of uranium, it can be found across the globe. And because ^{238}U is not usually present in thorium fuel there are fewer transuranic elements in the spent fuel [5].

Regardless of how the U.S. fuel cycle changes, better tools and techniques for measuring burnup and monitoring spent fuel will be required. One attractive option for non-destructively examining spent fuel is gamma spectroscopy. In this work, a multitude of fission products identified as candidates for burnup analysis and spent fuel monitoring, as proposed by Dennis and Usman [6], are scrutinized for their suitability for such a program. Consideration is given to half-life, fission yield, branching ratios, thermal neutron absorption cross section, production modes and fuel matrix diffusivity. Based on these parameters, the best isotopes for non-destructive burnup analysis and spent fuel monitoring have been identified.

2. Traditional Tools, Techniques and Conventional Isotopes for Burnup Analysis

A report was published by US Nuclear Regulatory Commission [7] discussing various aspects of spent fuel monitoring and the requirements of the measurements system. There are two broad groups of techniques available; “passive” measurement of delayed neutrons and gamma and “active” interrogation by either a pulsed neutron source or a weak steady state source and subsequently monitoring the gamma and/or neutron emissions. For safe transportation of spent nuclear fuel it is critical to have a reliable and efficient monitoring system capable of on-site, accurate measurement of the spent fuel to ensure compliance with the safety criteria. Gamma measurement is one non-destructive technique (NDA) for spent fuel monitoring, analyzing the radiation emitted by irradiated nuclear fuel assemblies to determine parameters such as burnup, cooling time, and a qualitative verification of the irradiation history [8]. These parameters can be calculated with the help of flux measurements in the core and following the path of the fuel assembly as it proceeds with its burnup cycle. These calculations can be experimentally verified by the above

mentioned techniques. Willman and co-workers [9] have investigated ^{137}Cs ($T_{1/2}$ = 30.1 years), ^{134}Cs ($T_{1/2}$ = 2.1 years) and ^{154}Eu ($T_{1/2}$ = 8.6 years) as indictors of cooling time and irradiation history since these isotopes dominate the gamma spectrum of spent fuel after five years of cooling time [7]. Moreover, the isotope has very small neutron absorption cross sections and hence negligible burnup history dependence and its fission yields from ^{235}U and ^{239}Pu is approximately the same. Willman and co-worker [10] has reported the success of using ^{154}Eu while Dennis and Usman [11] reported the potential of using ^{106}Ru. Because of their relatively long half-lives, these isotopes are most useful for analyzing used fuel after about 10 years of cooling. Focus of this manuscript is to analyze new isotopes for their suitability as a burnup indicator. The conventional fission isotopes (^{137}Cs, ^{154}Eu, ^{106}Ru etc.) already considered for burnup analysis are not included in this discussion with the exception of ^{134}Cs which is included for comparison. Interested reader may refer to literature [8-11] for discussion on the conventional burnup isotopes.

Another NDA technique for power reactor released spent fuel is based on neutron measurements. A series of neutron absorptions in ^{238}U leads to the production of ^{244}Cm. Spontaneous fission of ^{244}Cm provides a source of "delayed neutron". Since the half-life of ^{244}Cm is 18.1 years, neutron intensity from ^{244}Cm is a measure of burnup. This technique is highly sensitive to cooling time, and initial enrichment for the spent fuel. Additional information on neutron measurement based burnup calculation is available in the literature [12].

Additionally, chemical assay with mass spectroscopic techniques [13] have historically been applied to determine isotopic composition of spent nuclear fuel but these techniques requires fuel sample destruction and can take a long time for sample analysis

and results. Recent new attempts for spent nuclear fuel analysis include use of digital measurement of Cherenkov [14]. A patent is also been filed by Dowdy and co-workers [15] on the application of Cherenkov radiation for irradiated fuel monitoring.

Focus of this manuscript is to compare the advantages of various isotopes for gamma emission based spent fuel measurement. While other techniques are available but gamma measurement based spent fuel monitoring is by far the most commonly used technique.

3. Important Indicators Characteristics for Burnup Analysis and Fuel Monitoring

Burnup measurement are useful for a number of applications including; pre-transportation compliance certification, monitoring of spent fuel for Special Nuclear Material (SNM) accountability and proliferation deterrence, monitoring during storage for historic burnup analysis and online burnup measurement for next generation reactors for fuel cycle optimization. Additional spent fuel monitoring is required during reprocessing operation. For each of these application one or more of the techniques described in the previous section is better suited than others.

Half-life of the burnup indicator isotope is one characteristic that can dramatically impact its suitability for different applications; online applications, interim storage (short-term) and long-term storage (historical data). A nuclide with a half-life between minutes and days is ideal for online burnup determination but useless for historical data collection. For interim storage-pool monitoring, the indicator's half-life should be between a few days and a few years. Burnup indicators for long-term storage applications should have half-lives greater than few years.

Another desirable characteristic for burnup and used fuel monitoring indicators is a simple production mode and a simple decay chain. Generally, it is significantly more complicated to track the decay of a candidate isotope with multiple decay modes and multiple production modes, which via direct fission and by decay of several fission products. However, in certain situations this can be an advantage. A single production path (production from single parent nuclide or direct production from fission) coupled with a high fission yield ensures that a detectable amount of the isotope would be present. Since the emitted gamma rays must potentially penetrate several layers of fuel, cladding, and moderator, a high energy gamma ray (on the order of MeV) with a high branching ratio is also necessary for detectability.

It is also important for the indicator isotope to remain in the fuel where it was created after it is produced. Therefore, the neutron capture cross-section must be as low as possible and must not exceed more than a few barns so that product atoms density is independent of burnup history. Small neutron absorption cross section also ensures that burnup indicator isotope generated from fission is not subsequently consumed by parasitic neutron absorption. Low fission product migration at high temperatures is another desirable characteristic. The fission product must ideally remain where it was created. Any migration of fission products will skew the burnup profile of the assembly [16].

4. Candidate Isotopes

^{137}Cs, ^{134}Cs and ^{154}Eu are commonly used isotopes for burnup analysis and fuel monitoring. Recently Willman et al. investigated two correlations between burnup and the intensity of these isotopes. They proposed a linear correlation between burnup and the intensity of the 661.7 keV ^{137}Cs peak while they found that ^{154}Eu and ^{134}Cs is related to the

square of burnup [9]. Hawari and co-workers [17] have considered gamma spectrometry of Cs-137 and Eu-154 for online burnup monitoring of pebble bed reactors. Jansson and co-workers [18] provide corroborating evidence that there is a correlation between ^{137}Cs intensity and burnup for Pressurized Water Reactor (PWR) assemblies [18]. Dennis and Usman [11] proposed ^{106}Ru isotope for MOX fuel burnup analysis. They studied the feasibility of using ^{106}Ru as a burnup indicator for UO_2 fuel and as a means for discriminating between MOX and UO_2 fuel. Their ORIGEN-ARP (Oak Ridge Isotope Generation and Depletion Code – Automatic Rapid Processing) simulations showed a linear correlation between primary photopeak intensity and MOX fuel assembly burnup for ^{137}Cs and ^{106}Ru. They relied on using peak ratios rather than raw peak counts to normalize and remove the burnup history dependence.

This paper analyzes the list of candidate isotopes proposed by Dennis and Usman [6] for their suitability for burnup analysis application. These isotopes are listed in Table 1. To complete the analysis, data was collected on the half-life, fission yield, branching ratios, diffusivity, and neutron absorption cross section for each of the candidate isotope. Some nuclides lacked data for some of these characteristics, leaving room for additional research. However, based on an analysis of the data that was available, the best isotopes for burnup analysis and irradiated fuel monitoring have been identified.

There are some isotopes in Table 1 that decay with virtually identical photon energies. For example, ^{137m}Ba, ^{98}Tc, and ^{132}Cs have almost same photon energy and emission probability values. It would be difficult to distinguish these isotopes based on gamma spectroscopy alone. However, their half-lives differ by orders of magnitude. ^{137m}Ba has a half-life of 2.55 min, which will decay quickly. The half-life of ^{98}Tc is 4.2 million

years, making it practically stable. ^{132}Cs has half-life of 6.48 days. For these situations one may consider using an unfolding technique to determine correct apportionment of summed peak and separating say ^{137m}Ba from ^{98}Tc.

Table 1. Reference isotopes for burnup analysis and spent fuel monitoring [6]

Simulation Energy (keV)	Potential Isotope	Energy (MeV)	Photon Emission Probablity	Simulation Energy (keV)	Potential Isotope	Energy (MeV)	Photon Emission Probablity
76.6110	^{243}Am	0.07467	0.66	617.82	^{108m}Ag	0.61437	0.90393
	^{206}Bi	0.074969	0.54146		^{43}K	0.61749	0.80514
	^{61}Co	0.067412	0.85		^{190m}Os	0.61608	0.9862
	^{73}Se	0.067	0.7729601		^{144}Pm	0.61801	0.98597
	^{44}Ti	0.07838	0.97619	626.15	^{43}K	0.61749	0.80514
93.2640	^{49}Cr	0.090639	0.532		^{144}Pm	0.61801	0.98597
101.5900	^{67}Ga	0.93311	0.357		^{148m}Pm	0.62997	0.88998
134.9000	^{99m}Tc	0.14051	0.8907	659.46	^{137m}Ba	0.66165	0.8998
143.2200	^{99m}Tc	0.14051	0.8907		^{132}Cs	0.66769	0.97423
	^{85m}Kr	0.15118	0.75278		^{130}I	0.66854	0.96129
159.8700	^{52}Fe	0.016868	0.966		^{132}I	0.66769	0.987
	^{56}Ni	0.15838	0.98795		^{97}Nb	0.6579	0.9809
176.5300	^{52}Fe	0.016868	0.966		^{126}Sb	0.66633	0.99619
	^{111}Ln	0.17128	0.9024	667.78	^{137m}Ba	0.66165	0.8998
193.1800	^{90}Y	0.20251	0.96631		^{98}Tc	0.65241	0.99745
	^{166m}Ho	0.18442	0.726		^{132}Cs	0.66799	0.97423
	^{190m}Os	0.18673	0.702		^{130}I	0.66854	0.96129
226.4900	^{85m}Sr	0.23169	0.84725		^{132}I	0.66769	0.987
	^{132}Te	0.22816	0.88	692.76	^{97}Nb	0.6579	0.9809
276.4400	^{203}Hg	0.27919	0.773		^{126}Sb	0.66633	0.99619
	^{203}Pb	0.27919	0.768		^{94}Nb	0.70293	1
318.0800	^{192}Ir	0.31651	0.82853	717.74	^{144}Pm	0.69649	0.99492
	^{5}1Ti	0.32008	0.929		^{126}Sb	0.695	0.99619
	^{157}Dy	0.32616	0.938		^{108m}Ag	0.72295	0.90499
326.4000	^{194m}Ir	0.32845	0.929	751.05	^{166m}Ho	0.71169	0.54087
	^{51}Ti	0.32008	0.929		^{126}Sb	0.7205	0.53794
	^{157}Dy	0.32616	09.38		^{244}Am	0.746	0.67

Table 1 continued.

359.71	^{73}Se	0.3611	0.965		^{52}Mn	0.74421	0.9
	^{190m}Os	0.36109	0.9488		^{97m}Nb	0.74336	0.9796
	^{131}I	0.36448	0.81164	759.37	^{98}Tc	0.74535	0.99819
376.36	^{43}K	0.37276	0.87273		^{95}Zr	0.75671	0.55345
	^{204m}Pb	0.89915	0.99164		^{95}Nb	0.76579	0.99808
	^{200}Tl	0.36794	0.873	767.7	^{95}Tc	0.76579	0.9382
434.64	^{108m}Ag	0.43393	0.89881		^{95}Zr	0.75671	0.55345
	^{202}Tl	0.43956	0.915		^{82}Br	0.77649	0.8331
	^{69m}Zn	0.43863	0.94889		^{132}I1	0.77261	0.76196
484.6	^{181}Hf	0.48203	0.825	792.68	^{95}Nb	0.76579	0.99808
	^{194m}Ir	0.48286	0.97		^{95}Tc	0.76579	0.9382
	^{87}Y	0.4847	0.9394	809.33	^{134}Cs	0.79584	0.854
	^{90m}Y	0.47953	0.9099		^{210}Tl	0.7997	0.9896
492.93	^{190}Os	0.50255	0.9778		^{206}Bi	0.8031	0.9889
	^{103}Ru	0.49708	0.889		^{58}Co	0.81076	0.9943
	^{87}Y	0.4847	0.9394		^{136}Cs	0.8185	0.997
534.56	^{130}I	0.53609	0.99		^{166m}Ho	0.81031	0.57136
	^{133}I	0.52987	0.8632		^{56}Ni	0.81185	0.85996
	^{135m}Xe	0.52656	0.80997	1592	^{96}Tc	0.81254	0.81803
601.17	^{134}Cs	0.6047	0.976		^{210}Tl	0.7997	0.9896
	^{124}Sb	0.60271	0.978001		^{140}La	1.5965	0.9549

Table 2 lists the candidate isotopes from Table 1 with their half-lives and divides them into groups based on their usefulness for online burnup analysis, interim storage monitoring, and long-term or historical data applications. A cut off of ten minutes was used as the lower limit for online measurement system. This choice is based on the fact that at least 2-3 minutes would be required to transport the irradiated fuel to location where it can be measured. And a minimum of one minute count might be necessary for good statistics of the peak counts. However, if there is a slight uncertainty in the cooling/transport time the quality of measurement can be adversely impacted for a short lived isotope. Therefore

a ten minute lower limit is set for half-life for online burnup application. Hence, radioisotopes with half-lives less than ten minutes are not considered useful for any of these applications. This choice of ten minutes is also to ensure that during the measurement time (that is one min count) the activity is only going to reduce by less than 7%. Four isotopes are placed in Group 0 with half-lives less than 10 minutes and therefore minimum to no usefulness. There are 21 isotopes in Group 1 having half-lives between 10 minutes and 24 hours. Nuclides in Group 1 are suitable for online burnup analysis. For online measurement too long half-life is not useful either. The upper limit for online burnup applications half live is set at 24 hours. These choices are somewhat arbitrary. There are 30 isotopes in Group 2 with half-lives between 24 hours and 5 years. Group 2 nuclides are ideal for interim-storage pool monitoring applications. Group 3 encompasses potential tracers for long-term storage applications. There are six isotopes in Group 3 with half-life of 5 years or more. These isotopes are possibly best suited for historical data validations and long-term spent fuel monitoring.

a) Online burnup analysis – Candidate Isotopes

For the three applications in mind, next step is to evaluate the best isotopes for each application in regards to their physical properties; fission yield, branching ratio and gamma energies, neutron absorption cross section and diffusion parameters. Group 1 is candidate isotopes for online monitoring. Table 3 provides half-lives, emission probabilities (branching ratio), the corresponding gamma energies and fission yields (thermal neutron fission yield from uranium and plutonium) for all candidate isotopes for group 1. The last column in the table lists gamma yield (PxFY) which is the product of fission yield and emission probability and can be used as a figure of merits for an isotope's suitability as a

Table 2. Candidate isotopes grouped by half-life for burnup analysis [19]

	NOT USEFUL (GROUP 0)		ONLINE ANALYSIS (GROUP 1)		INTERIM STORAGE ANALYSIS (GROUP 2)		LONG-TERM STORAGE (GROUP 3)	
	Less than 9 min	**($T_{1/2}$) (min)**	**10 min – 24 hours**	**($T_{1/2}$) (min)**	**24 hours-5 years**	**($T_{1/2}$) (days)**	**5 years-more**	**($T_{1/2}$) (year)**
1	^{97m}Nb	0.9683	^{190m}Os	9.9	^{200}Tl	1.088	^{44}Ti	58.9
2	^{210}Tl	1.3	^{49}Cr	42.3	^{82}Br	1.47	^{108m}Ag	418
3	^{137m}Ba	2.55	^{204m}Pb	67.2	^{140}La	1.6785	^{166m}Ho	1200
4	^{51}Ti	5.77	^{85m}Sr	67.63	^{203}Pb	2.163	^{243}Am	7390
5			^{97}Nb	72.1	^{90}Y	2.67	^{94}Nb	20300
6			^{61}Co	99	^{111}In	2.8	^{98}Tc	4200000
7			^{132}I	137.7	^{132}Te	3.20		
8			^{90m}Y	191.4	^{67}Ga	3.26		
9			^{85m}Kr	268.8	^{87}Y	3.35		
10			^{99m}Tc	360	^{96}Tc	4.28		
11			^{73}Se	429	^{52}Mn	5.59		
12			^{157}Dy	488.4	^{56}Ni	6.075		
13			^{52}Fe	496.5	^{206}Bi	6.243		
14			^{244}Am	606	^{132}Cs	6.48		
15			^{130}I	741.6	^{131}I	8.0252		
16			^{69m}Zn	825.6	^{202}Tl	12.31		
17			^{135m}Xe	917.4	^{126}Sb	12.35		
18			^{95}Tc	1200	^{136}Cs	13.16		
19			^{133}I	1248	^{95}Nb	34.985		
20			^{43}K	1338	^{103}Ru	39.247		
21			^{200}Tl	1566	^{148m}Pm	41.3		
22					^{181}Hf	42.38		
23					^{203}Hg	46.594		
24					^{124}Sb	60.2		
25					^{95}Zr	64.032		
26					^{58}Co	70.86		
27					^{192}Ir	73.828		
28					^{194m}Ir	170		
29					^{144}Pm	363		
30					^{134}Cs	753.725		

burnup indicator. PxFY is in fact number of discrete energy gammas released per fission. Higher the PxFY is better suited the isotope would be for burnup applications. Table 3 also lists the ratio of the fission yield for ^{235}U and ^{239}Pu. This ratio is an indicator of the isotope's usefulness to be used as a discriminator between ^{235}U and ^{239}Pu.

Table 3. Group 1 fission product and decay characteristics [20, 21, 22, 23]
(Potential candidates for online measurements)

Isotope	Half-life (mins)	Emission Probability (%)	Energy (keV)	^{235}U Th. Fiss. Yield	^{239}Pu Th. Fiss. Yield	FY Ratio (^{235}U/^{239}Pu)	PxFY (^{235}U) Gamma yield
^{43}K	1338	86.8 79.16 11.85	372.76 617.49 396.86	N/A	N/A	N/A	N/A
^{49}Cr	42.3	53.2 30.32 16.39	90.64 152.93 62.29	N/A	N/A	N/A	N/A
^{52}Fe	496.5	99.18 1.64 0.21	168.69 377.75 1727.57	N/A	N/A	N/A	N/A
^{61}Co	99	84.67 0.79 3.62	67.42 841.7 909.2	N/A	N/A	N/A	N/A
^{69m}Zn	825.6	94.8 100.0	438.63 573.9	1.0604E-11	7.0227E-10	0.01509976	1.0053E-11 1.0604E-11
^{73}Se	429	69.84 97.0 0.27	67.07 361.2 510	5.1100E-17	2.0330E-19	251.352680	3.5688E-17 4.9567E-17 1.3797E-19
^{85m}Kr	268.8	75 0.300 0.01 14	151.195 129.81 451.0 304.87	5.8987E-05	2.3275E-05	2.53440460	4.424E-05 1.7696E-07 5.8987E-09 8.2582E-06
^{85m}Sr	67.63	96.0 97.49 1.12 0.11 0.32	151.19 231.86 129.82 731.80 238.78	1.4735E-13	2.1241E-11	0.00693691	1.4145E-13 1.4365E-13 1.6503E-15 1.6208E-16 4.7150E-16
^{90m}Y	191.4	100. 97.25 90.74 0.32	2318.97 202.53 479.51 681.8	5.2570E-08	1.1327E-06	0.04641017	5.2570E-08 5.1125E-08 4.7702E-08 1.6822E-10
^{95}Tc	1200	1.95 3.74 93.82	947.67 1073.71 765.79	8.2435E-17	2.6280E-16	0.31367960	1.6075E-18 3.0831E-18 7.7341E-17
^{97}Nb	72.1	1.09 0.15 98.23	1024.4 1268.62 657.94	1.0704E-04	6.5215E-04	0.16413044	1.1667E-06 1.5056E-07 1.0514E-04
^{99m}Tc	360	88.5 0.023	140.511 142.683	2.8512E-10	2.7839E-08	0.010241823	2.5233E-10 6.5577E-14

Table 3 continued.

^{130}I	741.6	99. 96.03 82.17	536.07 668.54 739.51	1.5510E-06	3.2879E-05	0.04717187	1.5354E-06 1.4894E-06 1.2744E-06
^{132}I	137.7	98.7 75.6 17.57	667.71 772.60 954.55	1.0393E-04	1.5148E-03	0.068611905	1.0258E-04 7.8574E-05 1.8261E-05
^{133}I	1248	0.356 0.309 1.81 0.539 0.645 1.49 0.457 1.23 4.47 0.551 1.49 2.33 86.3	262.70 422.903 510.530 617.978 680.252 706.575 768.360 856.278 875.328 1052.39 1236.44 1298.22 529.870	1.0232E-03	6.8765E-03	0.14880330	3.6427E-06 3.1618E-06 1.8521E-05 5.5153E-06 6.5999E-06 1.5246E-05 4.6762E-06 1.2586E-05 4.5739E-05 5.6381E-06 1.5246E-05 2.3841E-05 8.8306E-04
^{135m}Xe	917.4	1.47 0.1 0.07 80.8	786.9 1133.0 1358.0 526.56	1.8117E-03	7.5384E-03	0.24032192	2.6631E-05 1.8117E-06 1.2682E-06 1.4638E-03
^{157}Dy	488.4	93 0.26 1.33	326.34 83.04 182.42	2.6950E-18	1.6595E-15	0.0016239	2.5064E-18 7.0070E-21 3.5844E-20
^{190m}Os	9.9	94.88 97.79 98.62	361.2 502.5 616.5	N/A	N/A	N/A	N/A N/A N/A
^{200}Tl	1566	87.0 13.75 29.93	367.94 579.30 1205.75	N/A	N/A	N/A	N/A
^{204m}Pb	67.2	94.2 99.17 91.5	374.76 899.15 911.74	N/A	N/A	N/A	N/A
^{244}Am	606	66. 28 16.4	743.97 897.85 153.86	N/A	N/A	N/A	N/A

We have somewhat arbitrarily selected a lower limit of gamma yield per fission of 10^{-6} to identify the most attractive isotopes for burnup interrogation. For online application since the cooling time is small isotopes an isotope with lower than 10^{-6} gamma yield may still be useful, therefore we have set the gamma yield usefulness limit to 10^{-8}. At this point it is important to notice the data gaps, for many isotopes (marked as N/A – not available). For these isotopes fission yield information is either not available at all or is available with

large discrepancies between the sources of information. Therefore additional work is required to evaluate the effectiveness of these isotopes as burnup indicator.

Some of the isotopes, such as ^{73}Se, ^{85m}Sr are not suited for burnup analysis because their low gamma yields (PxFY). Some of the isotopes such as ^{190m}Os have no fission yield (and hence gamma yield) available in the literature. Candidate isotopes without gamma yield values or with values below 10^{-8} are not considered suitable for online burnup analysis. ^{130}I emits a 668.54 keV photon with an emission probability of 96.03%, while ^{132}I emits a 667.1 keV photon with an emission probability of 98.7%. Because of their similar photon emission energies, distinguishing them from one another would be difficult even with high resolution spectroscopy. However, the fission yield for ^{132}I is two orders of magnitude higher than that of ^{130}I, therefore most of the gamma in this case would come from for ^{132}I (note that the emission yields of the gammas of interest are very similar). In cases where the fission yield difference is not as large, but there is significant difference in the half-lives (for example, half-life of ^{130}I is almost five times longer than ^{132}I) one would rely on standard unfolding techniques to separate the contribution from the individual peaks.

Table 4 lists thermal neutron absorption cross sections and number of production paths for group 1 candidate isotopes. Thermal neutron cross section is an important parameter for a candidate burnup analysis isotope. A large neutron cross section would mean that the isotope will exhibit large burnup history dependence. Therefore a low thermal neutron absorption cross section is desired. Moreover, any burnup indicator with large thermal neutron cross section will be lost by neutron absorption. Therefore at 2.65E+06 b, the thermal absorption cross section of ^{135m}Xe is much too high to be used as

a tracer for online burnup analyses. On the other hand, ^{97}Nb and ^{132}I have an absorption cross section of 0 b; the lowest of the isotopes in Group 1 therefore making them a very attractive candidate for burnup analysis.

Table 4. Group 1 candidate isotopes thermal absorption cross section and production mode for online burnup analysis [24]

Isotope	Thermal Absorption Cross Section (barns)	Number of Production Modes
^{132}I	0.00E+00	1
^{97}Nb	0.00E+00	1
^{49}Cr	1.72E-02	2
^{61}Co	1.73E-02	1
^{85m}Kr	2.35E-02	1
^{43}K	1.18E+00	1
^{52}Fe	1.74E+00	2
^{190m}Os	3.90E+00	1
^{90m}Y	6.50E+00	1
^{69m}Zn	7.24E+00	1
^{133}I	9.69E+00	1
^{95}Tc	1.41E+01	1
^{130}I	1.80E+01	1
^{85m}Sr	1.91E+01	1
^{200}Tl	1.95E+01	1
^{73}Se	2.18E+01	1
^{99m}Tc	2.29E+01	1
^{157}Dy	1.17E+02	1
^{244}Am	6.00E+02	1
^{204m}Pb	7.03E+02	1
^{135m}Xe	2.65E+06	1

The ideal online burnup tracer would only be produced by fission. However, two isotopes in Group 1, ^{49}Cr and ^{52}Fe, are also produced by the decay of other fission products,

making them less than ideal candidates. Any burnup analysis algorithm based on an isotope with multiple production modes will show cooling time and burnup history dependence and therefore should be avoided.

Table 5 shows the diffusion properties of the Group 1 isotopes. Where possible the diffusion coefficient in UO_2 is provided, but for many candidates this information is not readily available. High diffusion rates would lead to significant migration of the isotope from its original location of birth to other areas. This migration will skew the measurement results, and will make certain sections of high burnup fuel not to be recorded appropriately. Therefore, high diffusion rates are not desirable for isotopes being considered for burnup analysis. There are significant knowledge gaps in regards to diffusion coefficients of fission isotopes. Ideally these diffusion coefficients must be measured in MOX and UO_2 fuel matrix separately at the elevated temperature comparable to fuel operating temperatures. Much of this information is missing. There is limited data on uranium diffusion and none on MOX. When UO_2 diffusion data was missing, to provide predictive data as a helpful tool diffusion coefficient in other materials is listed in table 5. For example, there is no diffusion coefficient for Os in fuel material is available, however diffusion coefficient of 1.07×10^{-9} cm^2/s (at 1100 ^0C) is reported in pyrrhotite ($OsPO_5$) which too varies with temperatures [25]. Reference cited in the table may be a good starting point for an interested reader to explore additional information. Needless to say that more work is needed in the area of isotope diffusion rates for many isotopes of interest. It is also difficult to predict the diffusive characteristics of MOX fuel without experimental data and how it would compare with UO_2.

Table 5. Diffusion coefficients of candidate isotopes for online burnup analysis

Isotopes	DIFFUSION	Isotopes	DIFFUSION
^{43}K	K in melilite : $D=1.22x10^{-16}$ cm^2/s at 900 ^0C [26]	^{99m}Tc	Tc in dense Bentonite : $D=8x10^{-7}$ cm^2/s Tc in dense metalic Molybdenum : $D=5.1x10^{-13}$ cm^2/s at 600 ^0C [44,27]
^{49}Cr	Cr in β-Uranium : $D=3.6x10^{-10}$ cm^2/s at 670 ^0C $D=6.45x10^{-11}$ cm^2/s at 680 ^0C $D=3.80x10^{-10}$ cm^2/s at 695.8 ^0C $D=5.36x10^{-10}$ cm^2/s at 712.7 ^0C [30]	^{130}I	Iodine in UO_2 : $D=5.0x10^{-14}$ cm^2/s at 1650 ^0C $D=3.0x10^{-15}$ cm^2/s at 1400 ^0C [28]
^{52}Fe	Fe in Fe_3O_4: $D=1.63x10^{-8}$ cm^2/s at 1199 ^0C $D=1.59x10^{-9}$ cm^2/s at 1200 ^0C [29]	^{132}I	Iodine in UO_2 : $D=5.0x10^{-14}$ cm^2/s at 1650 ^0C $D=3.0x10^{-15}$ cm^2/s at 1400 ^0C [28]
^{61}Co	Co in β-Uranium : $D=9.3x10^{-9}$ cm^2/s at 691.5 ^0C $D=1.16x10^{-8}$ cm^2/s at 706.3 ^0C $D=1.33x10^{-8}$ cm^2/s at 717.0 ^0C $D=1.90x10^{-8}$ cm^2/s at 741.0 ^0C [30]	^{133}I	Iodine in UO_2 : $D=5.0x10^{-14}$ cm^2/s at 1650 ^0C $D=3.0x10^{-15}$ cm^2/s at 1400 ^0C [28]
^{69m}Zn	Zn in $LiTaO_3$: $D=3.055x10^{-14}$ cm^2/s at 900 ^0C Zn in $CuInSe_2$ bulk crystal: $D=5.0x10^{-11}$ cm^2/s at 550 ^0C [31,32]	^{135m}Xe	Xe in UO_2: $D=2.5x10^{-14}$ cm^2/s at 1400 ^0C [33]
^{73}Se	Se in PbSe : $D=0.5x10^{-13}$ cm^2/s at 400 ^0C $D=1x10^{-12}$ cm^2/s at 500 ^0C $D=0.8x10^{-10}$ cm^2/s at 800 ^0C Se in Carbon steel : $D=2x10^{-32}$ cm^2/s [34,35]	^{157}Dy	Dy on the W(111) facet : $D=5.0x10^{-8}$ cm^2/s at 827 ^0C [36]
^{85m}Sr	Sr in $Bi_2Sr_2CuO_4$: $D=3.4x10^{-13}$ cm^2/s at 775 ^0C $D=1.1x10^{-11}$ cm^2/s at 800 ^0C Sr in Carbon steel : $D=9.7x10^{-8}$ cm^2/s [34,37]	^{190m}Os	Os in Pyrrhotite($OsPO_5$) : $D=1.07x10^{-9}$ cm^2/s at 1100 ^0C [25]

Table 5 continued.

^{85m}Kr	Kr in crushed UO_2 : $D=6.7x10^{-17}$ cm^2/s at 900 ^0C $D=8.3x10^{-15}$ cm^2/s at 1100 ^0C [38]	^{200}Tl	Tl in KCl: $D=0.8x10^{-11}$ m^2/s at 300 ^0C Tl in Tl Amalgam : $D=0.98x10^{5}$ cm^2/s at 1200 ^0C [39,40]
^{90m}Y	Y in UO_2 : $D=6.8x10^{-8}$ cm^2/s at 1150-1450 ^0C [41]	^{204m}Pb	Pb in Zircon : $D=1.77x10^{-16}$ m^2/s at 1251 ^0C Pb in solid PbTl 50%Pb : $D=1.86x10^{-12}$ cm^2/s at 206 ^0C [42,43]
^{95}Tc	Tc in dense Bentonite : $D=8x10^{-7}$ cm^2/s Tc in dense metallic Molybdenum : $D=5.1x10^{-17}$ m^2/s at 600 ^0C [35,44]	^{244}Am	Am in UO_2: $D=4.5x10^{-11}$ cm^2/s for high O potential $D=6.0x10^{-10}$ cm^2/s for low O potential [45]
^{97}Nb	Nb in UO_2: $D=7.99x10^{-11}$ cm^2/s at 1096 ^0C $D=4.82x10^{-11}$ cm^2/s at 1380 ^0C [41]		

b) Interim Storage (short term monitoring) – Candidate Isotopes

For interim storage analysis isotopes from third column of table 2 were selected for further analysis. Table 6 displays half-lives, emission probabilities (branching ratio), the corresponding gamma energies for all candidate isotopes for group 2. Similar to group 1, the last column in the table lists gamma yield which is the product of fission yield and emission probability and the other two columns list the ratio of the fission yield for ^{235}U and ^{239}Pu and fission yields (thermal neutron fission yield from uranium and plutonium). The data in Table 6 is used in conjunction with the data in Tables 7 and 8 to evaluate usefulness of these isotopes for spent fuel monitoring program. The criteria for isotopes in Group 2 are similar to those used for Group 1. If a candidate's gamma yield (PxFY) value is less than 10^{-8}, it is considered as unsuitable tracer for spent fuel monitoring. Several

candidates were eliminated from Group 2 because of their low gamma yield (PxFY) values for example, ^{67}Ga, ^{111}In, and ^{148m}Pm. Candidate isotopes were also excluded if their gamma yield could not be determined due to lack of data, for example; ^{56}Ni and ^{203}Hg.

Table 6. Group 2 fission product and decay data [20,21,22,23]

Isotope	Half-life (days)	Emission Probability (%)	Energy (keV)	^{235}U Th. Fiss. Yield	^{239}Pu Th. Fiss. Yield	FY Ratio (^{235}U/^{239}Pu)	PxFY (^{235}U)
^{52}Mn	5.59	90.0 94.5 100.0	744.23 935.54 1434.09	N/A	N/A	N/A	N/A
^{56}Ni	6.075	98.8 49.5 86. 0	158.38 749.95 811.85	N/A	N/A	N/A	N/A
^{58}Co	70.86	30.0 99.45 0.69 0.52	511.0 810.759 863.00 1674.72	N/A	N/A	N/A	N/A
^{67}Ga	3.26	38.81 21.41 16.64	93.31 184.58 300.22	1.1934E-17	2.91553E-16	0.040932523	4.6316E-18 2.5551E-18 1.9858E-18
^{82}Br	1.470	71.06 43.53 83.4	554.35 619.11 776.52	3.82137E-07	8.99942E-06	4.24624E-02	2.7155E-07 1.6634E-07 3.1870E-07
^{87}Y	3.35	82.2 89.84	388.53 484.81	3.52878E-15	1.01775E-12	0.003467237	2.9007E-15 3.1738E-15
^{90}Y	2.67	N/A 0.000001	1760.70 2186.24	3.69872E-08	7.96964E-07	0.046410126	N/A 3.6987E-16
^{95}Zr	64.032	0.27 44.27 54.38	235.69 724.193 756.729	1.27051E-03	1.25467E-03	1.01262E+00	3.4304E-06 5.6245E-04 6.9090E-04
^{95}Nb	34.985	0.03 0.01 99.808	204.12 561.88 765.803	1.06041E-06	5.65875E-06	1.87393E-01	3.1812E-10 1.0604E-10 1.0584E-06
^{96}Tc	4.28	99.76 82.00 97.57	778.22 812.54 849.86	N/A	N/A	N/A	N/A
^{103}Ru	39.247	0.071 0.384 0.289 0.344 91.31 0.855 5.78	39.76 53.275 294.98 443.80 497.08 557.04 610.33	2.35624E-07	1.26480E-05	0.018629349	1.6729E-10 9.0480E-10 6.8095E-10 8.1055E-10 2.1515E-07 2.0146E-09 1.3619E-08

Table 6 continued.

^{111}In	2.8	0.003 90.65 94.09	150.81 171.28 245.35	2.9712E-15	1.6524E-12	0.001798112	8.9136E-20 2.6934E-15 2.7956E-15
^{124}Sb	60.2	98.3 7.46 1.360 2.287 10.81 0.743 1.892 1.841 1.588 1.043 2.623 1.222 0.675 47.79 5.51	602.727 645.853 709.320 713.781 722.784 790.711 968.199 1045.128 1325.508 1355.175 1368.160 1436.561 c1488.88 1690.975 2090.936	2.70379E-08	2.69957E-07	1.00156E-01	2.6578E-08 2.0170E-09 3.6772E-10 6.1836E-10 2.9228E-09 2.0089E-10 5.1156E-10 4.9777E-10 4.2936E-10 2.8201E-10 7.0920E-10 3.3040E-10 1.8251E-10 1.2921E-08 1.4898E-19
^{126}Sb	12.35	83.27 99.6 99.6	414.7 666.5 695.0	8.75506E-06	1.37397E-05	0.637208964	7.2903E-06 8.7200E-06 8.7200E-06
^{131}I	8.0252	2.607 6.06 81.2 7.26 1.796	80.185 284.305 364.48 636.989 722.911	3.90977E-05	2.29304E-04	0.170505966	1.0193E-06 2.3693E-06 3.1747E-05 2.8385E-06 7.0219E-07
^{132}Te	3.20375	14.96 1.96 88.0	49.72 116.30 228.16	1.52851E-02	2.25318E-02	0.678379002	2.2867E-03 2.9959E-04 1.3451E-02
^{132}Cs	6.48	0.75 0.96 99.45 84.48 11.94 6.88	505.79 630.19 667.71 464.47 567.16 1031.66	7.36827E-10	2.97953E-09	0.247296386	5.5262E-12 7.0735E-12 7.3277E-10 6.2247E-10 8.7977E-11 5.0694E-11
^{134}Cs	753.725	8.37 15.38 97.65 85.5 8.7 3.017	563.243 569.32 604.72 795.83 801.945 1365.186	4.43390E-08	3.85859E-06	1.14910E-02	3.7112E-09 6.8193E-09 4.3297E-08 3.7910E-08 3.8575E-09 1.3377E-09
^{136}Cs	13.16	42.17 99.7 79.76	340.55 818.51 1048.07	3.48339E-05	6.13750E-04	5.67558E-02	1.4689E-05 3.4729E-05 2.7784E-05

Table 6 continued.

^{140}La	1.6785	20.8 2.995 46.1 4.392 23.72 5.58 2.73 7.04 0.531 95.40 0.845 3.412	328.761 432.513 487.022 751.653 815.781 867.839 919.533 925.198 950.988 1596.20 3 2347.84 7 2521.30	5.20771E-05	1.01954E-04	5.10790E-01	1.0832E-05 1.5597E-06 2.4008E-05 2.2872E-06 1.2353E-05 2.9059E-06 1.4217E-06 3.6662E-06 2.7653E-07 4.9682E-05 4.4005E07 1.7769E-06
^{144}Pm	363	43.78 98.5 99.49	476.78 618.01 696.49	4.6662E-14	1.2900E-12	0.036172093	2.0429E-14 4.5962E-14 4.6424E-14
^{148m}Pm	41.3	22.2 2.47 1.10 12.56 3.92 18.66 5.35 6.75 94.9 12.54 5.48 89.0 32.8 17.17 20.3	75.8 98.48 189.63 288.11 311.63 414.07 432.78 501.26 550.27 599.74 611.26 629.97 725.70 915.33 1013.81	8.78357E-11	4.03712E-08	0.002175702	1.9500E-11 2.1695E-12 9.6619E-13 1.1032E-11 3.4432E-12 1.6390E-11 4.6992E-12 5.9289E-12 8.3356E-11 1.1015E-11 4.8134E-12 7.8174E-11 2.8810E-11 1.5081E-11 1.7831E-11
^{181}Hf	42.38	43.3 5.85 0.86 15.12 0.703 80.5 0.233	133.021 136.26 136.86 345.93 475.99 482.18 615.17	N/A	N/A	N/A	N/A
^{192}Ir	73.828	31.2 86.94 50.26	308.46 316.51 468.07	N/A	N/A	N/A	N/A
^{194m}Ir	170	93 97 62	328.5 482.6 600.5	N/A	N/A	N/A	N/A
^{200}Tl	1.088	87.0 13.75 29.93	367.94 579.30 1205.75	N/A	N/A	N/A	N/A
^{202}Tl	12.31	91.5 0.59 0.07	439.51 520.3 960.1	N/A	N/A	N/A	N/A

Table 6 continued.

^{203}Pb	2.163	80.9 3.35 0.75	279.2 401.32 680.51	N/A	N/A	N/A	N/A
^{203}Hg	46.594	81.48	279.2	N/A	N/A	N/A	N/A
^{206}Bi	6.243	40.79 99 66.23	516.18 803.10 881.01	N/A	N/A	N/A	N/A

Table 7 lists thermal neutron absorption cross sections and number of production paths for group 2 candidate isotopes. In this table ^{192}Ir has the highest value of absorption cross section. Similar to group 1, for storage-pool monitoring applications (group 2) low thermal neutron absorption cross section is desired. Any burnup indicator with large thermal neutron cross section will be highly dependent on burnup history. Therefore at 1.42E+03 b, the thermal absorption cross section of ^{192}Ir is much too high to be used as a tracer for online burnup analyses. On the other hand, ^{56}Ni, ^{206}Bi, and ^{203}Pb having multiple modes of production is not suitable for interim-storage monitoring applications.

Table 8 shows the diffusion properties for group 2 isotopes. Where possible the diffusion coefficient in UO_2 is provided, but for most candidates this information is not readily available. As discussed earlier, high diffusion rates are not desirable for isotopes being considered for burnup analysis. Diffusion coefficients data is provided for many of these isotopes in other materials due to limited information available in the literature. For instance, there is no diffusion coefficient within the fuel element for Ni isotope; however data is available for Ni diffusion in copper and aluminum. The available data also shows significant temperature dependence. Diffusion coefficients in the table 8 are not sufficient and need for further research on diffusion coefficients in UO_2 and MOX fuels is obvious.

Table 7. Group 2 candidate isotopes thermal absorption cross section and production mode for storage fuel burnup analysis [24]

Isotope	Thermal Absorption Cross Section (barns)	Number of Production Modes
^{134}Cs	0.0000E+00	1
^{103}Ru	0.0000E+00	1
^{148m}Pm	0.0000E+00	1
^{132}Te	2.0000E-03	1
^{95}Zr	1.2000E+00	1
^{140}La	2.7000E+00	1
^{90}Y	3.5000E+00	1
^{203}Hg	4.9480E+00	1
^{56}Ni	5.0230E+00	3
^{126}Sb	5.8000E+00	1
^{95}Nb	7.0000E+00	1
^{203}Pb	9.8709E+00	2
^{206}Bi	1.0400E+01	2
^{67}Ga	1.0760E+01	1
^{202}Tl	1.1402E+01	1
^{136}Cs	1.30000E+1	1
^{82}Br	1.6630E+01	1
^{124}Sb	1.7400E+01	1
^{194m}Ir	1.7600E+01	1
^{87}Y	1.8361E+01	1
^{200}Tl	1.9500E+01	1
^{96}Tc	2.35440E+1	1
^{144}Pm	3.5380E+01	1
^{132}Cs	3.7035E+01	1
^{111}In	4.3100E+01	1
^{52}Mn	5.3366E+01	1
^{181}Hf	8.0000E+01	1
^{131}I	8.0000E+01	1
^{58}Co	1.6508E+02	1
^{192}Ir	1.4212E+03	1

Table 8. Diffusion coefficients of candidate isotopes for spent fuel monitoring

Isotopes	DIFFUSION	Isotopes	DIFFUSION
^{52}Mn	Mn in CdTe: $D=9.72\times10^{-11}$ cm^2/s at 800 ^{0}C $D=8.70\times10^{-14}$ cm^2/s at 600 ^{0}C [46]	^{132}Te	Te in UO_2 : $D=1.7\times10^{-12}$ cm^2/s at 1400 ^{0}C [47]
^{56}Ni	Ni in copper : $D=4.67\times10^{-24}$ m^2/s at 340 ^{0}C Ni in aluminum : D: 5.12×10^{-13} cm^2/s at 450 ^{0}C [48,49]	^{132}Cs	Cs in UO_2: $D=1.14\times10^{-18}$ cm^2/s at 1227 ^{0}C $D=1.0\times10^{-17}$ cm^2/s at 1327 ^{0}C [50]
^{58}Co	Co in β-Uranium : $D=9.3\times10^{-9}$ cm^2/s at 691.5 ^{0}C $D=1.16\times10^{-8}$ cm^2/s at 706.3 ^{0}C $D=1.33\times10^{-8}$ cm^2/s at 717.0 ^{0}C $D=1.90\times10^{-8}$ cm^2/s at 741.0 ^{0}C [30]	^{134}Cs	Cs in UO_2: $D=1.14\times10^{-18}$ cm^2/s at 1227 ^{0}C $D=1.0\times10^{-17}$ cm^2/s at 1327 ^{0}C [50]
^{67}Ga	Ga in GaSb : $D=3.83\times10^{-18}$ cm^2/s at 551 ^{0}C D: 9.33×10^{-16} cm^2/s at 640 ^{0}C [51]	^{136}Cs	Cs in UO_2: $D=1.14\times10^{-18}$ cm^2/s at 1227 ^{0}C $D=1.0\times10^{-17}$ cm^2/s at 1327 ^{0}C [50]
^{82}Br	Br in NaCl: $D=2.27\times10^{-16}$ cm^2/s at 20 ^{0}C $D=1.52\times10^{-13}$ cm^2/s at 500 ^{0}C [52]	^{140}La	La in molten Uranium: $D=4.2\times10^{-7}$ cm^2/s at 1200 ^{0}C [53]
^{87}Y	Y in UO_2 : $D=6.8\times10^{-8}$ cm^2/s at 1150-1450 ^{0}C [41]	^{144}Pm	Pm in Silicon: $D=1\times10^{-13}$ cm^2/s at 1100 ^{0}C $D=1.5\times10^{-12}$ cm^2/s at 1250 ^{0}C [54]
^{90}Y	Y in UO_2 : $D=6.8\times10^{-8}$ cm^2/s at 1150-1450 ^{0}C [41]	^{148m}Pm	Pm in Silicon: $D=1\times10^{-13}$ cm^2/s at 1100 ^{0}C $D=1.5\times10^{-12}$ cm^2/s at 1250 ^{0}C [54]
^{95}Nb	Nb in UO_2: $D=7.99\times10^{-11}$ cm^2/s at 1096 ^{0}C $D=4.82\times10^{-11}$ cm^2/s at 1380 ^{0}C [41]	^{181}Hf	Hf in α-Zr: $D=4.0\times10^{-24}$ m^2/s at 500 ^{0}C $D=1.5\times10^{-20}$ cm^2/s at 842 ^{0}C [55]
^{95}Zr	Zr in Titanite: $D=3.46\times10^{-19}$ cm^2/s at 753 ^{0}C $D=1.21\times10^{-15}$ cm^2/s at 1050 ^{0}C [56]	^{192}Ir	Ir in Silicon : $D=3.1\times10^{-20}$ cm^2/s at 550 ^{0}C [57]

Table 8 continued.

^{96}Tc	Tc in dense Bentonite : $D=8x10^{-11}$ m^2/s Tc in dense metalic Molybolenum : $D=5.1x10^{-14}$ cm^2/s at 600 ^0C [44,27]	^{194m}Ir	Ir in Silicon : $D=3.1x10^{-20}$ cm^2/s at 550 ^0C [57]
^{103}Ru	Ru in SiC: $D=55x10^{-12}$ cm^2/s at 1850 ^0C $D=8x10^{-12}$ cm^2/s at 1650 ^0C Ru in Aluminum: $D= 5.1x10^{-10}$ cm^2/s at 600 ^0C [58,59]	^{200}Tl	Tl in KCl: $D=0.8x10^{-7}$ cm^2/s at 300 ^0C Tl in Tl Amalgam : $D=0.98x10^{5}$ cm^2/s at 1200 ^0C [39,40]
^{111}In	In in In-Sn alloy : $D=2.29x10^{-18}$ cm^2/s at 25 ^0C [60]	^{202}Tl	Tl in KCl : $D=0.8x10^{-10}$ cm^2/s at 300 ^0C $D=1.2x10^{-6}$ cm^2/s at 350 ^0C [39,40]
^{124}Sb	Sb in $TiSi_2$: $D=3x10^{-14}$ cm^2/s at 550 ^0C $D=1.3x10^{-13}$ cm^2/s at 600 ^0C $D=1.5x10^{-12}$ cm^2/s at 700 ^0C [61]	^{203}Pb	Pb in Zircon : $D=1.77x10^{-16}$ cm^2/s at 1251 ^0C Pb in solid PbTl 50%Pb : $D=1.86x10^{-12}$ cm^2/s at 206 ^0C [42,43]
^{126}Sb	Sb in $TiSi_2$: $D=3x10^{-14}$ cm^2/s at 550 ^0C $D=1.3x10^{-13}$ cm^2/s at 600 ^0C $D=1.5x10^{-12}$ cm^2/s at 700 ^0C [61]	^{203}Hg	Hg in Ag_3Sn : $D=6.04x10^{-11}$ cm^2/s at 50 ^0C Hg in Ag_2Hg_3 : $D=1.53x10^{-9}$ cm^2/s at 50 ^0C [62,63]
^{131}I	Iodine in UO_2 : $D=5.0x10^{-14}$ cm^2/s at 1700 ^0C $D=3.0x10^{-15}$ cm^2/s at 1400 ^0C [28]	^{206}Bi	Bi in nanocrystalline copper : $D=2.3x10^{-15}$ cm^2/s at 100 ^0C [64]

c) Long-term storage/Historic data – Candidate Isotopes

For long-term storage monitoring application (group 3) only six isotopes were identified in table 2. Table 9 lists data aggregated from the literature to identify the best isotopes from Group 3 (5 years < $T_{1/2}$) for historical data burnup analysis. The data presented here includes the thermal fission yields from ^{235}U and ^{239}Pu, important photon emission probabilities, and corresponding gamma ray energies. Similar to the previous groups the product of fission yields and gamma emission is also listed as the figure of merit

for the isotope's suitability for tracer applications. Isotopes with a gamma yield of less than 10^{-8} were not consideration useful. Unfortunately, the highest gamma yield in Table 9 (from ^{94}Nb) is still an order of magnitude below this criterion. For group 3 application long-term storage historic burnup data reconstruction it is possible to count for extended period of data and therefore lower gamma yield are acceptable. Moreover, due to long cooling time many of the interfering short lived gamma emitter would decay away making low intensity measurements possible. With this possibility in mind, thermal absorption cross sections, number of production modes and diffusion coefficients of group 3 isotopes are presented in Tables 10 and 11 respectively.

Table 9. Group 3 fission product and decay data [20,21,22,23]

Isotope	Half-life (years)	Emission Probability (%)	Energy (keV)	^{235}U Th. Fiss. Yield	^{239}Pu Th. Fiss. Yield	FY Ratio (^{235}U/^{239}Pu)	PxFY (^{235}U)
^{44}Ti	58.9	69.84 97.0 0.27	67.07 361.2 510.0	N/A	N/A	N/A	N/A
^{94}Nb	20300	99.815 99.892	702.639 871.114	1.44759E-09	9.51964E-08	1.5206E-02	1.4449E-09 1.4460E-09
^{98}Tc	4200000	100 102	652.41 745.35	8.87586E-09	4.16934E-09	2.1288E+00	8.8758E-09 9.0533E-09
^{108m}Ag	418	99.1 98.41 99.5 76.2	433.94 614.28 722.91 79.13	2.9300E-10	9.4100E-06	3.1137E-05	2.9036E-10 2.8834E-10 2.9153E-10 2.2326E-10
^{166m}Ho	1200	72 .0 54.14 56.88	184.41 711.68 810.29	9.40646E-13	1.32047E-09	7.1236E-04	6.7726E-13 5.0926E-13 5.3503E-13
^{243}Am	7390	5.89 67.20.346 0.115 0.56	43.53 74.66 86.71 141.90 117.60	N/A	N/A	N/A	N/A

The thermal absorption cross sections and number of production modes for Group 3 candidates are listed in Table 10. Several of the isotopes listed in the table have rather convoluted production path with multiple modes. For example ^{243}Am is produced in a thermal reactor through three different paths. This makes it an unattractive candidate for burnup analysis. The same is true for ^{44}Ti which has four production paths.

Table 10. Group 3 candidate isotopes thermal absorption cross section and production modes for online burnup analysis [24]

Isotopes	Thermal Absorption Cross Section (barns)	Number of Production Modes
^{243}Am	0.000000E+0	3
^{94}Nb	0.000000E+0	1
^{98}Tc	9.300000E-1	1
^{44}Ti	9.726000E-1	4
^{108m}Ag	5.070600E+1	1
^{166m}Ho	2.838660E+3	1

Table 11 shows diffusion properties of candidate isotopes. Only Am and Nb diffusion coefficients are available in UO_2 fuel for other isotopes diffusion coefficient in other materials are reported as reference information. Ideally diffusion coefficient should be available in UO_2 or MOX fuel material at elevated temperature comparable to the fuel temperature in the reactor. In the absence of the desired information available data is reported as starting point. For example, diffusion coefficient for Ti is 79×10^{-14} m^2/s at 1010 ^{0}C and 0.25×10^{-14} m^2/s at 700 ^{0}C in pure copper. Significant variation with temperature is obvious from the data [65]. Data gaps are obvious stressing the need for collection of diffusion coefficient values for these isotopes in UO_2 and MOX fuel at high temperatures.

Table 11. Diffusion coefficients of candidate isotopes for historical data

Isotopes	DIFFUSION	Isotopes	DIFFUSION
^{44}Ti	Ti in pure copper : D=79x10^{-10} cm^2/s at 1010 ^{0}C D: 0.25x10^{-10} cm^2/s at 700 ^{0}C [65]	^{108m}Ag	Ag in SiC : D=1.0x10^{-14} cm^2/s at 1200 ^{0}C Ag in Cadmium : D=2.63x10^{-11} cm^2/s at 220 ^{0}C D=2.29x10^{-10} cm^2/s at 280 ^{0}C [66,67]
^{94}Nb	Nb in UO_2: D=7.99x10^{-11} cm^2/s at 1096 ^{0}C D=4.82x10^{-11} cm^2/s at 1380 ^{0}C [41]	^{166m}Ho	Ho in barium titanate : D=4.3x10^{-14} cm^2/s at 1200 ^{0}C D: 4.7x10^{-13} cm^2/s at 1400 ^{0}C [68]
^{98}Tc	Tc in dense Bentonite : D=8x10^{-7} cm^2/s Tc in dense metalic Molybolenum : D=5.1x10^{-13} cm^2/s at 600 ^{0}C [44,27]	^{243}Am	Am in UO2: D=4.5x10^{-11} cm^2/s for high O potential D=6.0x10^{-10} cm^2/s for low O potential [45]

Table 12. Candidate isotopes comparison for three burnup applications

	ONLINE ANALYSIS (GROUP 1)		INTERIM STORAGE ANALYSIS (GROUP 2)		LONG-TERM STORAGE (GROUP 3)	
	Isotope	**Remarks**	**Isotope**	**Remarks**	**Isotope**	**Remarks**
1	^{190}Os (m)	1	^{200}Tl	1,4	^{44}Ti	1,3,4
2	^{49}Cr	1,3,4	^{82}Br	5	^{108m}Ag	5*
3	^{204m}Pb	1,2	^{140}La	4*	^{166m}Ho	1,2
4	^{85m}Sr	1,4	^{203}Pb	1,3	^{243}Am	1,3
5	^{97}Nb	5	^{90}Y	1,4	^{94}Nb	5
6	^{61}Co	1,4	^{111}In	1	^{98}Tc	5*
7	^{132}I	5	^{132}Te	5		
8	^{90m}Y	4*	^{67}Ga	1		
9	^{85m}Kr	5*	^{87}Y	1,4		
10	^{99m}Tc	1	^{96}Tc	1		
11	^{73}Se	1	^{52}Mn	1		
12	^{157}Dy	1,2,4	^{56}Ni	1,3		
13	^{52}Fe	1,3,4	^{206}Bi	1,3		

Table 12 continued.

14	^{244}Am	1,2	^{132}Cs	1		
15	^{130}I	5	^{131}I	5		
16	^{69m}Zn	1	^{202}Tl	1,4		
17	^{135m}Xe	2	^{126}Sb	5*		
18	^{95}Tc	1	^{136}Cs	5		
19	^{133}I	5	^{95}Nb	5		
20	^{43}K	1	^{103}Ru	5		
21	^{200}Tl	1,4	^{148m}Pm	1		
22			^{181}Hf	1		
23			^{203}Hg	1,4		
24			^{124}Sb	5*		
25			^{95}Zr	5*		
26			^{58}Co	1,2,4		
27			^{192}Ir	1,2		
28			^{194m}Ir	1		
29			^{144}Pm	1		
30			^{134}Cs	5		

Remarks – 1) Not Suitable due to low or missing gamma yield 2) Not Suitable due to high neutron x-section 3) Not Suitable due to multiple production 4) Not Suitable due to high diffusion rate 5) Suitable based on available data *) Perhaps acceptable

Suitable Isotopes of Burnup Monitoring

Based on the available information the three lists of candidate isotopes for the three applications; online burnup analysis, interim-storage and long-term storage were evaluated and the results is shown in table 12. The list is not in any specific order, however, the remarks may be helpful in narrowing down the choice for a certain application to a single or small group of isotopes.

Best suited candidate isotopes for three applications are listed in table 13 with gamma energies and yields. Based on the available measurement resources and the

application users would have to select the gamma peaks of interest to be measured for analysis. For example, for on-line burnup analysis ^{97}Nb is identified as a good candidate with 657.94 keV (yield of 1.05E-04) and 1268.62 keV (yield of 1.50E-07). If the available measurement system does not offer good energy resolution at low energies one may have to rely on 1268.62 keV low yield peak while if high resolution system is available one could measure 657.94 keV.

Table 13. Best candidate isotopes for three burnup applications with characteristic data

	ONLINE ANALYSIS (GROUP 1)			**INTERIM STORAGE ANALYSIS (GROUP 2)**			**LONG-TERM STORAGE (GROUP 3)**		
	Isotope ($T_{1/2}$) (min)	**Gamma Energy (keV)**	**Gamma Yields**	**Isotope ($T_{1/2}$) (days)**	**Gamma Energy (keV)**	**Gamma Yields**	**Isotope ($T_{1/2}$) (years)**	**Gamma Energy (keV)**	**Gamma Yields**
1	^{97}Nb (72.1)	1268.62 657.94	1.50E-07 1.05E-04	^{82}Br* (1.47)	554.35 619.11 776.52	2.71E-07 1.66E-07 3.18E-07	^{108m}Ag* (418)	433.94 614.28 722.91 79.13	2.90E-10 2.88E-10 2.91E-10 2.23E-10
2	^{132}I (137.7)	667.71 772.60 954.55	1.02E-04 7.86E-05 1.83E-05	^{132}Te (3.20)	49.72 116.30 228.16	2.28E-03 2.99E-04 1.34E-02	^{94}Nb (20300)	702.639 871.114	1.44E-09 1.44E-09
3	^{85m}Kr (268.8)	75 0.300 0.01 14	151.195 129.81 451.0 304.87	^{131}I (8.025)	80.185 284.30 364.48 636.98 722.91	1.01E-06 2.36E-06 3.17E-05 2.83E-06 7.02E-07	^{98}Tc* (42E+5)	652.41 745.35	8.87E-09 9.05E-09
4	^{130}I (741.6)	536.07 668.54 739.51	1.54E-06 1.49E-06 1.27E-06	^{126}Sb* (12.35)	414.7 666.5 695.0	7.29E-06 8.72E-06 8.72E-06			
5	^{133}I (1248)	262.70 422.903 510.530 617.978 680.252 706.575 768.360 856.278 875.328 1052.39 1236.44 1298.22 529.870	3.64E-06 3.16E-06 1.85E-05 5.51E-06 6.59E-06 1.52E-05 4.67E-06 1.25E-05 4.57E-05 5.63E-06 1.52E-05 2.38E-05 8.83E-04	^{136}Cs (13.16)	340.55 818.51 1048.07	1.46E-05 3.47E-05 2.77E-05			
6				^{95}Nb (34.98)	204.12 561.88 765.803	3.18E-10 1.06E-10 1.05E-06			

Table 13 continued.

7				^{103}Ru* (39.24)	39.76 53.275 294.98 443.80 497.08 557.04 610.33	1.67E-10 9.04E-10 6.80E-10 8.10E-10 2.15E-07 2.01E-09 1.36E-08			
8				^{124}Sb* (60.2)	602.727 645.853 709.320 713.781 722.784 790.711 968.199 1045.128 1325.508 1355.175 1368.160 1436.561 c1488.88 1690.975 2090.936	2.65E-08 2.01E-09 3.67E-10 6.18E-10 2.92E-09 2.00E-10 5.11E-10 4.97E-10 4.29E-10 2.82E-10 7.09E-10 3.30E-10 1.82E-10 1.29E-08 1.48E-19			
9				^{95}Zr* (64.03)	235.69 724.193 756.729	3.43E-06 5.62E-04 6.90E-04			
10				^{134}Cs (753.7)	563.243 569.32 604.72 795.83 801.945 1365.186	3.71E-09 6.81E-09 4.32E-08 3.79E-08 3.85E-09 1.33E-09			

*) Diffusion Data not available to UO_2

5. Conclusions and Recommendations

The best isotopes for online burnup analysis, interim storage monitoring, and long-term storage monitoring have been investigated. Considering group 1 isotopes in table 2 and all the burnup indicator parameters that discussed before, ^{130}I, ^{132}I, ^{133}I for all corresponding energy levels are better candidate for the online burnup analysis while ^{97}Nb is also a good candidate. ^{132}I has a small (0.0686) fission yield ratio making it a good candidate for plutonium identification. But the low gamma energies from ^{132}I is would make it a bit challenging to separate the peak out from the possible noise from Compton from higher energies and other sources. The possibility of relying on 1024.4 keV from ^{97}Nb

is not as attractive because of the low gamma yield of only 1.1667E-06. Therefore ^{132}I seems to be a better candidate. Because of the small difference between the emission energy from ^{130}I (668.54 keV) ^{132}I (667.71 keV) the two peaks will be practically inseparable but due to the low gamma yield of ^{130}I (1.4894E-06) as compared to ^{132}I (1.0258E-04) one can assume that the entire peak is from ^{132}I.

In short, ^{132}I seems to be a good candidate for on-line burnup analysis. Other isotopes like ^{85}Kr(m) is not as attractive due to its low emission energy (151.195 keV and 304.87 keV) and hence being prone interference. Iodine is also an attractive candidate for burnup analysis due to its low diffusion rate (~10^{-14} cm^2/s) in UO_2 at the elevated temperature. Another good candidate is ^{97}Nb at the energy level of 1024.4 keV and 657.94 keV. Even though ^{135}Xe(m) looks very good candidate given the circumstances, it has very large thermal neutron absorption cross section ($2.65x10^6$ barn) it will not be considered a good candidate for the analysis.

For the interim storage (short-term) monitoring there are several candidate isotopes. However, the list reduces to only a few once consideration is given to gamma yield and emission energies. The good candidate isotopes include; ^{140}La, ^{136}Cs, ^{134}Cs, ^{131}I, ^{95}Zr and ^{103}Ru. From the list ^{140}La is of particular interest due to its high emission energy (2521.30 keV) and significantly large gamma yield of (1.7769E-06). However it has a large diffusion rate (4.2E-07 cm^2/s) in molten uranium making it not so attractive. The two isotopes of cesium are well known for their usefulness as a burnup indicator and need not to be discussed. From the remaining choices, ^{131}I is an attractive option. The two energies of interest from ^{131}I are 636.98 keV and 722.91 keV with the respective yields of 2.8385E-06 and 7.0219E-07. ^{131}I also have a nonzero neutron absorption cross section make its use

somewhat history dependent. ^{95}Zr is also a good candidate but it has two drawbacks. Firstly while the gamma yields are high, the emission energies are relatively low in the 700 keV range. The other issue with ^{95}Zr is the unavailability of its diffusion rate information in the fuel matrix. This knowledge gap must be filled to make use of this very attractive candidate. ^{103}Ru is potentially a good candidate for plutonium identification because of the large difference in the fission yield from uranium vs. plutonium. However, it has the same issue of missing information on the diffusion rate in UO_2. The other issue with the possible use of ^{103}Ru is the low emission energies with the maximum being 610.33keV. In short the only alternate to the use of cesium is ^{131}I isotopes for interim storage monitoring unless the data gaps are addressed for other isotopes.

There are only six isotopes for long term storage monitoring. From those six only ^{108m}Ag*, ^{94}Nb and ^{98}Tc* are viable options. ^{98}Tc has a very long half live (42E+05 yrs) which will result very low count rates. Moreover, the emission energies are also low (652.41 keV and 745.35 keV). ^{108m}Ag has a large difference in the fission yield from uranium vs. plutonium (fission yield ratio of 3.1137E-05) but its diffusion rate in UO_2 is not known and it has a nonzero absorption cross section. Therefore the only good candidate for long term storage monitoring is ^{94}Nb. It has a half-life of 20300 years with a low diffusion rate of $\sim 10^{-11}$ cm^2/s. It has almost zero neutron absorption cross section making it burnup history independent and decent gamma yield of 1.44E-09. Based on this analysis ^{94}Nb is the only good candidate for long-term storage monitoring.

REFERENCES

[1] Nuclear waste repository safe for future generations, 1663 LANL Sci/Tech Magazine. December 2008. Retrieved September 19, 2010.

[2] Nuclear Energy Institute, Plutonium and Uranium Reprocessing, http://www.nei.org/resourcesandstats/documentlibrary/nuclearwastedisposal/policybrief/advancedfuelcycle, Accessed on 13, April, 2013, Created on March 2010.

[3] Shaw Areva MOX Services, LLC, 2008, September 27. MOX Project [Online]. Available: http://www.moxproject.com/.

[4] United States Enrichment Corporation, Megatons to Megawatts Program, http://www.usec.com/news/megatons-megawatts-program-recycles-450-metric-tons-weapons-grade-uranium-commercial-nuclear-fu, Accessed on 13 April, 2013, Created on 9 July 2012.

[5] International Atomic Energy Agency, Thorium Fuel cycle-Potential benefits and challenges, IAEA-TECDOC-1450, page 1-2, May 2005, Austria.

[6] M. L. Dennis, S. Usman, "Feasibility Study of MOX Fuel Online Burnup Analysis", Proceedings of ICAPP '06. Reno, NV. June 2006.

[7] B.B. Bevard, J.C. Wagner, C.V. Parks, and M. Aissa, "Review of Information for Spent Nuclear Fuel Burnup Confirmation", NUREG/CR-6998, 2009.

[8] Håkansson, A., Bäcklin, A., Hildingson, L., Danielson, N. 1993. Results of spent-fuel NDA with HRGS. In: Proceedings of the 15th Annual Esarda meeting, Rome, Italy.

[9] C. Willman, and et al., "Nondestructive assay of spent nuclear fuel with gamma-ray spectroscopy", Annals of Nuclear Energy 33, (2006), 427-438.

[10] C. Willman, and et al., "A nondestructive method for discriminating MOX fuel from LEU fuel for safeguards purpose", Annals of Nuclear Energy 33, (2006), 766-773.

[11] M. L. Dennis, S. Usman, Feasibility of 106Ru peak measurement for MOX fuel burnup analysis. Nuclear Engineering and Design, 240 (2010), 3687-3696.

[12] K.A. Jordan, G. Perret, "A delayed neutron technique for measuring induced fission rates in fresh and burnt LWR fuel", Nuclear Instruments and Methods in Physics Research A 634, 91-100, (2011)

[13] Kiyoshi Inoue and et al., "Burnup determination of Nuclear Fuel", Mass Spectroscopy, 17, (1969), 830-842.

[14] S. Grape and et. al., "Modeling Cherenkov light from irradiated nuclear fuel assemblies using GEANT4", IAEA-CN-184/88, The IAEA Symposium on International Safeguards, Vienna, Austria, November 1-5, 2010.

[15] E. Dowdy et. al., "Method of monitoring irradiated nuclear fuel using Cerenkov radiation", US Patent No. 4,389,568, Jun. 21, 1983

[16] Crane, T.W., Hsue, S.T., Lee, J.C., Talbert Jr., W.L., 1978. Nondestructive assay methods for irradiated nuclear fuels. Los Alamos National Lab., Los Alamos, NM, LA-6923, pp. 2-8

[17] A. Hawari, et.al., Assessment of Online Burnup Monitoring of Pebble Bed Reactor Fuel Using Passive Gamma Ray Spectrometry, IEEE Transaction of Nuclear Science, Vol. 49, 1249 (2002)

[18] P. Jansson, A. Håkansson, and A. Backlin, Gamma-ray Measurements of Spent PWR Fuel and Determination of Residual Power, http://jansson.net/publications/isv_7_1997.pdf, Accessed on April 2013, Created on October 1997, p.12.

[19] J. R. Parrington, et. al., Nuclides and Isotopes Chart of the Nuclides Fifteenth Edition, Lockheed Martin Company, NY, 1996.

[20] www.ndc.jaea.go.jp

[21] www-nds.iaea.org

[22] http://ie.lbl.gov/fission.html

[23] K. Tasaka, et. al., JNDC Nuclear Data Library of Fission Products, Japan Atomic Energy Research Institute, JAERI 1287, June 3, 1983.

[24] http://www-nds.iaea.org/exfor/endf.htm#1

[25] James M. Brenan et. al., Diffusion of Osmium in pyrrhotite and pyrite: implications for closure of the Re-Os isotopic system, Earth and Planetary Science Letters, 180, (2000), 399-413.

[26] M. Ito and J. Ganguly, Potassium diffusion in melilite; Experimental studies and constraints on the thermal history and size of planetesimals hosting CAIs, Meteoritics & Planetary Science 39, (2004), 1911-1919.

[27] I. E. Alekseev and A. E. Antropov, Accelerated Transfer of 99mTc impurity atoms at polymorphic transition in irradiated molybdenum metal, Radiochemistry, 44, (2002), 336-369.

[28] G. Stankunas and et. al., Modeling the influence of nuclear fuel microstructure on fission product release, Lithuanian Journal of Physics, 46, (2006), 271-275.

[29] N. L. Peterson, W.K Chen and D. Wolf, Correlation and isotope effects for cation diffusion in magnetite, J. Phys Chem Solids, 41, (1980) 709-719.

[30] M.P Dariel, M. Blumenfeld, and G. Kimmel, Diffusion of Cobalt in BetaUranium, J. Applied Physics, 41, (1970) 1480-1483

[31] I. Song and et. al., Diffusion of Zn in stoichiometric LiTaO3, Journal of Crystal Growth, 270, (2004), 568-572.

[32] M. Benabdeslem, and et. al., Diffusion of Zn in CuInSe2 bulk crystals, Journal of Crystal Growth, 274, (2005), 144-148.

[33] W. Miekeley and F.W. Felix, Effect of stoichiometry on diffusion of xenon in UO2, Journal of Nuclear Materials, 42, (1972), 297-306.

[34] T.B. Caldwell, Ancillary Equipment Residual Radioactivity Estimate to support tank closure activities for F-tank farm, CBU-PIT-2005-00120, June 16, 2005

[35] R. L. Guldi and et, al., Difusion of lead and selenium in lead selenide, J. Applied Physics, 44, (1973), 4896-4907.

[36] T. Biernat, R. Blaszczyszyn, Surface diffusion of dysprosium on the W(111) facet, Applied surface science, 230, (2004), 81-87.

[37] N. Chen and et, al., Diffusion of Sr in Bi2Sr2Can-1Cu2n+4 , J. Mater. Res., Vol. 8, No. 10, (1993), 2465-2470.

[38] A. B. Auskern, The diffusion of krypton-85 from uranium dioxide powder, Metallurgy and ceramics, 1960.

[39] K. Gaswami and et., al., Determination of the diffusion coefficient of thallium in KCl crystal by electron irradiation, Solid-state science and technology, (1980), 1855-1856.

[40] W. T. Foley, M.T.H. Liu, Tracer diffusion of thallium in thallium amalgams, Canadian Journal of Chemistry, 42, (1964), 2607-2609.

[41] J.I Federer and R.A. Padgett, Jr., Diffusion studies of 95Nb in polycrystalline UO2 between 1100 and 2100 0C, Journal of Nuclear Material, 17, (1965), 294-304.

[42] D.J. Cherniak, E.B. Watson, Pb diffusion in zircon, Chemical geology, 172, (2000), 5-24.

[43] H.A. Resing and N. H. Nachtrieb, Self-diffusion of lead, thallium and bismuth in the solid lead-thallium system, J. Phys. Chem. Solids, 21, (1961), 40-56.

[44] N.G. Sawatsky and D.V. Oscarson, Diffusion of Technetium in dense bentonite, Water, air, and soil pollution, 57-58, (1991), 449-456.

[45] I. Sato, K. Tanaka, and T. Arima, Diffusion behaviors of plutonium and americium in polycrystalline urania, Materials Science and Engineering, 9, (2010), 012005.

[46] N. Y. Jamil and D. Shaw, The diffusion of Mn in CdTe, Semicond. Science Technology, 10, (1995), 952-958.

[47] Dominique Bayen, Release of Volatile Fission Products from Uranium Dioxide-MS Thesis, University of California, Nuclear Engineering Department, 1983.

[48] A. Almazouzi and et. al., Diffusion of iron and nickel in single-crystalline copper, Physical Review B, 54, (1996), 857-863.

[49] Ken-Ichi Hirano, R.P. Agarwala and Morris Cohen, Diffusion of Iron, Nickel and Cobalt in Aluminum, Acta Metallurgica, 10, (1962), 857-863.

[50] G. Busker, R.W. Grimes, M. R. Bradford, The diffusion of Iodine and caesium in the UO2±x lattice, Journal of Nuclear Materials, 279, (2000), 46-50.

[51] K. Sunder and et. al., Zinc and Gallium diffusion in gallium antimonide, Physical Review B, 75, (2007), 245210-1 - 245210-9.

[52] M. Hess and et. al., Diffusion constants of Br in NaCl measured by Rutherford backscattering spectroscopy, Journal of Applied Physics, 105, (2009), 124910-124915.

[53] J. Hovingh, Diffusion of Lanthanum in Molten Uranium, Department of Nuclear Engineering, University of California, Berkeley, California.

[54] D. E. Nazyrov, G. S. Kulikov, R. Sh. Malkovich, Diffusion of Promethium in Silicon, Tech. Physics Letter, 23, (1997), 68-69.

[55] F. Dyment and et. al., Diffusion of Hf in α-Zr, Applied Physics A, 51, (1990), 29-33.

[56] D. J. Cherniak, Zr diffusion in titanite, Contrib Mineral Petrol, 152, (2006), 639-647.

[57] A. Rodriguez and et. al., RBS characterization of the iridium diffusion in silicon, Nuclear Instruments and Methods in Physics Research B, 161-163, (2000), 663-667.

[58] K. Fukuda and K. Iwamoto, Diffusion Behavior of Fission Product in Pyrolytic Silicon Carbide, Journal of Nuclear Materials, 75, (1978), 131-144.

[59] F. Dyment and et. al., Ru Self-diffusion and Ru diffusion in Al, Defect and Diffusion Forum, 237-240, (2005), 402-407.

[60] Masaharu Komiyama and et. al., Diffusion coefficients of indium and tin in In-Sn alloys determined by Auger electron spectroscopy using xenon ion bombardment, Journal of Materials Science Letters, 5, (1986), 673-674.

[61] P. Gas and et. al., Diffusion of Sb, Ga, Ge, and (As) in TiSi2, Journal of Applied Physics, 63, (1988), 5335-5345.

[62] T. Okabe, A. L. Hines, R.F Hochman, Diffusion of mercury in Ag3Sn, Journal of Applied Physics, 47, (1976), 49-52.

[63] P. J. Shires, A.L. Hines, and T. Okabe, Diffusion of mercury in Ag2Hg3, Journal of Applied Physics, 48, (1977), 1734-1735.

[64] H. J. Höfler and et. al., Diffusion of bismuth and gold in nanocrystalline copper, Journal of Applied Physics, 74, (1993), 3832

[65] Y. Iijima, K. Hoshino, and K. Hirano, Diffusion of Titanium in Copper, Metallurgical Transactions A, 8A, (1997), 997-1001.

[66] E. López-Honorato and et. al., Silver Diffusion in Silicon Carbide Coatings, Journal of the American Ceramic Society, 94, (2011), 3064-3071.

[67] A. K. Jha and et. al., Diffusion of Silver in Cadmium, Scripta Metallurgica, 6, (1972), 495-500.

[68] J. Itoh and et. al., Diffusion and solubility of holmium ions in barium titanate ceramics, Journal of Materials Research, 19, (2004), 3512-3520.

V. SPENT FUEL INTERROGATION USING DELAYED FAST NEUTRON SPECTRUM AT MISSOURI UNIVERSITY OF SCIENCE AND TECHNOLOGY REACTOR

T. Akyurek, S. Usman

Department of Mining and Nuclear Engineering, Missouri University of Science & Technology, Rolla, MO, 65401, USA

Abstract

Interrogation of nuclear fuel and Plutonium (Pu) and Uranium (U) discrimination was performed using Missouri University of Science and Technology Reactor (MSTR) fuel by non-destructive (NDA) method. Post-irradiated delayed fast neutron spectra were obtained for two pairs of burnt and fresh fuels. Burnup and ^{239}Pu conversions were calculated based on neutron emission intensity ratios. After 100 kW high power runs, all fuel elements showed three distinct regions of neutron spectra; a distinct low energy peak followed by intermediate energy region without distinct peak but a wide hump, followed by a high energy peak with a long tail. At 10 kW low powers, intermediate energy hump and low energy peak seems to merge together while the high energy peak still remains distinct. Based on data from 10 kW power runs, the burnup values of F1 and F2 fuel elements were estimated to be 149 MWD/T and 196 MWD/T, respectively. ^{239}Pu conversion since 1992 for low enriched (19.75%) fuel elements was calculated as 0.24 g for F1 and 0.32 g for F2. Results based on high power runs of 100 kW provided comparable burnup of 217 MWD/T for F2. However the results for F1 were approximately 10 times higher perhaps due to unique burnup history and consequently high poison build-up. These experimental burnup results compare well with the reactor burnup calculation as reported to Nuclear Regulatory Commission (NRC).

1. Introduction

The nondestructive analysis (NDA) is an important technique for monitoring spent fuel for burnup credit calculations, accountancy of special nuclear material, safeguard and ensuring adherence to proliferation control programs. NDA is a well-established technique and can utilize either fission product gamma or the delayed neutrons. The primary objective of this work is to develop a technique capable of determining Plutonium burnup (Pu) content of the original fuel using delayed fast neutron based non-destructive method. Missouri University of Science and Technology Research Reactor (MSTR) was utilized for validation of the technique. Willman and co-workers reported NDA method for discriminating mixed oxide (MOX) fuel from low enriched uranium (LEU) fuel using gamma signature of fission products [1]. Dennis and Usman [2] reported a similar technique evaluating the feasibility of using gamma ray spectroscopy for MOX fuel discrimination. Subsequently they identified ^{106}Ru isotope as their isotope of choice [3] for burnup indicator and MOX fuel discriminator using gamma ray spectroscopy at MSTR. The gamma ray based NDA method is the only commercially available technique for measuring the composition of Plutonium and Uranium (U) in the spent fuel [4]. The technique has the drawback that it relies on the lowest energy direct peaks from Pu and U. The emitted gamma rays can be lost in the background since these isotopes emit low energy photons which make discrimination of Pu content from U difficult especially in MOX fuel analysis. However, Willman and coworkers were able to accomplish discrimination of MOX fuel and Uranium fuel using nondestructive gamma spectroscopy by obtaining ^{134}Cs/^{154}Eu ratio experimentally [1,5]. Akyurek and coworkers compiled a list of candidate isotopes for Pu-U discrimination for various applications [6]. Nondestructive analysis can

also be developed based on neutron measurements. Zhao [7] investigated the feasibility of using neutron measurement techniques for pebble bed reactor fuels for online burnup measurement. In fact, a technique based on the combination of the delayed neutron and gamma technique was developed to measure relative fission rate ratios between spent fuel and new uranium fuel [8]. Delay thermal neutron measurement technique is also being developed at Paul Scherrer Institut in Switzerland where the goal is re-irradiation at zero power and mapping the delayed neutron post irradiation to characterize the interfaces between burnt and fresh fuel assemblies using BF_3 detector as reported by Jordan and Perret [9]. Due to the detector being used at Paul Scherrer Institut their analysis relay on thermal neutron measurements which would introduce undesired additional uncertainty because of moderation process.

With recent Megatons to Megawatts program, the U.S. nuclear power industry is planning to introduce MOX fuel in the present fleet of nuclear reactors [10]. According to the agreement 35 metric tons (MT) of weapon-grade plutonium will be converted into MOX fuel [11]. Duke Energy utilized AREVA's MOX fuel assemblies for their Catawba Nuclear Station in 2005 starting a new era of nuclear fuel cycle in U.S. Regardless of how the U.S. nuclear fuel cycle evolves, better tools and techniques for measuring burnup and monitoring spent fuel will be required. Burnup measurement is important for various applications such as; burnup credit validation and verification, pre-transportation compliance certification, monitoring spent fuel for Special Nuclear Material (SNM) control, accountability, monitoring during storage for historic burnup analysis and possibly online burnup measurement for next generation reactors.

As a tool for technique development and validation, MSTR can be used for burnup analysis and discrimination of Pu and U content using nondestructive neutron measurements with LEU fuel. This research focused on developing a technique to be able to discriminate MOX(Pu) from LEU fuel using delayed fast neutron measurements. Bubble Technologies (BTI) Portable Spectroscopic Neutron Probe (N-Probe) detector [12] was used in this study to collect fast delayed neutron spectra from various fuel elements.

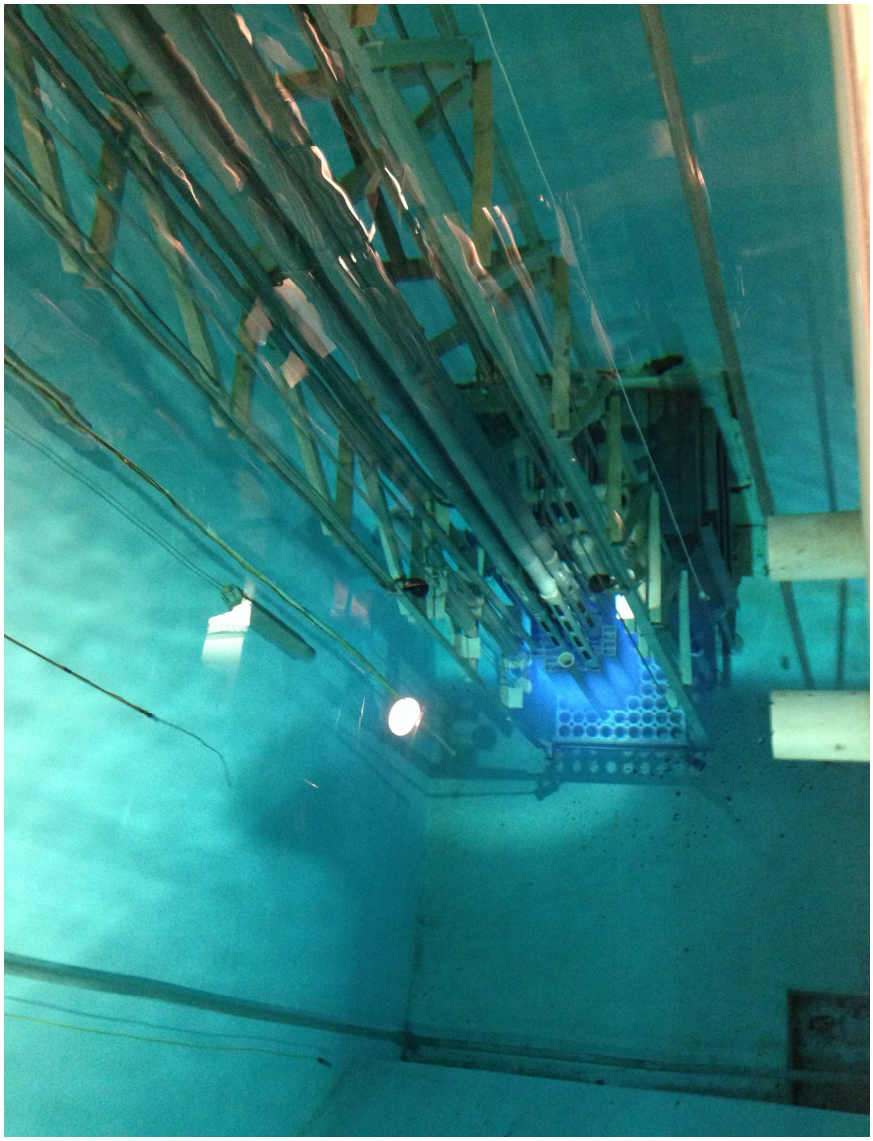

Figure 1. Picture of MST Reactor pool and core with Cherenkov radiation

2. Description of MST Reactor

Fig. (1) shows MSTR which is a swimming pool reactor licensed by NRC to operate at 200 kW thermal power. MSTR has been in operation for more than 50 years. It is the first nuclear reactor in the state of Missouri that serves as an excellent facility for research and training.

The reactor pool contains 32,000 gallons of high purity water in a pool which is 30 feet deep, 9 feet wide and 19 feet long. The reactor core is movable in the pool and there are two modes of operation; the T mode and the W mode. Reactor is said to be in the "T" mode when the core is moved close to the thermal column providing improve thermalization. On the other hand, when the reactor core is pushed away from the graphite it is said to be in "W": or water mode. The reactor core was refueled to LEU fuels in 1992 [13] and the LEU fuels have been in use since then. The reactor core consists of 15 fuel elements and 4 control rods. Fig. (2) shows a mock fuel element and the configuration of fuel plates in each fuel element. Each fuel element consists of 9 fuel plates and each plate contained 12.5 g of enriched ^{235}U at the beginning of its life.

Figure 2. Picture of fuel element and fuel plates

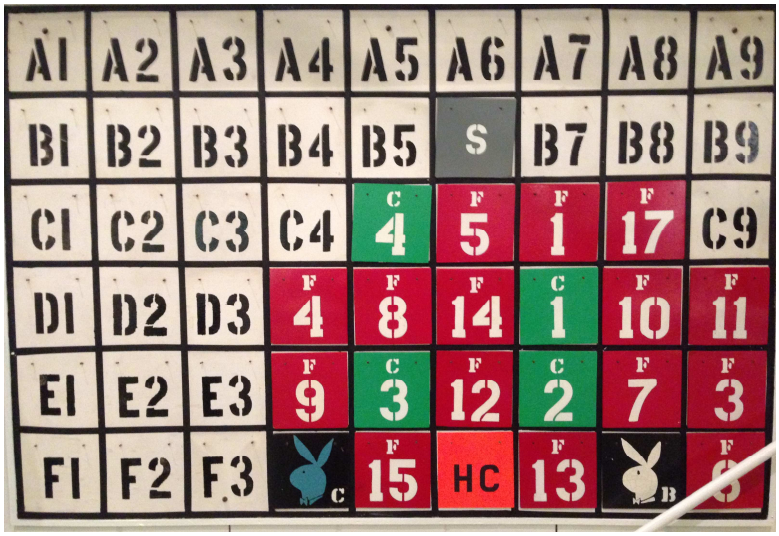

Figure 3. Picture of the MST reactor core grid plate. Rabbits represent experimental facilities (Cadmium and Bare), an "F" above the number represents a fuel assembly, a "C" above the number represents a control rod, "HC" is the hot cell and "S" represents a source for reactor start-up.

The fuel is in the form of Uranium Silicide-Aluminum (LEU U_3Si_2-Al) with 19.75 ± 0.2 wt% enriched ^{235}U. The silicon content of U_3Si_2 is 7.5 ± 0.4 wt%. MSTR current fuel configuration (called T121 to specify that it is close to the thermal column) is shown in Fig. (3). The beam port, which was used in our experiments, is located near the fuel element "F11". Table 1 shows the burnup and conversion history of the reactor core fuel elements as reported to NRC. During the last 23 years of operation with LEU, the core went through many core re-configurations and consequently the burnup of various fuel elements are significantly different. Some new and used fuel elements are still available in the reactor pool storage and can be used as Pu free elements. These new fuel elements can be used to compare with irradiated U element to developed burnup measurement and discrimination technique. Old fuel is expected to have higher quantities of Pu content and hence the difference in post irradiation delayed neutron measurement can be related to Pu contents of the fuel.

Table 1. MST Research reactor Fuel Burnup/Conversion History since 1992 [21].

Reporting Period	Total kW/hr to date	Burnup assigned to fuel element #	U-235 burnup to date in grams	U-235 burnup and conversion per reporting period in grams	U-235 burnup and conversion to date in grams	Conversion Plutonium to date in grams
07/23/92 - 03/31/93	3557.0		0.1549	0.1834	0.1834	0.0285
04/1/93 - 03/31/94	12205.5	1g, F-3	0.5315	0.4458	0.6292	0.0977
04/01/94 - 03/31/95	16793.3		0.7313	0.2365	0.8657	0.1344
04/01/95 - 03/31/96	25707.6		1.1195	0.4595	1.3252	0.2057
04/01/96 - 03/31/97	31450.8		1.3696	0.2961	1.6213	0.2517
04/01/97 - 03/31/98	38239.7	1g, F-2	1.6653	0.3500	1.9713	0.3060
04/01/98 - 03/31/99	48390.3		2.1073	0.5232	2.4945	0.3872
04/01/99 - 03/31/00	55710.8		2.4261	0.3674	2.8619	0.4358
04/01/00 - 03/31/01	61842.8	1 g, F-1	2.6931	0.3161	3.1780	0.4849
04/01/01 - 03/31/02	65676.2		2.8600	0.1977	3.3757	0.5157
04/01/02 - 03/31/03	78537.7		3.4201	0.6630	4.0387	0.6186
04/01/03 - 03/31/04	112199.4	1 g, F-7 1 g, F-8	4.8861	1.7353	5.7740	0.8879
04/01/04 - 03/31/05	142557.5	1 g, F-9	6.2143	1.5685	7.3425	1.1282
04/01/05 - 03-31-06	183355.0	1g, F-12 1g, F-13	7.9992	2.1079	9.4504	1.4512
04/01/06 - 03/31/07	202098.6	1g, F-5	8.8192	0.9684	10.4188	1.5996
04/1/2007- 03/31/08	216161.9		9.4345	0.7266	11.1454	1.7109
04/1/2008- 03/31/09	226442.9	1g, F-4	9.8843	0.5312	11.6766	1.7923
4/1/2009 - 3/31/2010	244391.9	1g, F-10	10.6696	0.9274	12.6040	1.9344
4/1/2010 - 3/31/2011	256130.7		11.1831	0.6065	13.2105	2.0273
4/1/2011 - 3/31/2012	282811.1	1g, F-14	12.2980	1.3168	14.5272	2.2292
4/1/2012 - 3/31/2013	305806.5	1g, F-15	13.3041	1.1881	15.7153	2.4112
4/1/2013 - 3/31/2014	341338.0	1g, C-1 1g, C-2	14.8586	1.8358	17.5511	2.6925

Table 1 shows approximate burnup history of MSTR fuel. The fuel is shuffled periodically and the most irradiated element is assigned burnup credit in the units of g of ^{235}U. It is important to recognize the approximate nature of burnup credit assignment to various fuel elements. Periodically, the most burnt element is assigned with total core burnup in grams. While this information is rather crude, in the absence of anything better it is being used as the approximate burnup of a specific element. Over the years, burnup value (in grams) has been assigned to various fuel elements in the core. This randomly assigned burnup approximation does not represent the actual burnup value in a particular fuel element. Therefore, a better burnup calculation or measurement is needed for the reactor core. Table 1 also shows the approximate conversion of ^{238}U to ^{239}Pu based on the total kW-hr of reactor run time.

3. Theory of Delayed Neutrons

Fission produces a large number of isotopes many of them being neuron rich. These neutron rich isotopes are the source of delayed neutrons. Decay of neutron rich isotopes and production of delayed neutrons plays significant role for controlling the nuclear reactors even though they comprise only about 1% of the total neutrons released from fission. There are over 250 well known precursors responsible for delayed neutron [14]. However, dealing with these individual precursors for reactor kinetics is computationally impractical. Therefore these neutron precursors are grouped together with isotopes of similar half-lives. Traditionally, 6-groups of delayed neutron have been used but other grouping schemes are also reported in the literature. For example, Isaev and co-workers [15] proposed 12-groups of delayed neutrons based on Iodine and Bromine. While other studies have recommend eight group for delayed neutron for reactor kinetics [16]. These

grouping of neutron rich precursors/fission products is based on their half times. For example, ^{87}Br (has half-life of 55.6 seconds) is known to produce delay neutron and is grouped as the longest lived precursor. Other probable neutron precursors are ^{137}I, ^{89}Br, ^{139}I, ^{85}As, ^{9}Li from thermal fission of ^{235}U.

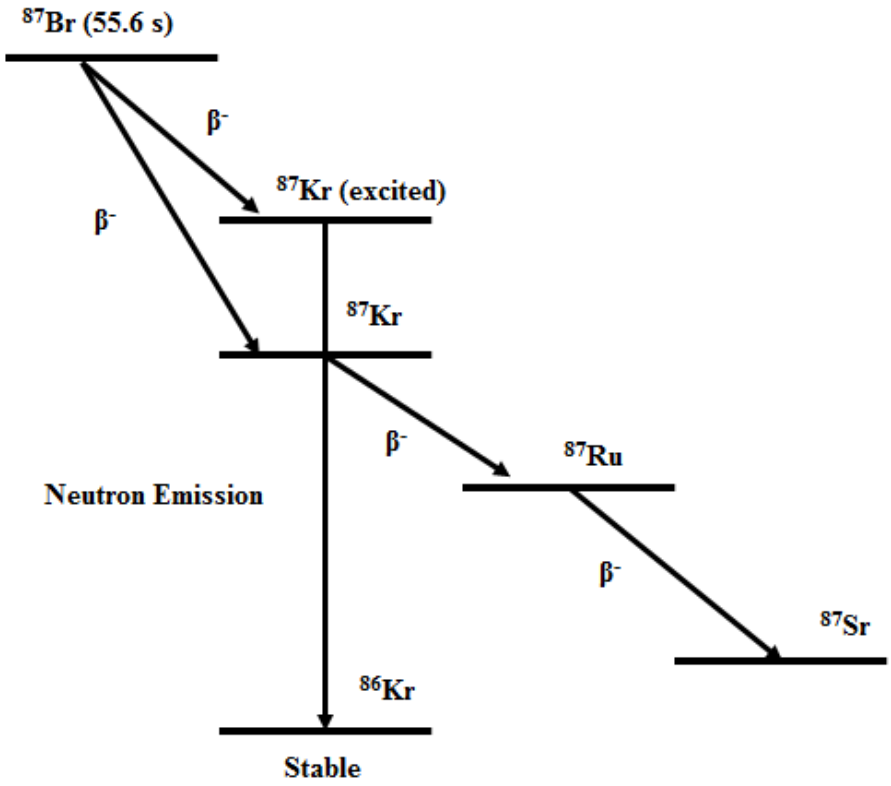

Figure 4. An illustration of the neutron emission from ^{87}Br isotope

When a precursor undergoes β-decay, it will end up in an excited daughter nucleus which then emits a neutron. Therefore, the delay in neutron production is based on precursor's half-life. For example, Fig. (4) shows the delayed neutron emission ^{87}Br. The β-decay goes through with two different branches and ^{87}Br isotopes can take two different paths [17]. It is only when ^{87}Kr goes through neutron emission decay mode that a neutron is produced.

There are many decay chains that are important in the delay neutron emission. The precursors can be described with six groups (*i*), each of them characterized by decay constant (λ_i), and a fractional yield (β_i). The term β_i is defined by the fraction of all the fission neutrons emitted in fission which appear as delayed neutrons in the *i*th group. Table 2 lists the properties of the typical 6 groups of delayed neutrons released during the fission of ^{235}U, ^{233}U, ^{239}Pu and ^{238}U. It is important to also recognize that the energy spectrum of the delayed neutron from each precursors is different and hence their effectiveness to cause subsequent fission is also different. Various aspects of neutrons and their impact on reactor kinetics are covered well in the report by Nuclear Energy Agency (NEA) Nuclear Science Committee [18].

Assuming all the delayed neutrons are produced by decay of a fission product, the number of total neutrons post shutdown can be estimated by sum of exponential weighted by the fission yield of the respective precursor;

$$N(t) = \sum_i w_i . e^{-\lambda_i t} \quad (1)$$

where w_i is the fission yield of precursor and t is the time post shutdown. Eq. (1) provides the time dependence of delay neutrons per fission.

For thermal neutron systems, the lower average delayed neutron energy can decrease the resonance absorption and leakage during slowing down which results in an increase reactivity impact. The delay neutron energy spectra for different isotopes are available in literature [20]. In general, thermal reactor delayed neutrons are more effective in sustaining fission chain reactions than prompt neutrons.

Table 2. Characteristic 6-group delay neutron parameters for ^{235}U, ^{233}U, ^{239}Pu, ^{238}U [19].

Group	Decay Constant λ_i (1/s)	Mean Life $\tau=1/\lambda_i$ (sec)	Half Life $\ln 2/\lambda_i$ (sec)	Fission Yield w_i (n/fission)	Fraction Yield β_i
Thermal Fission in ^{235}U					
1	0.0124	80.645	55.720	0.00052	0.000215
2	0.0305	32.786	22.720	0.00346	0.001424
3	0.111	9.009	6.220	0.0031	0.001274
4	0.301	3.322	2.300	0.00624	0.002568
5	1.14	0.877	0.610	0.00182	0.000748
6	3.01	0.332	0.230	0.00066	0.000273
Total				**0.0158**	**0.0065**
Thermal Fission in ^{233}U					
1	0.0126	79.365	55.000	0.00057	0.000224
2	0.0337	29.673	20.570	0.00197	0.000777
3	0.139	7.194	5.000	0.00166	0.000655
4	0.325	3.076	2.130	0.00184	0.000723
5	1.13	0.884	0.615	0.00034	0.000133
6	2.5	0.44	0.277	0.00022	0.000088
Total				**0.0066**	**0.0026**
Thermal Fission in ^{239}Pu					
1	0.0128	78.125	54.280	0.00021	0.000073
2	0.0301	33.222	23.040	0.00182	0.000626
3	0.124	8.064	5.600	0.00129	0.000443
4	0.325	3.076	2.130	0.00199	0.000685
5	1.12	0.892	0.618	0.00052	0.000181
6	2.69	0.371	0.257	0.00027	0.000092
Total				**0.0061**	**0.0021**
Fast Fission in ^{238}U					
1	0.0132	75.757	52.380	0.00054	0.00019
2	0.0321	31.152	21.580	0.00564	0.00203
3	0.139	7.194	5.000	0.00667	0.0024
4	0.358	2.793	1.900	0.01599	0.00574
5	1.41	0.709	0.490	0.00927	0.00333
6	4.02	0.248	0.172	0.00309	0.00111
Total				**0.0412**	**0.0148**

4. Experimental Setup

In order to investigate spent fuel and Pu/U content with delay neutron spectrum, NDA was performed using N-Probe Liquid scintillator detector at the Missouri S&T nuclear reactor (MSTR) beam port. Three aspects of experimental setup; MSTR fuel, N-Probe Liquid scintillator detector setup and MSTR nuclear beam port facility are importan for data collection and are discussed here.

MSTR fuel was described in the previous section. The beam port is the link between the reactor pool and the neutron detector, through the pool wall to the basement where delay neutron detection equipment was located. The beam port is made up aluminum beam tube and closed at its end in the reactor pool. Fig. (5) shows a drawing of the beam port, Bubble Technologies (BTI) N-Probe neutron detector, the MST fuel grid which identifies fuel element “F11” as the location closest to the beam port termination. The beam port is 15.24 cm in diameter without the shutter assembly. Stainless steel shutter assembly allows beam collimation and is configurable with dimension of 7.6 cm x 5.1 cm.

MSTR has a 5.8 cm lead gamma shielding which can be placed in the beam port to stop undesired gamma radiation. For all measurements during this study the gamma shield was present in the beam. Even if there was no lead gamma shielding, detector has the ability to discriminate the gamma radiation out from neutrons. The photon shielding is located 1.75 m away from grid location D9 (fuel element “F11”). In “T” mode only grid location D9 (fuel element F11 in Fig. 5) is in the line of the beam port and the detector is almost exclusively reading the F11 neutrons. Therefore it is assumed that all the neutrons detected in this configuration are for F11.

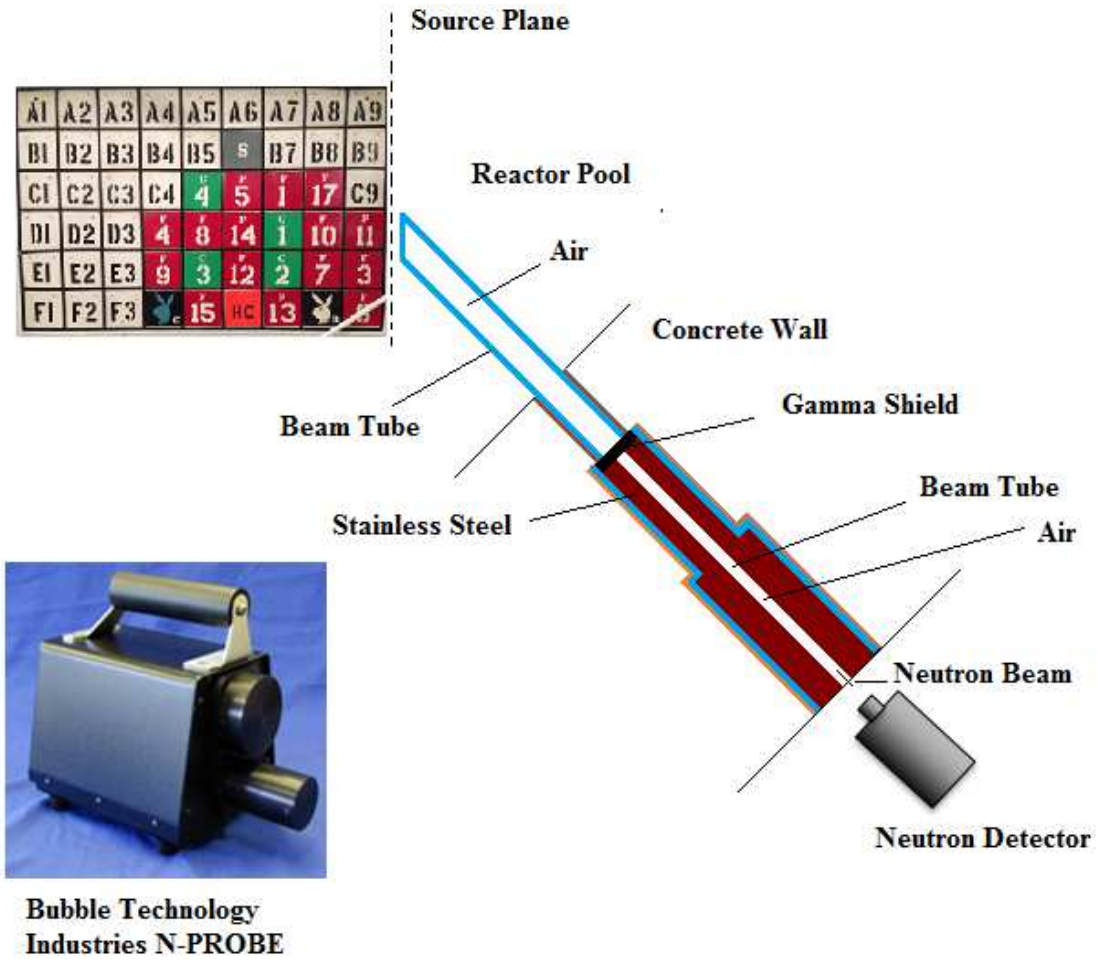

Figure 5. MST nuclear reactor beam port facility. Schematic shows the MST reactor grid plate, aluminum beam port with stainless steel shutter assembly and the N-Probe neutron detector which provides both thermal and fast neutron spectrum.

Grid location D9 under T-mode, as shown in Fig. (5) (location of "F11") was used for all experiments. Ideally, the fuel assembly under interrogation should be removed from the grid and placed near the underwater counting system. However, no resources were available for underwater fuel measurements, therefore, countings were performed from D10 location through the beam port. These measurements can therefore be regarded as "bulk measurements" of the core with most delayed neutron contribution coming from the closest fuel element D10. Effect of reactor power (10 kW and 100 kW power) on the

delayed neutron production was also investigated because it is anticipated that at higher power the moderator density will be reduced and the neutron energy spectrum will shift towards the high energy side and as a result there will be a shift in the production rate of certain precursors. Data for irradiated at various reactor powers (10 kW and 100 kW power) were collected after 15 minutes of operation at a particular power. The reason for operating the reactor for 15 minutes is to allow for precursors to reach their steady state concentrations. Longest lived precursor has a half-life of less than one minute and would reach steady state in 15 minutes. The attenuating mediums are 0.13 m of water, 1 cm of 1100-H14 Aluminum, 5.8 cm of lead shielding, and approximately 6.39 m of air [21]. Delayed fast neutron data was collected for 30 minutes after shutdown. Thermal neutron measurements were not taken into account for this study because of the attenuating mediums between the reactor core fuel element located at D9 and the neutron detector. Due to the geometry of the measurement low thermal neutron counts were recorded; not sufficient for any analysis and investigating of spent fuel.

Although the fuel elements in our experiments were different than LWR fuel elements, the same fundamental NDA method can be developed further for different LWR fuels. In this study, four different fuel elements were used to interrogate the burnup analysis and Pu/U discrimination. The two fuel elements (F1 and F2) were fairly used in the reactor core since 1992. “F1” fuel element (old fuel) mostly burnt at the edge of core grid while “F2” fuel element (old fuel) burnt in the middle of the core. The other two “new” fuel elements (F11 and F16) stayed in storage unit in pool since 1992 except F11 was used for a couple months in 2007 in the core. Using these two old and two new fuel elements, the burnup and Pu conversion values can be determined in a unit of gram with NDA method.

Bubble Technology Industries (BTI) portable neutron spectrometer (N-Probe) was used for collecting all experimental data. N-Probe is a detector for measurement of nuclear facilities, spent fuel storage areas, waste processing operations [12]. Fig. (5) also shows the N-Probe spectrometer which contains 5cm x 5cm diameter NE-213 liquid scintillator detector to measure fast neutrons between 800 keV and 20 MeV as well as spherical ^{3}He detector to measure thermal neutrons between 0 to 1.5 MeV based on $^{3}He(n,p)^{3}H$ reaction [22]. NE-213 liquid scintillator, which contains purified xylene, naphthalene, activators and wave-shifter, has an excellent pulse shape discrimination properties [23]. Therefore, NE-213 liquid scintillator used in BTI fast neutron probe is able to remove undesirable photons from the signal. Besides, these two detectors work simultaneously and pulse-height distributions from both are shown during the measurements. The two spectra can be switched by simple command in the software application. The combination of thermal and fast neutron measurements provide new capability for spent fuel interrogation. Post shutdown fast neutron spectroscopy has not been reported in the literature, particularly for burnup analysis.

The software interface currently available with the detector however does have a serious shortcoming; it does not allow the user to separate second by second (which is the smallest data acquisition time) spectra information for any detailed analysis. While the data can be displayed on the screen, there is no mechanism for the user to download the information, and manipulate the data. Furthermore, one second minimum acquisition time is perhaps too long for the initial measurements just after the shutdown where good statistics are possible with sub-second collection time. On the other hand, much of the short lived isotopes' information is lost by lumping the data into per second bins.

Four different core configurations were used for the data collection during this study. In February 2014, two tests were performed in "T" mode; T119 when the location D9 was occupied by the fuel element F2 and T120 when the location D9 was occupied by F11. Fuel element F2 was a well-used element (mostly in the center of the core) since 1992. Fuel element F11 was comparatively new fuel with an estimated burnup close to 0 MW-hours. The burnup value for entire core was approximately 300 MW-hours and no specific burnup information about single fuel element was available. Therefore, the burnup information between fuel elements F11 and F2 was investigated. Since there is a significant burnup difference between F11 and F2, one would expect some Pu build-up in F2. In October 2014, two additional tests were performed in "T" mode; T121 when the location D9 was occupied by the fuel element F16 and T122 when the location D9 was occupied by F1. Fuel element F1 is a well-used element (mostly at edge of core grid). Fuel element F16 was new fuel with 0 MW-hours burnup. In October 2014, the burnup value for entire core was approximately 340 MW-hours, however, no specific burnup information was available for individual elements. The burnup information between fuel elements F11 and F2 was investigated and Pu build-up calculated in unit of gram based on the experimental results.

For every new core configuration, all safety test and calibrations were performed including; regulating and safety shim rod calibrations, calculation of shutdown margin and excess reactivity etc. These results are documented in the reactor log book. In general, the placement of the new fuel element resulted in an increase of the reactivity of the core, always a senior reactor operator was available to run the reactor as per Nuclear Regulatory Commission (NRC) regulations. The total reactivity worth was 8.578% $\Delta k/k$ for 120T core

configuration, 9.229% Δk/k for 121T core configuration, 9.497% Δk/k for 122T core configuration [21].

5. Results

Cumulative delayed fast neutron data for 30 min count post shutdown were collected for four different fuel elements; two almost new and the other two significantly aged fuel elements. Neutron energy spectra showed the dependence on the reactor power during irradiation and the age of the fuel element. A pair of used (old) and fresh (new) fuel (F1 and F11, respectively) was used to collect delayed neutron data in February 2014 and another pair of used and fresh fuel (F2 and F16, respectively) was analyzed in October 2014. As mentioned before delayed fast neutron data were taken after 15 minutes of irradiation at two power levels; 10 kW and 100 kW power. The reason for operating the reactor for 15 minutes is to allow for short lived precursors to reach their steady state concentrations. Longest lived common precursor ^{87}Br has a half live of 55 seconds and would reach the steady state in 15 minutes. In all cases there were two distinct regions; a low energy peak followed by a high energy peak ending with an exponential tail. For high power runs, the region between the high energy and the low energy appears to contain a bumpy region which disappears at low power runs. Nevertheless, this continuum region shows a distinct feature of the neutron energy spectrum after high power run.

Figs. (6) and (7) show the cumulative (time integrated) energy spectra of F2 (old) and F11 (new) after 10 kW and 100 kW power runs, respectively. In the case of low reactor power there was a very prominent peak at low energy. The low energy peak showed higher intensity for the old fuel. This low energy peak had a long tail which ended at the second

high energy peak. It is interesting to note that the intensity of the high energy peak is higher for the new fuel than the old fuel.

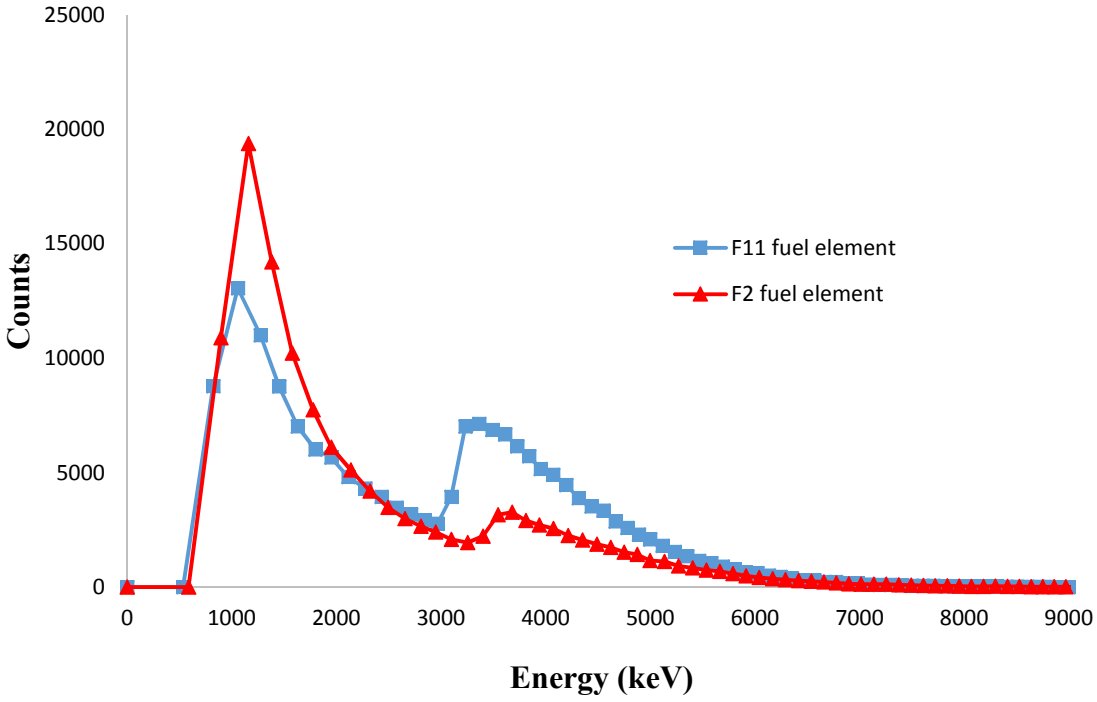

Figure 6. Delayed fast neutron spectrum for F2 and F11 fuel at 10 kW power.

When the neutron spectra for the old and new fuels were compared for high power run, the intensity of low energy peak for old fuel was less than the new fuel. Intensity-wise the order of the high energy peak remained unchanged; that is the new fuel had a higher intensity high energy peak than the old fuel. This observation is consistent with delayed neutron fraction of U (0.0065) being larger than Pu (0.0021). However, the order of the low energy peak was reversed; the intensity of the old fuel was lower than the new fuel. Moreover, the region between the two peaks was now seen to show a broad peak or a bumpy region with higher intensity for the new fuel than the old fuel. Based on these observations it seems that the low energy peak has some power dependence not desirable

for any burnup analysis. It might be advantageous to rely on the full integrated energy spectrum for any burnup analysis

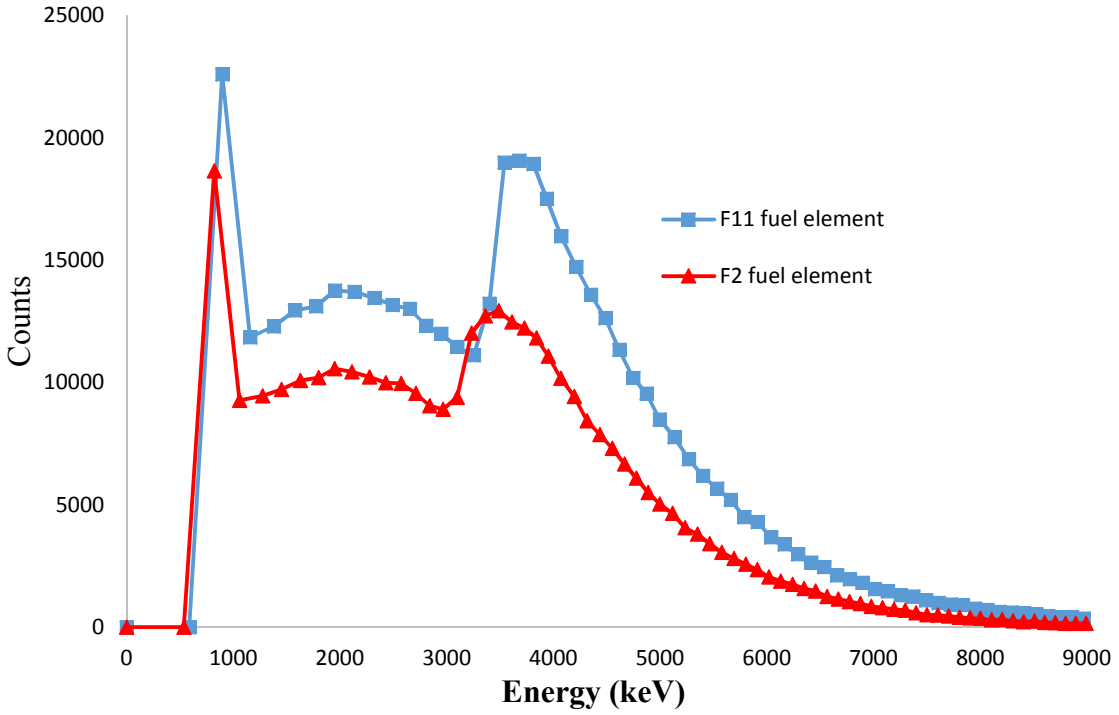

Figure 7. Delayed fast neutron spectrum for F2 and F11 fuel at 100 kW power.

Figs. (8) and (9) show the temporal response of fast delay neutrons. For all cases, there is a pattern of build-up for the first 20 seconds. While the net neutron counts are due to an agglomeration of many isotopes, there seems to be a trend of build-up in the majority of the isotopes to produce the net build-up effects. For the low power runs, low energy neutrons dominate the total counts during the first 100 seconds after shutdown. This is not the case for high power runs where the high energy neutrons dominate for the entire period after the shutdown. It is important to note that after 130 seconds, for both cases of 10 kW and 100 kW the high energy neutrons suggesting no power dependence. For this reason data for this time period is useful for burnup analysis.

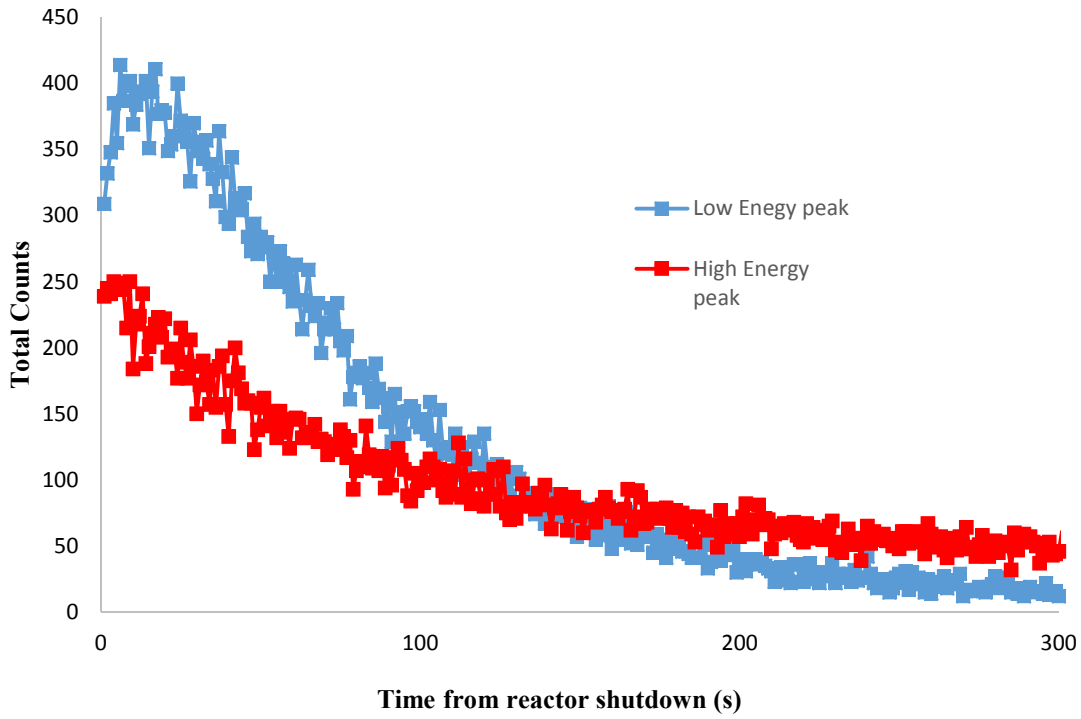

Figure 8. Temporal response of high and low energy peaks after 10 kW shutdown.

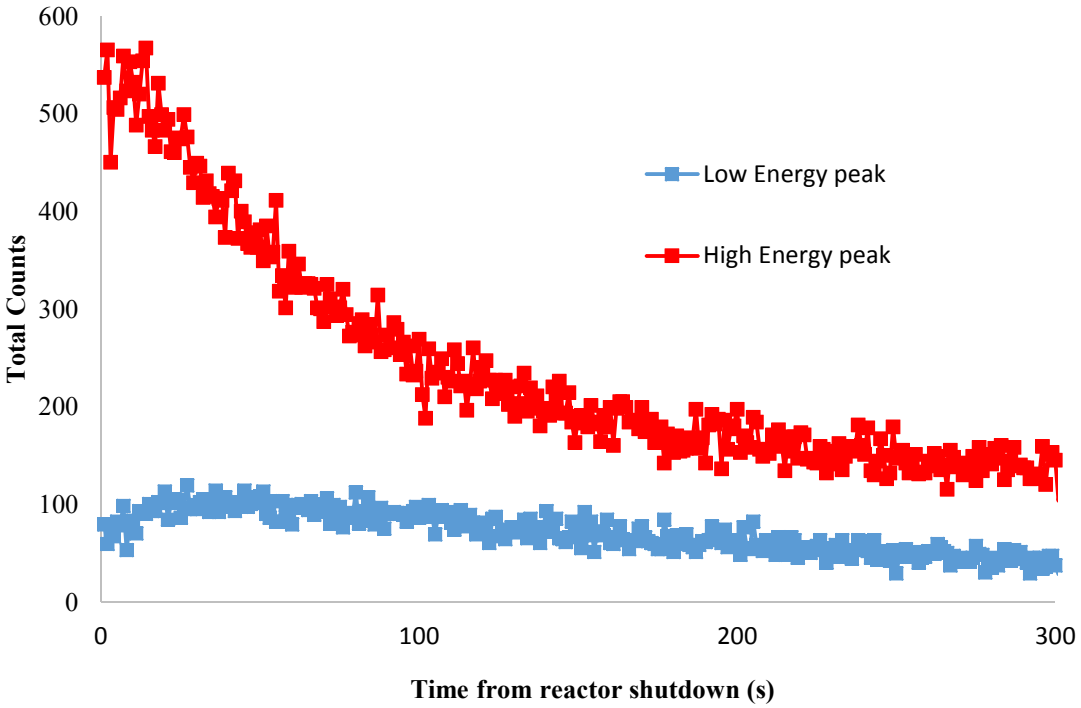

Figure 9. Temporal response of high and low energy peaks after 100 kW shutdown.

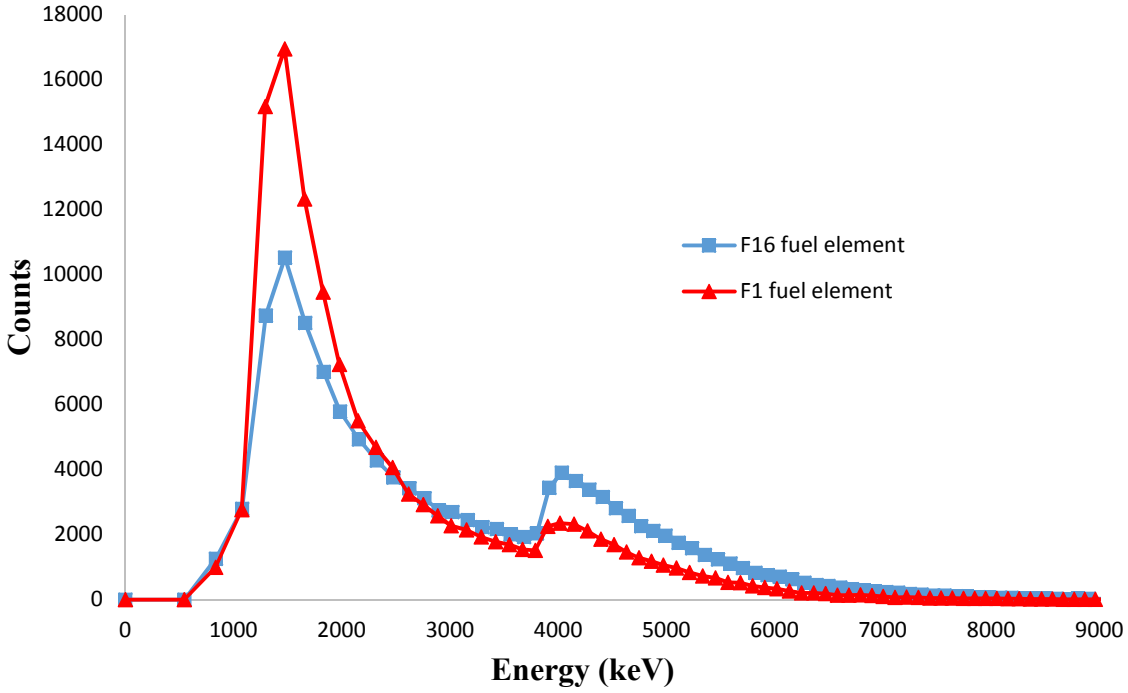

Figure 10. Delayed fast neutron spectrum for F1 and F16 fuel at 10 kW power.

To confirm the experimental data from F2 and F11 fuel elements, another pair of burnt (F1) and fresh (F16) fuel spectra was collected. Results for second experiment showed similar behavior as described above. The low energy peak of F1 fuel was dominant in contrast to high energy peak of F16 fuel at 10 kW reactor power (see Fig. 10). However, at 100 kW power the low energy peaks were not as prominent as the previous experiment. However, similar bump region and high energy peaks were observed (see Fig. 11). A slightly shift in peak locations was observed for the higher energy peaks of F2 and F11 which could be due to the detector calibration drift.

After collecting all fuel elements' spectra, the data needed to be manually separated second by second for further analysis since the software does not offer automatic data extraction. While for some very short lived isotopes one second may be too long of an interval to capture accurate build-up and decay history, but in general one second bin

provided a reasonable picture of precursor build-up and decay. Assuming the delayed neutrons were arriving at the detector right after reactor shutdown, delayed fast neutron decaying data was acquired by extracting the energy spectra for every second. Fig. (12) shows the cumulative temporal response of F2 and F11 after 10 kW power run. For low power runs, a noticeable initial build-up and decay of the precursor responsible for the low energy peak is observed. Same is true for the other pair of old (F1) and new (F16) fuel elements. It is quite interesting that the build-up is not for the same fuel elements after high power runs (see Figs. 14 and 15).

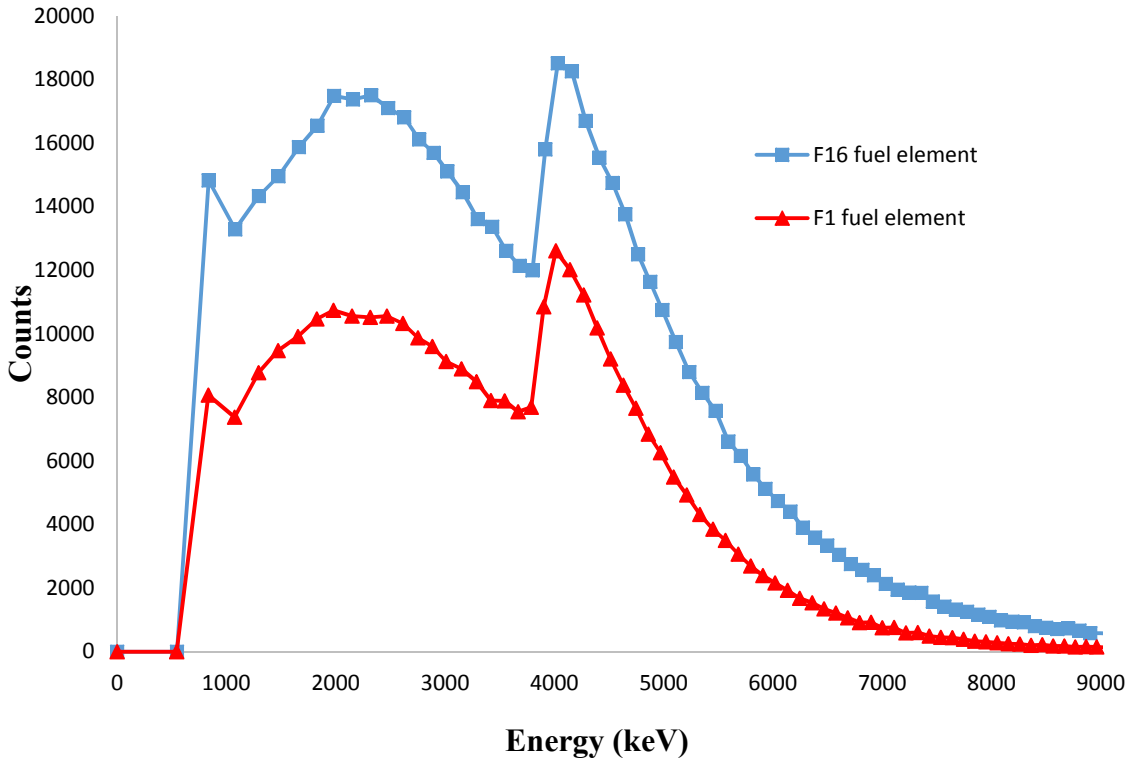

Figure 11. Delayed fast neutron spectrum for F1 and F16 fuel at 100 kW power.

A similar build-up was reported by Jordan and Perret [9]. As seen in their Fig. (3) [9], there is an obvious build-up for fresh fuel as well as for all burned fuels. The time to

reach peak build-up is approximately 10-15 seconds. They attributed this rise in the neutron count rates to the fuel movement – "The arrival of the sample in the measurement position is seen as a bump in the time series." However, the duration of the bump lasted for approximately 10-15 second which is much longer and not consistent with their conclusion. It is believed that the bump that was also observed in the present study (even without any fuel element movement) is the result of the precursor build-up and decay.

If we assume that the neutron precursor (which admittedly is not a single isotope but an agglomeration of many isotopes) is a single isotope with a decay constant of λ_P which is produced either directly from fission with a yield of γ_P or by radioactive decays of a parent isotope P with a decay constant of λ_P, one can write the transient concentration equation of the precursor as;

$$\frac{dP(t)}{dt} = \lambda_{P'} P' + \gamma_P \bar{\Sigma} \phi_T - \lambda_P P - \sigma_{aP} \phi_T P \qquad (2)$$

The steady state concentration at a given power would then be;

$$P = \frac{\lambda_{P'} P' + \gamma_P \bar{\Sigma} \phi_T}{\lambda_P + \sigma_{aP} \phi_T} \qquad (3)$$

At high power/flux if the absorption cross section is large, the concentration would be small; exactly what we observed after high power runs that the build-up was negligible. To better illustration, 3D version of the delayed fast neutron count rate with corresponding time and energy graphs are shown in Figs. (16), (17), (18) and (19) for each fuel elements at 100 kW run.

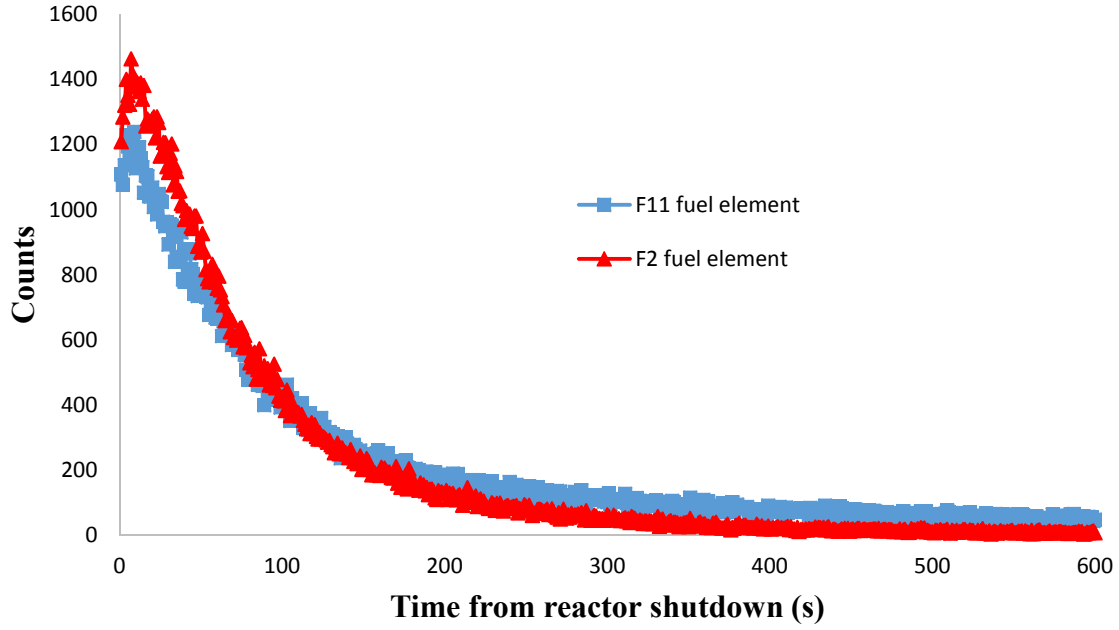

Figure 12. Fast neutron count rate from F2 and F11 fuel at 10 kW power run.

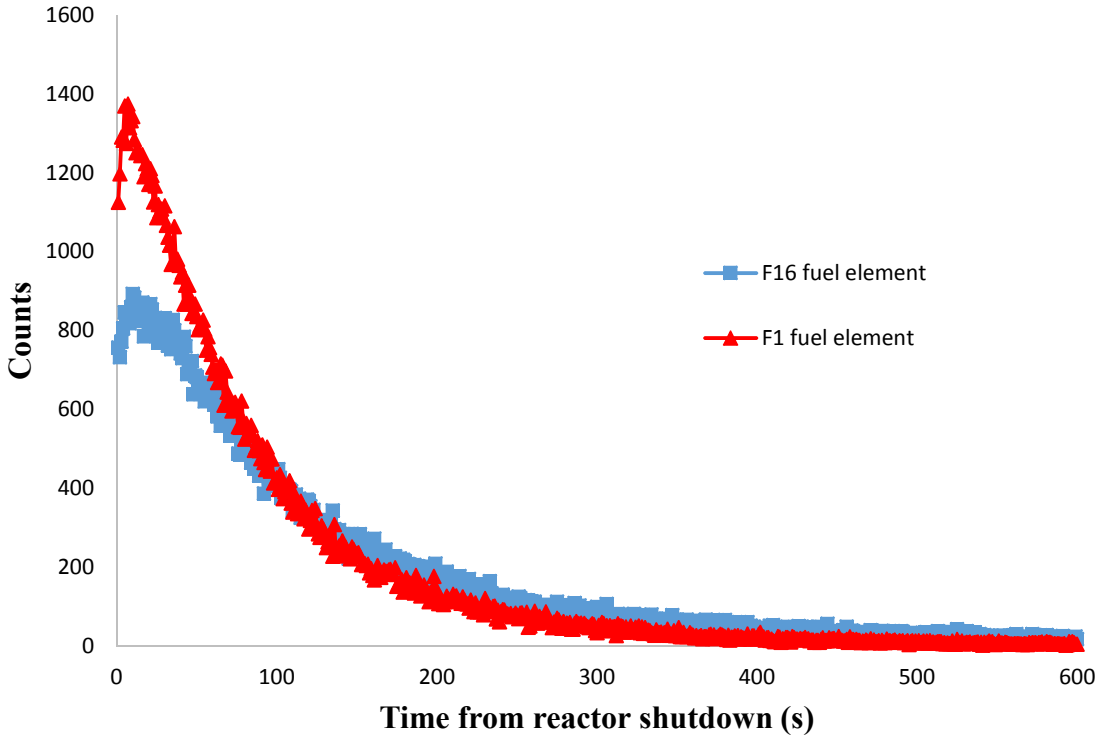

Figure 13. Fast neutron count rate from F1 and F16 fuel at 10 kW power run.

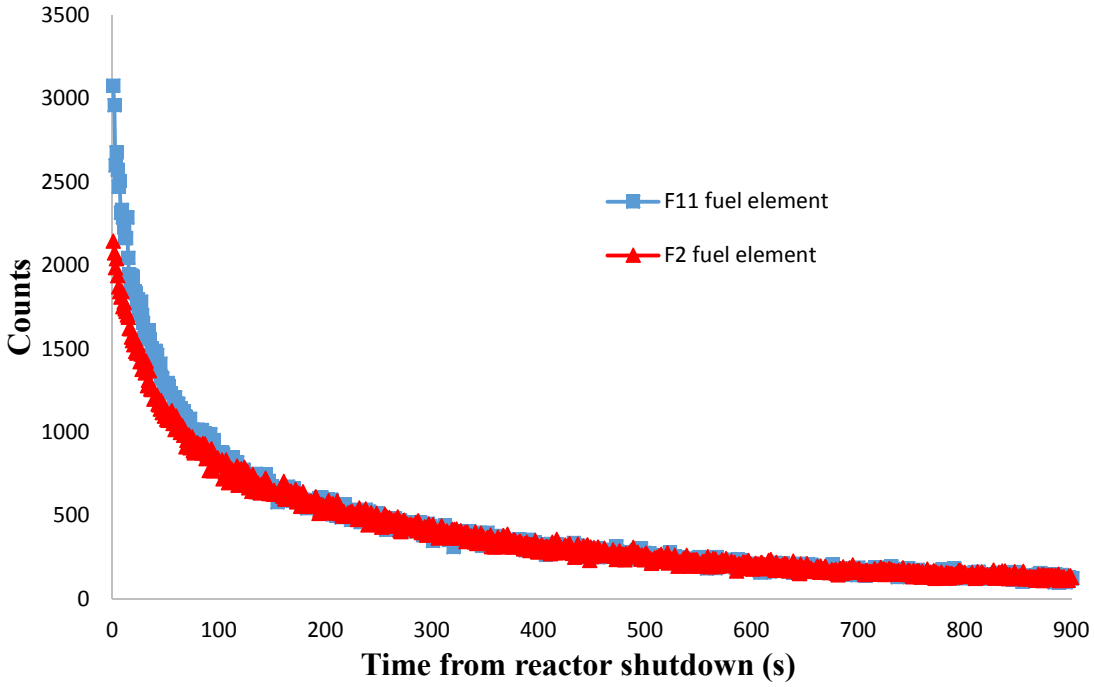

Figure 14. Fast neutron count rate from F2 and F11 fuel at 100 kW power run.

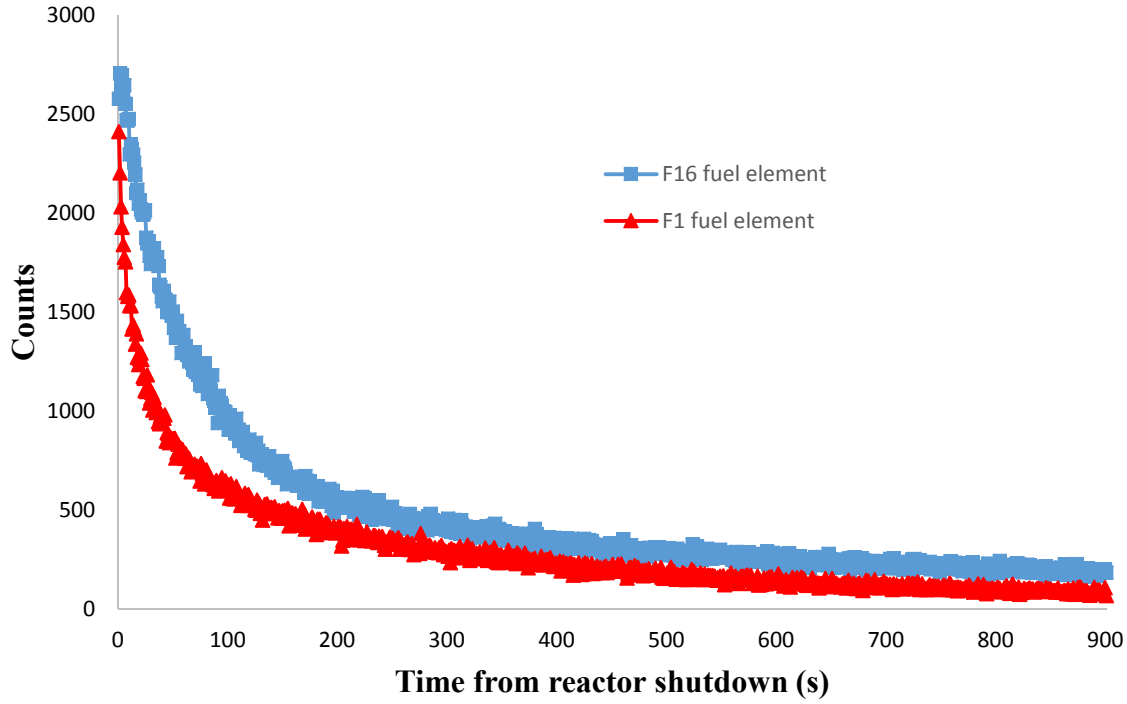

Figure 15. Fast neutron count rate from F1 and F16 fuel at 100 kW power run.

Although measurements were taken for 1800 seconds the 3D graphs were shown for 250 seconds only. The count rates from used fuels were less than fresh fuels. F11 (new) and F16 (new) fuel elements were shown seemingly similar count rates with corresponding energies and times as well as F2 (old) and F1 (old) fuel elements. However, all the 3D graphs showed that there is an energy dependence on fast delayed neutron count rates. The different count rates made a curve from high energy level to low energy level when data collection time increased. The curve for old fuel elements became straight at around 50 seconds while the curve for new fuel elements disappeared and became straight at around 80 seconds. This indicates that fuel elements have different burnup history.

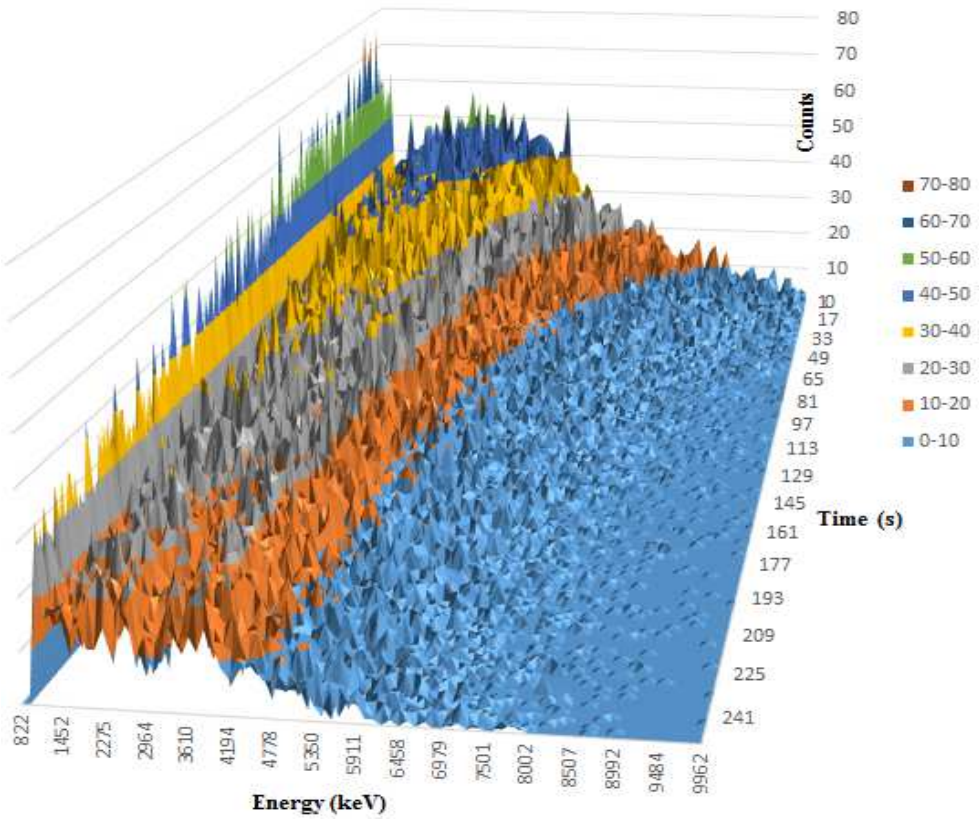

Figure 16. 3D graph for fast neutron count rate from F2 fuel at 100 kW power run.

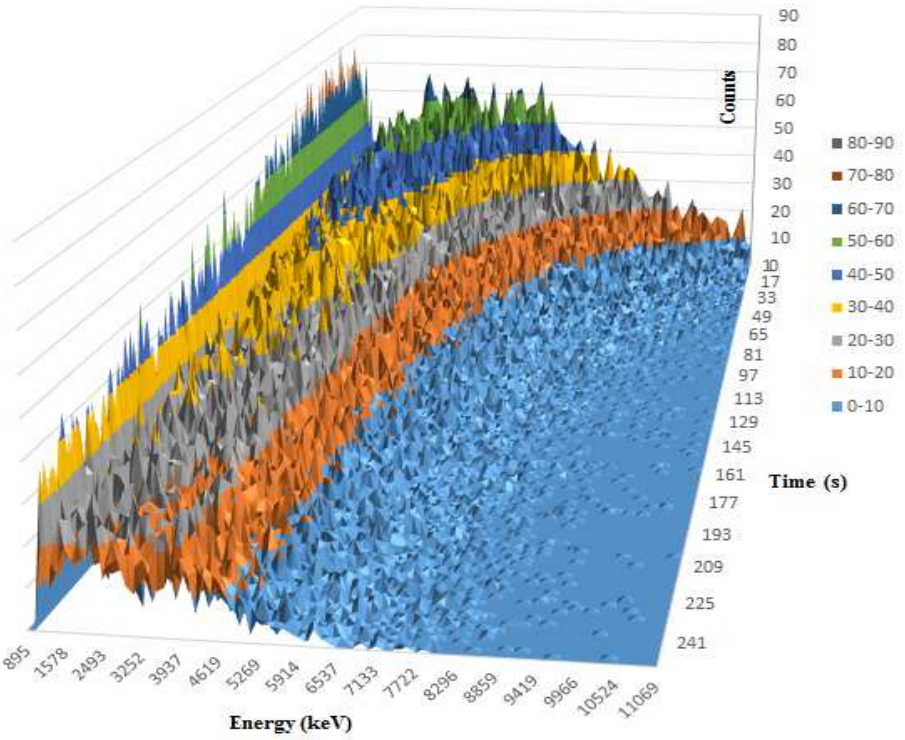

Figure 17. 3D graph for fast neutron count rate from F11 fuel at 100 kW power run

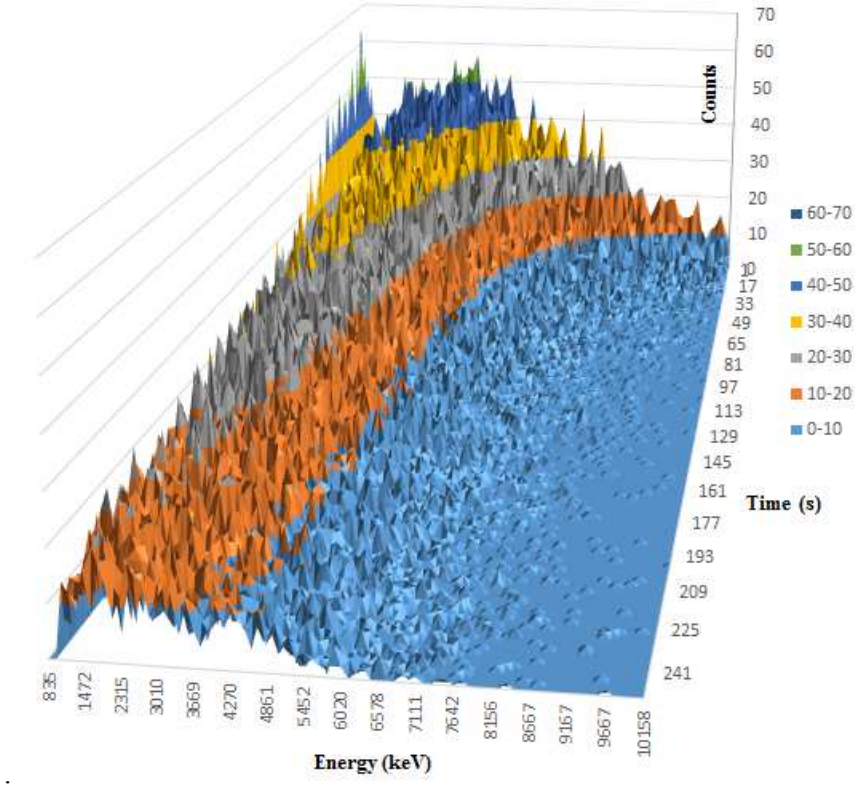

Figure 18. 3D graph for fast neutron count rate from F1 fuel at 100 kW power run

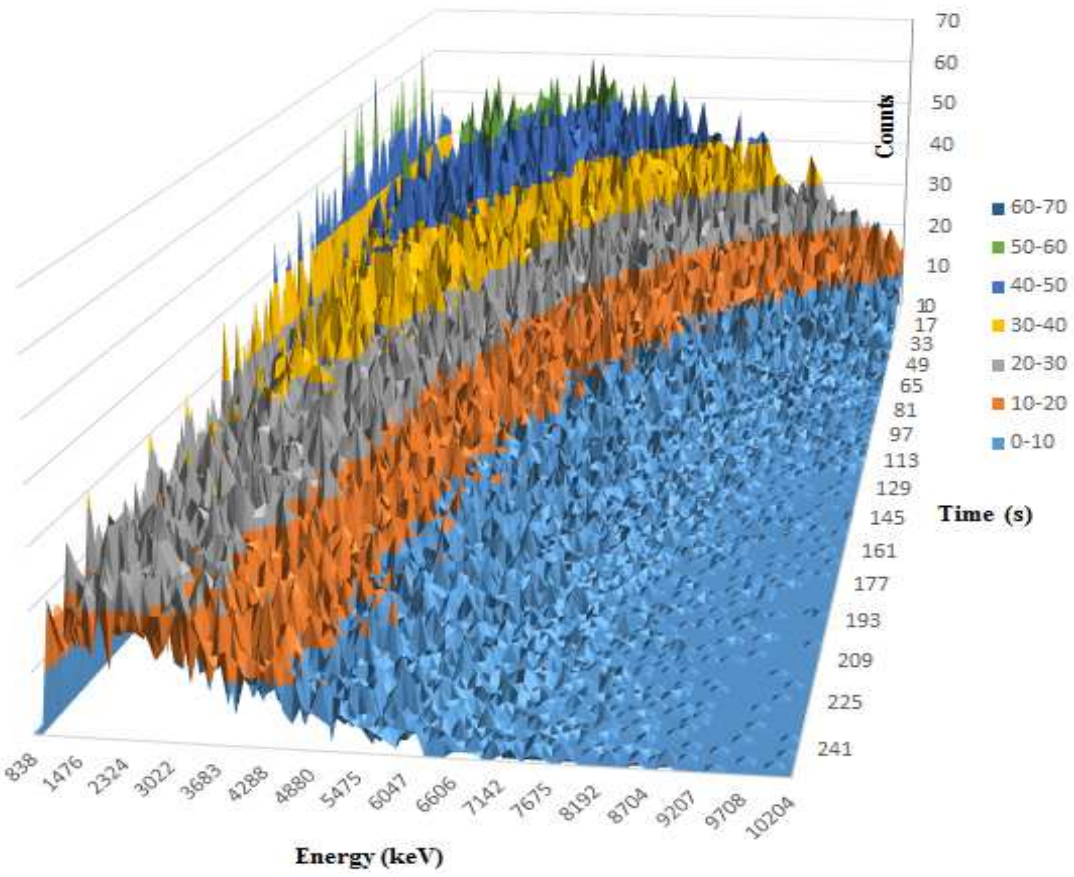

Figure 19. 3D graph for fast neutron count rate from F16 fuel at 100 kW power run

When ^{238}U isotope is exposed to neutrons, it absorbs neutrons to become ^{239}U which undergoes two beta decays to eventually produce ^{239}Pu isotope. Fuel elements F1 and F2 has been in use for over 20 years, therefore one would expect more ^{239}Pu production in them than the new F11 and F16 fuel elements in the reactor core. It was assumed that F11 and F16 fuel elements were fresh without any Pu while F1 and F2 contained Pu produced since 1992; the beginning of their life.

$$^{238}_{92}U + {}^{1}_{0}n \rightarrow {}^{239}_{92}U \xrightarrow{\beta^-} {}^{239}_{93}Np \xrightarrow{\beta^-} {}^{239}_{94}Pu \qquad (4)$$

Production of ^{239}Np can lead to second beta decay to produce ^{239}Pu, however ^{239}Np has a large thermal neutron absorption cross section of 37 barns. This means if neptunium remains in the reactor at high power the production of ^{239}Pu will be reduced. However, the unique burnup of MSTR facilitates production of ^{239}Pu. During the long shutdown periods particularly during the evenings and weekend ^{239}Np get ample opportunity to go through the beta decay and produce ^{239}Pu. A half-life of 2.3 days is short enough for weekends to produce large quantity of ^{239}Pu.

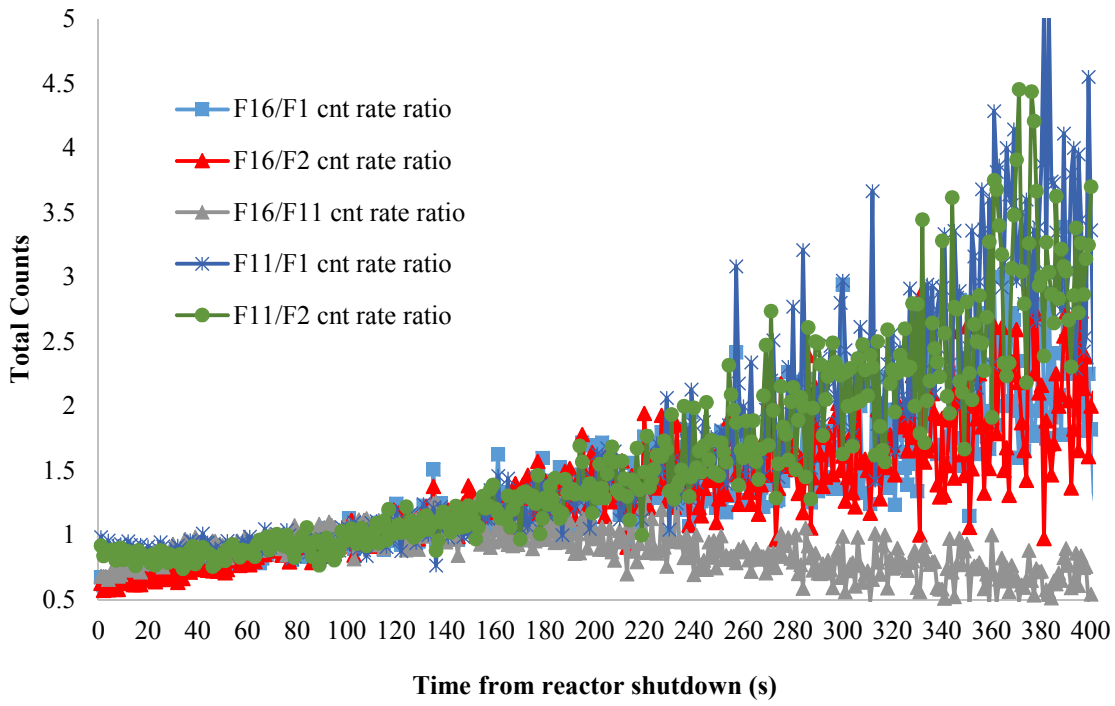

Figure 20. Fuel element fractions for integrated spectrum at 10 kW power run

The ratios between fuel elements were examined to be able to calculate the burnup values. As discussed before, it seems there is some power dependence for low energy peaks after low power runs. Therefore, burnup analysis is based on integrated total count spectrum; a quantity much easier to measure. Fig. (20) shows integrated total count ratios

between 0 and 400 seconds at 10 kW run. First 100 second of the count ratios of fuel elements showed significant low energy contribution and hence power history dependence. This power history dependence would add additional undesirable uncertainty. Based on the 3D graphs (Figs.16-19) it was decided to base burnup predictions as well as Pu/U ratio estimates on the total neutron counts between 150-400 seconds when using post high power run data. The data for this period of time showed little dependence on the low energy neutrons and hence burnup history dependence. This somewhat arbitrary choice is consistent with methodologies proposed by other researchers. For example, Jordan and Perret [9] relied on thermal neutron counts from 60-240 seconds for their analysis. For low power runs, the total neutron counts showed large statistical fluctuation after 130 seconds. Therefore, for low power runs cumulative neutron counts ratios between 100 and 130 seconds were used.

Ideally, it is expected that F16/F1, F16/F2, F11/F1 and F11/F2 ratios must be higher than 1.0 since the F16 and F11 fuel elements were new fuels and should emit more delayed neutrons than F1 and F2. It is also expected that F16/F11 ratio must be around 1.0 since they both were new fuels. However, all the ratios in the beginning were lower than 1.0. In fact, F16/F11 ratio is around 0.6 which indicates F16 fuel element has higher burnup than F11. After 130 seconds of the data collection at 10 kW power, F1 and F2 fuels were produced only the background counts while F11 and F16 fuels were still showing fission fast delayed neutrons. In this case count ratios of the fuels were much higher than initial ratios after 130 seconds. Therefore, one has to rely on integrated total count ratios between 100 and 130 seconds for 10 kW power burnup calculations (see Fig. 21).

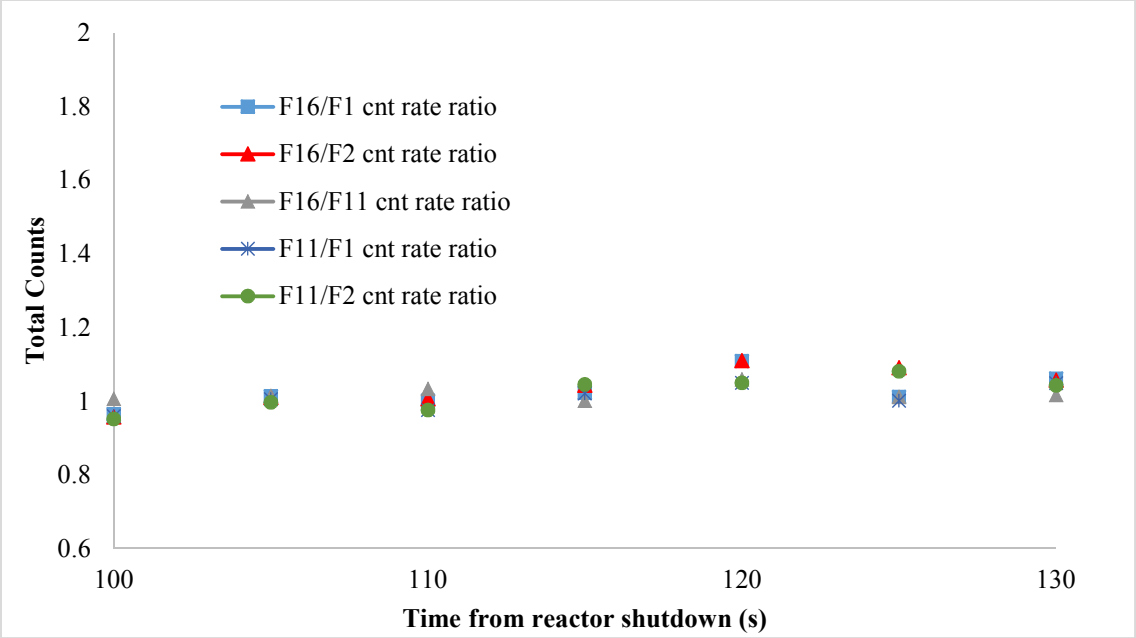

Figure 21. Best fuel element fractions at 10 kW power run between 100 and 130 s.

Table 3 shows average neutron emission ratios for various fuel elements between 100 and 130 seconds after 10 kW power and their corresponding error. It is expected that all values should be more than 1.0 since F11 and F16 fuel elements were actually new fuel elements. All the ratios were measured to be more than 1.0 and also show that F2 was slightly more burned than F1.

Table 3. Fuel element ratios and errors between 100 and 130 seconds at 10 kW run.

Fuel fraction	Average	Error
F16/F1	1.002903132	± 0.066683242
F16/F2	1.038606284	± 0.025532915
F11/F1	1.011960808	± 0.0990654
F11/F2	1.015806226	± 0.013807403

Table 4 shows the fuel elements and their calculated burnup values based on delayed fast neutron measurements in unit of both gram (g) and megawatt day per metric

ton (MWD/T). Since we assumed that F11 and F16 were fresh, no burnup values were assigned for these fuel elements. Because each fresh fuel element contained 112.5 gram of enriched ^{235}U, F11 and F16 fuel elements must have 112.5 g ^{235}U fuel at the time of measurement. Using Fig. (21) and corresponding Table 3 of neutron emission ratios, the burnup values were calculated. According to calculations, F1 fuel burned 1.33 g of ^{235}U and F2 fuel burned 1.75 g of ^{235}U and their corresponding burnup values are 149 MWD/T and 196 MWD/T, respectively. Collectively, F1 and F2 fuels burnt only a total of 3.08 g of ^{235}U over 20 years. These predictions are actually matching with reactor burnup calculations as reported to NRC. Using a conversion factor (0.1839) [21] from the MS&T reactor ^{239}Pu production was calculated to be 0.57 g.

Table 4. Burnup calculations and ^{239}Pu production at 10 kW run

Fuel Elements	Remaining Fuel (g)	Burnup (g)	Burnup (MWD/T)	^{235}U Burnup & Conversion (g)	^{239}Pu Conversion (g)
F11	112.50	0.00	0	0.00	0.00
F16	112.50	0.00	0	0.00	0.00
F1	111.17	1.33	149	1.57	0.24
F2	110.75	1.75	196	2.07	0.32
Total	446.92	3.08	345.00	3.65	0.57

Fig. (22) shows integrated total count ratios between 0 and 600 seconds at 100 kW run. First 100 seconds of the count ratios of fuel elements showed that there are some uncertainties in the ratios. Again, it is expected that F16/F1, F16/F2, F11/F1 and F11/F2 ratios must be higher than 1.0 since the F16 and F11 fuel elements were new fuels which they should be emitting more delayed neutrons than F1 and F2 fuels.

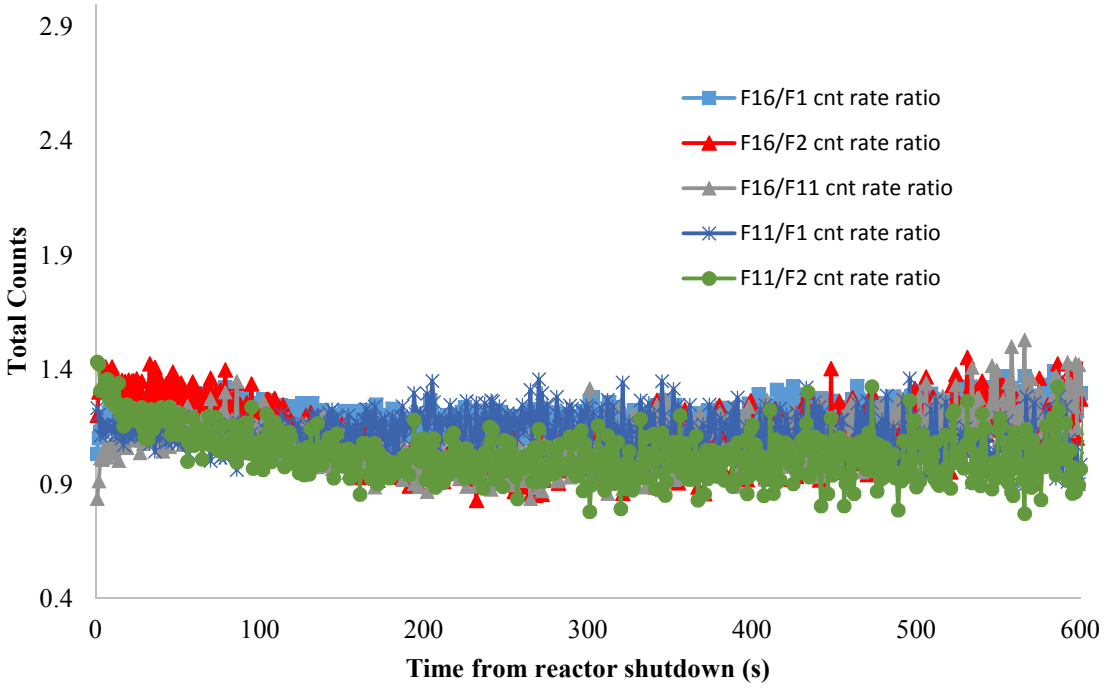

Figure 22. Fuel element fractions for integrated spectrum at 100 kW power run

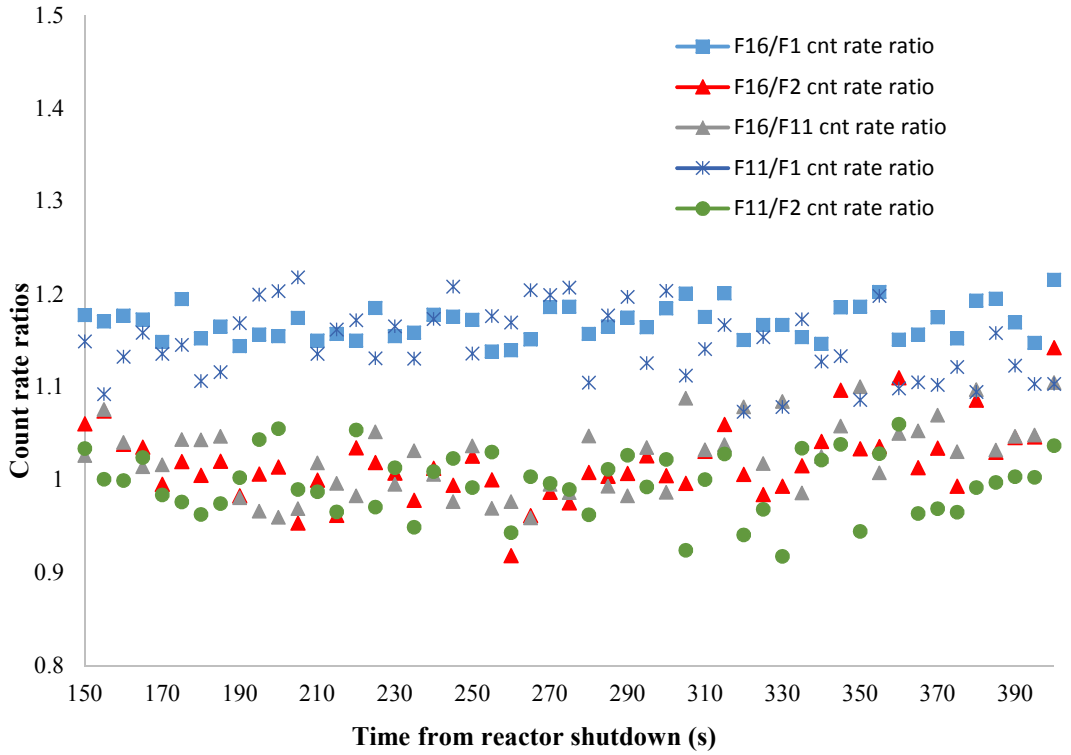

Figure 23. Best fuel element fractions at 100 kW power run between 150 s and 400 s.

Again, time interval was carefully selected for burnup calculations because of the high fluctuations from the beginning of data collection and high background contribution towards the tail end. The higher burnup cases, delayed neutrons died out faster and reached background count level earlier than fresh fuels. Therefore, the best time interval for fuel burnup analysis was selected between 150 and 400 seconds for 100 kW power runs.

Fig. (23) shows delayed fast neutron fuel element ratios between 150 and 400 seconds after 100 kW power run. There are two important outcomes of these ratios (see Table 5); one, F16 and F11 being fresh always produce ratios larger than 1 (F16/F1 and F11/F1) when compared to old fuel. Secondly, based on higher power run data F1 fuel seems to have higher burnup than F2. However, that is not true as discussed earlier due to the unique burnup history of F1.

Table 5. Fuel element ratios and errors between 150 and 400 second at 100 kW run

Fuel fraction	Average	Error
F16/F1	1.16861911	± 0.040678702
F16/F2	1.01768466	± 0.077681964
F11/F1	1.14586467	± 0.07747737
F11/F2	1.00427855	± 0.072539209

Table 6 shows calculated burnup values based on delayed fast neutron measurements in unit of both gram (g) and megawatt day per metric ton (MWD/T). Again, since we assumed F11 and F16 were fresh, no burnup values were assigned for these elements. According to the calculations F1 fuel burned 14.32 g of ^{235}U and F2 fuel burned 1.95 g of ^{235}U and their corresponding burnups are 1569 MWD/T and 217 MWD/T, respectively. ^{239}Pu production calculated as 0.36 g for fuel element F2 and total ^{239}Pu

production calculated as 2.99 g at 100 kW run. This prediction of 3 g ^{239}Pu production is also much higher due to the unique burnup history of F1.

Table 6. Burnup calculations and ^{239}Pu production at 100 kW run

Fuel Elements	Remaining Fuel (g)	Burnup (g)	Burnup (MWD/T)	^{235}U Burnup & Conversion (g)	^{239}Pu Conversion (g)
F11	112.50	0.00	0	0.00	0.00
F16	112.50	0.00	0	0.00	0.00
F1	98.18	14.32	1596	16.95	2.63
F2	110.55	1.95	217	2.31	0.36
Total	433.72	16.28	1813.00	19.27	2.99

The calculated fuel burnups for F2 from both high and low power runs are in reasonable agreement with two power based estimates and closely matching with the NRC reported values given in Table 1. However, the predicted burnup for F1 from high power run data is much higher than expected. This abnormality is probably because of the unique burnup history of F1 which was initially at location C7 of the reactor (see Fig. 3) when F16 was placed at D9 location for analysis. During this time high concentration of Xenon precursors would have been produced. Subsequently, the fuel was shuffled. During the reshuffling time Xenon would have build-up in F1. Moreover, C7 is in close proximity of the control rod at D7 which would strongly impact the neutron energy spectrum for F1. This possible exposure to fast neutron would lead to high fast fission factor for F1 and possible a changed in the delayed neutron precursor population. After this unique irradiation, F1 was then removed to D9 location for delayed neutron data collection. It is conceivable that some moderate to long live fission product with high neutron cross section

(such as Xenon) were still present in F1. Presence of these isotopes could have resulted in unexpectedly low fission rates and hence delayed neutron emissions. Because of this possible high poison, an unexpectedly low fission rate and high burnup was predicted for F1. For the previous tests (F2 and F11) fuel elements where in the storage before being tested and did not experience any unusual irradiation prior to their testing.

6. Conclusion

Since nuclear fuel cycle options are being reconsidered in the U.S., better tools and techniques for measuring burnup and monitoring spent fuel is highly desirable. In particular, non-destructive investigation by delayed fast neutron spectroscopy seems to be an efficient method to monitor nuclear fuel elements; especially MOX fuels because of the large difference in the delayed neutron fraction from ^{235}U (0.0065) and ^{239}Pu (0.0021). This over three fold decrease in delayed neutron is maintained even for the longest lived neutron precursors allowing measurements possible after even a minute or two post shutdowns. The purpose of this works is to propose an initial frame work for such a measurement technique for Pu/U discrimination applicable for MOX fuel. Obviously, for a robust technique develop a large database of post shutdown neutron count with high fidelity statistic is needed which is cost prohibitive for the current scope.

Even though the MSTR core does not contain MOX fuel elements, the reactor has been producing ^{239}Pu over the years. Production of ^{239}Pu is further facilitated by long shutdown times during evenings and weekend. Therefore the university reactors in general offer a significant research for technique development, verification and validation.

Using MSTR fuel, with the help of new (fresh) fuel and fairly burnt old fuel since 1992, the burnup values of the fuels were calculated using delayed fast neutron emission

rates. ^{235}U - ^{239}Pu conversion was also obtained with different fuel elements. Fuel burnup was calculated by taking the ratios of total time integrated fast delayed neutron emission rates post shutdown after running the reactor at two different powers. The specific time period for neutron data collection was selected to minimize reactor power history dependence and reduce uncertainties and fluctuations in the data. The results of burnup at 10 kW run was reasonable range and calculated to be 149.0 MWD/T and 196.0 MWD/T for F1 and F2 fuel elements, respectively. Total ^{239}Pu conversion for F1 and F2 fuel elements found to be 0.57 g. Burnup of F2 fuel element at 100 kW run calculated as 217.0 MWD/T and its ^{239}Pu conversion was estimated to be 0.36 g.

In addition to this technique development, the temporal response of neutron count rate was observed for the fast delayed neutrons. It is interesting to note that for low power runs initial build-up of delayed fast neutron precursor was observed (see Figs. (12) and (13)) for both F2-F11 fuel test and F1-F16 fuel test. This build-up is not apparent for high power runs. Also, low energy peaks for old fuels were higher than the fresh fuel at low power.

Ideally, data collection must be through underwater counting system but measurements were taken through a beam port with different mediums (discussed previously) causing thermalization of fast neutrons. It is also important to pay careful attention to the burnup history of all fuel elements being tested since our initial experiments suggested strong burnup history dependence when post measurement irradiations were at low power levels. Likewise, robust technique development would require careful time window selection for temporal neutron integration.

REFERENCES

[1] C. Willman, and et al., "A nondestructive method for discriminating MOX fuel from LEU fuel for safeguards purpose", Annals of Nuclear Energy 33, (2006), 766-773.

[2] M. L. Dennis and S. Usman, "Feasibility Study of MOX Fuel Online Burnup Analysis", Proceedings of ICAPP '06. Reno, NV. June 2006.

[3] M. L. Dennis and S. Usman, "Feasibility of 106Ru peak measurement for MOX fuel burnup analysis", Nuclear Engineering and Design, 240, (2010), 3687-3696.

[4] C. Riffard and et al., "MOX Fuel Characterization for Burnup Credit Application: Extension of Nondestructive Method Qualified for LEU Fuels", Nuclear Technology, 154, (2006), 186-193.

[5] C. Willman, and et al., "Nondestructive assay of spent nuclear fuel with gamma-ray spectroscopy", Annals of Nuclear Energy 33, (2006), 427-438.

[6] T. Akyurek and et al., "Review and characterization of best candidate isotopes for burnup analysis and monitoring of irradiated fuel", Annals of Nuclear Energy 69, (2014), 278-291.

[7] Z. Zhao, "Investigation on using neutron counting techniques for online burnup monitoring of pebble bed reactor fuels", PhD Dissertation, Nuclear and Radiological Engineering Department, University of Cincinnati, 2004.

[8] G. Perret and K.A. Jordan, "On the combination of delayed neutron and delayed gamma techniques for fission rate measurement in nuclear fuel", Institute of Electrical and Electronics Engineers, 978-1-4577-0927-2/2011.

[9] K.A Jordan and G. Perret, "A delayed neutron technique for measuring induced fission rates in fresh and burnt LWR fuel", Nuclear Instruments and Methods in Physics Research Section A, 634, (2011), 91–100.

[10] Shaw Areva MOX Services, LLC, 2008, September 27. MOX Project. ww.moxproject.com.

[11] United States Enrichment Corporation, Megatons to Megawatts Program, http://www.usec.com/news/megatons-megawatts-program-recycles-450-metrictons-weapons-grade-uranium-commercial-nuclear-fu, Accessed on 13 April, 2013, Created on 9 July 2012.

[12] H. Ing, and et. al., Portable Spectroscopic Neutron Probe, Radiation Protection Dosimetry, 126, (2007), 238-243.

[13] M. Straka, "Safety analysis report for the University of Missouri-Rolla Reactor with low enriched uranium fuel", License R-79, Docket 50-123, University of Missouri-Rolla, Rolla, MO, Ver. 1, Sect. 4, . (1998), pp. 2-5.

[14] M.C. Brady and T.R. England, "Delayed Neutron Data and Group Parameters for 43 Fissioning Systems", Nucl. Sci. and Eng., 103, (1989), 129.

[15] S.G. Isaev, and et. al., "Delayed neutrons as a probe of nuclear charge distribution in fission of heavy nuclei by neutrons", Progress in Nuclear Energy, 41, (2002), 117-124.

[16] J.M. Campbell and G.D. Spriggs, "8-Group Delayed Neutron Spectral Data for Hansen-Roach Energy Group Structure", Los Alamos Technical Report LANL 99-4000 (1999) and in the special issue of Progress in Nuclear Energy (2002).

[17] J.R. Lamarsh, Introduction to Nuclear Engineering, 3rd Edition, p. 87, (2001), Prentice Hall, New Jersey, USA

[18] A. D'Angelo and et. al., "Delayed neutron data for the major actinides", International Evaluation Co-operation, Nuclear Energy Agency Organization for Economic Co-Operation and Development, Volume 6, NEA/WPEC–6, (2002).

[19] W. M. Stacey, Nuclear Reactor Physics, p. 140, (2001), John Wiley & Sons Inc., New York, USA.

[20] T. Kawano, and et. al., "Calculation of delayed-neutron energy spectra in a quasiparticle random-phase approximation–Hauser-Feshbach model', Physical Review C, 78, (2008), 054601.

[21] C. Reisner, Senior Reactor Operator, Missouri University of Science and Technology, Rolla, MO, Private Communication, (March, 2014).

[22] Mobile Microspec Operational Manual, Bubble Technology Industries Inc (BTI), Revised: October 30, (2009).

[23] M. Karlsson, Absolute efficiency calibration of NE-213 liquid scintillator using 252Cf source, Master's Thesis, The Department of Nuclear Physics in Lund University, (1997), Lund, Sweden.

SECTION

3. CONCLUSIONS

This research is focused on spent fuel investigation using photon and fast neutron spectroscopy as well as different detector dead-time measurements and the count loss estimation in radiation detection systems. First, dead-time phenomenon of counting systems were investigated using dead-time models. The dead-time of different detection systems was calculated under different conditions using different methods. As it was discussed in previous sections, data lost is an important issue for high intensity radiation measurements (e.g., spent fuel investigation) and proper dead-time model should be selected for data correction for the counting systems. Second, the original plan was experimental interrogation of spent fuel elements using photon energy spectrum at MSTR. However, the difficulty of removing the lead shielding from beam port was prevented fuel investigation using photon energy spectrum. Therefore, only best isotopes were identified using photon energy, fission yield, branching ratio, half-life, branching ratios, production modes, fuel matrix diffusivity, and thermal neutron absorption cross section for MOX fuel burnup analysis and spent fuel monitoring. Candidate isotopes were previously identified performing ORIGEN ARP computer simulations. Third, spent fuel interrogation were performed and ^{235}U - ^{239}Pu conversion values obtained using NDA delayed fast neutron measurements at MSTR.

Using standard two-source method and the simple non-paralyzing model assumption, GM counter's dead-time dependence on applied voltage, operating temperature, and fatigue were obtained. Both ^{60}Co and ^{137}Cs sources were used for dead-time measurements. The results showed that plateau region is the best region for operating

with a minimum dead-time which is not sensitive to the applied voltage. The results also showed that there is a strong temperature dependence of dead-time, with a correlation coefficient of 0.93. Calculated dead-times using two-source methods were confirmed with oscilloscope methods. It is proven that one dead-time does not apply to all detectors and even for the same detector applicability of the same model under all operating condition is questionable. Therefore, dead-time model should be chosen carefully for the specific detector, operating conditions and radiation to be measured to correctly represent the physical measurement phenomenon. Using combination of attenuation law, paralyzing, and non-paralyzing models, dead-time of fast neutron detector was calculated. For fast neutron probe paralyzing dead-time calculated as 98.7μs and non-paralyzing dead-time calculated as 239.6 μs. This neutron detector was used to investigate the fuel element using delayed fast neutrons.

Using photon information, best isotopes obtained for burnup analysis by investigating half-life, fission yield, branching ratios, production modes, thermal neutron absorption cross section and fuel matrix diffusivity. ^{132}I and ^{97}Nb are identified as good isotope candidates for on-line burnup analysis. ^{132}I is also a good candidate for plutonium/uranium discrimination due to the large difference in the fission yield of the isotope. Cesium isotopes appears to be the best choices for interim storage monitoring. For the long-term storage monitoring ^{94}Nb is the most attractive candidate. It has a low diffusion rate of $\sim 10^{-11}$ cm^2/s, an almost zero neutron absorption cross section making it burnup history independent and decent gamma yield of 1.44E-09.

Nuclear fuel elements were investigated and Pu from U fuel discriminated using non-destructive (NDA) fast delayed neutron spectroscopy at Missouri University of

Science and Technology Reactor (MSTR). Using two sets of burnt and fresh fuels, delayed fast neutron spectra were obtained with different reactor powers after post-shutdown. At 10 kW power run, burnup values of F1 and F2 fuel elements were found to be 149 MWD/T and 196 MWD/T, respectively. ^{239}Pu conversion calculated as 0.57 g for low enriched (19.75%) fuel elements of F1 and F2 since 1992. The experimental burnup results compared with the reactor burnup calculations based on Nuclear Regulatory Commission (NRC) requirements and the results are closely matching. However, F1 fuel element burnup value at 100 kW power was higher than expected.

Analyzing the delayed fast neutron measurements using half-life information of each energy peaks and decay dynamics for all fuel elements and power runs will lead to identification of the neutron precursors. Therefore, precursor identification will be the future work of this particular study. Performing MCNP simulations (photon, thermal and fast neutron) of MSTR beam port for a specific fuel element is another suggestion for future work.

VITA

Tayfun Akyurek was born in Isparta, Turkey in 1981. He received his B.S. (Bachelor of Science) in Physics from Suleyman Demirel University (Isparta, Turkey) in 2003 and M.S. (Master of Science) in Physics from Suleyman Demirel University (Isparta, Turkey) in 2007. He also received his M.E. (Master of Engineering) in Nuclear Engineering from University of South Carolina (Columbia, SC, USA). During his master's program in Turkey, he went to University of Ghent, Belgium as an exchange student under the Erasmus Program for 6 months in 2005. After finishing his master program, he received scholarship from Ministry of National Education (Turkey) that allowed him to obtain his master and Ph.D. degrees in USA.

He has taught radiation detection and measurement, and reactor laboratory classes during his Ph.D. program in nuclear engineering department at MS&T. Tayfun is a student member of the American Nuclear Society. His research interests are nuclear spent fuel analysis using NDA methods, radiation detection and measurement as well as dead-time measurements and the count loss estimation in radiation detection systems. He has published several journal papers (some of them under review), and some conference papers during his Ph.D. program. In May 2015, he received his Ph.D. in Nuclear Engineering from Missouri University of Science and Technology. He is married and he has one daughter.